
Article:
Booth, S.G., Nedoma, A.J., Anthonisamy, N.N. et al. (2021) Perspectives for next generation lithium-ion battery cathode materials. APL Materials, 9 (10). 109201.

https://doi.org/10.1063/5.0051092

APL Materials

Perspectives for next generation lithium-ion battery cathode materials

Cite as: APL Mater. **9**, 109201 (2021); https://doi.org/10.1063/5.0051092
Submitted: 22 March 2021 . Accepted: 28 July 2021 . Published Online: 05 October 2021

Samuel G. Booth, Alisyn J. Nedoma, Nirmalesh N. Anthonisamy, et al.

Perspectives for next generation lithium-ion battery cathode materials

Cite as: APL Mater. 9, 109201 (2021); doi: 10.1063/5.0051092
Submitted: 22 March 2021 • Accepted: 28 July 2021 •
Published Online: 5 October 2021

View Online Export Citation CrossMark

Samuel G. Booth,[1,2,a] Alisyn J. Nedoma,[1,2,a] Nirmalesh N. Anthonisamy,[1,2] Peter J. Baker,[2,3] Rebecca Boston,[2,4] Hugo Bronstein,[2,5] Simon J. Clarke,[2,6] Edmund J. Cussen,[1,2,4] Venkateswarlu Daramalla,[2,7] Michael De Volder,[2,8] Siân E. Dutton,[2,7] Viktoria Falkowski,[2,6] Norman A. Fleck,[2,9] Harry S. Geddes,[2,6] Naresh Gollapally,[1,2] Andrew L. Goodwin,[2,6] John M. Griffin,[2,10] Abby R. Haworth,[2,10] Michael A. Hayward,[2,6] Stephen Hull,[2,3] Beverley J. Inkson,[2,4] Beth J. Johnston,[1,2] Ziheng Lu,[2,11] Judith L. MacManus-Driscoll,[2,11] Xabier Martínez De Irujo Labalde,[2,6] Innes McClelland,[1,2,3] Kirstie McCombie,[2,4] Beth Murdock,[10] Debasis Nayak,[2,11] Seungkyu Park,[2,8] Gabriel E. Pérez,[2,3] Chris J. Pickard,[2,11] Louis F. J. Piper,[2,12] Helen Y. Playford,[2,3] Simon Price,[13] David O. Scanlon,[2,14,15] Joe C. Stallard,[2,9] Nuria Tapia-Ruiz,[2,10] Anthony R. West,[2,4] Laura Wheatcroft,[2,4] Megan Wilson,[13] Li Zhang,[2,10] Xuan Zhi,[4] Bonan Zhu,[2,13] and Serena A. Cussen[1,2,4,a]

For affiliations, please see the end of the Reference section

ABSTRACT

Transitioning to electrified transport requires improvements in sustainability, energy density, power density, lifetime, and approved the cost of lithium-ion batteries, with significant opportunities remaining in the development of next-generation cathodes. This presents a highly complex, multiparameter optimization challenge, where developments in cathode chemical design and discovery, theoretical and experimental understanding, structural and morphological control, synthetic approaches, and cost reduction strategies can deliver performance enhancements required in the near- and longer-term. This multifaceted challenge requires an interdisciplinary approach to solve, which has seen the establishment of numerous academic and industrial consortia around the world to focus on cathode development. One such example is the Next Generation Lithium-ion Cathode Materials project, FutureCat, established by the UK's Faraday Institution for electrochemical energy storage research in 2019, aimed at developing our understanding of existing and newly discovered cathode chemistries. Here, we present our perspective on persistent fundamental challenges, including protective coatings and additives to extend lifetime and improve interfacial ion transport, the design of existing and the discovery of new cathode materials where cation and cation-plus-anion redox-activity can be exploited to increase energy density, the application of earth-abundant elements that could ultimately reduce costs, and the delivery of new electrode topologies resistant to fracture which can extend battery lifetime.

TABLE OF CONTENTS

I. INTRODUCTION

Electric-vehicle (EV) batteries presage a step change from internal combustion engines (ICE) to electric motors, offering lower running costs and reduced carbon emissions. Next-generation lithium-ion batteries (LIBs) will be largely driven by technological innovations in the cathode that will enable higher energy densities and also present opportunities for cost reduction since cathode materials remain the bottleneck to cost parity. Transformative cathode technology must meet a range of specifications, including higher capacity and power, longer first-lifetime, safer construction, sustainable sourcing of materials, lower cost, and greener manufacturing processes. Lithium-ion systems provide the highest specific energy density of current battery technologies; however, the cathode contributes substantially to both the cost and mass of the assembled unit. Cathode materials exhibit lower capacity relative to current commercially applied anode materials and therefore represent a limiting factor for electrochemical performance. Cathode formulations also often comprise low-abundancy transition metals (TMs) that are costly and may pose ethical concerns in the supply chain. A multi-objective approach to the development of cathode materials is therefore necessary to holistically streamline the design, synthesis, processing, and scale-up of lithium-ion batteries.

Efforts to address these challenges have seen the establishment of vibrant research consortia around the world, including the Faraday Institution FutureCat project in the UK, to pioneer the discovery and development of new cathode materials. Recognizing these challenges, we have established a research consortium that benefits from a depth of multidisciplinary expertise from within and extending beyond the battery field. Strong links have been formed with industrial collaborators to help solve industry-facing challenges and forge the interdisciplinary links to help bring next-generation materials to market. As this field continues to mature and materials development becomes more and more involved, we believe that there will be many developments as opposed to a one-size-fits-all solution. Instead, key advances in individual areas of study must be used to drive forward progress in all areas through a shared knowledge and expertise.

In this perspective, we set out what we see as the challenges related to the most mature next-generation cathode materials, high nickel content layered metal oxides, disordered rock salts, and spinels, along with design principles that we suggest are important to consider when establishing new cathode chemistries based on green, earth-abundant minerals. Materials discovery can now be driven by the application of computational structure searching to amplify the value of experimental work. Morphological control of the cathode structure can enhance the capacity and longevity of batteries, including the development of gradient compositions to counteract operationally induced cation migration as well as the production of hierarchical assemblies to fine tune the shape and size of cathode particles for optimal performance. We acknowledge that the development of new materials is continuously driven by the development of more sensitive measurement techniques. We therefore explore the new insights that can be gleaned, particularly through *operando* measurements, to uncover the structure and mechanism of the functioning electrode at a range of length scales. Finally, we examine the interplay between chemical and mechanical mechanisms that cause a loss of active material and diminish cell performance over the lifetime of a battery. We envision that this combined approach will enable a step change in cathode performance that supports the decarbonization of our energy and transport systems.

II. WHY THE CATHODE MATTERS

Simon Price and Megan Wilson

All technologies that support decarbonization through electrification—whether for energy generation, power conversion, or energy storage—have a "figure of merit": a metric that encapsulates their history, status, and prospects on the technology roadmap and provides a common focus for the research community and manufacturing industries.

Generally, this figure of merit relates in some way to cost reduction. In lithium-ion batteries, the figure of merit that matters most is the cost per kilowatt-hour, the manufacturing cost per unit of energy stored. This is typically stated in $/kWh. Driving this number down, while simultaneously ensuring that gravimetric and volumetric energy density targets are maintained, will be the critical factor in bringing EV technology to price parity with ICE vehicles.

As lithium-ion battery production continues to scale with the rapid growth of EVs, the driver of $/kWh cost reduction will move from reducing the numerator—the total manufacturing cost—to increasing the denominator, cell performance. This is because the absolute manufacturing cost of the cell, battery pack, or system eventually becomes limited by the fundamental costs of the bulk materials that increasingly dominate the cost structure. However, metrics such as energy density will continue to improve as new approaches are found to eke out additional performance from existing and novel materials. Such cell performance increases also pay dividends at the pack and system levels. Cells account for about 70% of the cost of today's battery systems, and in broad terms, a 10% increase in cell

storage capacity (for no increase in absolute cost) leads to a corresponding reduction not only in cell cost per kWh but also in pack and system cost per kWh.

Moving inside the cell, the key drivers of cost per kWh are the anode and cathode energy density and raw materials costs. Figure 1(a) shows a conventional wet-electrolyte cell using a standard graphite anode and a cathode chemistry at the leading edge of the mainstream: $LiNi_{0.8}Mn_{0.1}Co_{0.1}O_2$ (NMC811). For this particular configuration, the cathode active material accounts for a little over one-third of the cell mass and volume and, depending on the purchase price, about one-half of the cell cost. The anode active material, by contrast, occupies more of the cell volume but less mass and just a fraction of the cost: one-fifth of the cost of the cathode active material and about one-tenth of the total cell cost.

Given the cathode's disproportionate influence on today's cell performance and cost, finding ways to "shrink" the cathode—in volume and mass, but particularly in cost—is perhaps the key challenge facing the battery industry. Cathode electrochemical performance has increased in recent years as the mainstream industry focusing on nickel-rich ternary materials, such as NMC811 and above. Much excitement in the industry today also focuses on the anode, particularly on "silicon-rich" anode technologies. The incorporation of silicon into conventional graphite anodes increases the energy capacity. Capacity improvements on the anode will require a higher cathode loading to balance the cell, exacerbating the challenge of reducing the cathode cost [Fig. 1(b)].

Based on data sourced from tier 1 cathode manufacturer annual reports and initial public offering prospectuses (2019), the raw material precursors of mainstream cathode active material variants already account for about 80% of the total cathode active material manufacturing cost at large-scale producers in China [Fig. 1(c)]. In other words, there is little room to reduce the cost of existing cathode raw materials by streamlining the materials manufacturing process. When considering novel cathode active materials, their absolute cost (in $/kg) can only be greater than that of conventional materials if they bring gains in performance that put them on parity, or better, than conventional materials in $/kWh terms.

Not only will the driver of future cost reduction ($/kWh) move from absolute manufacturing cost reductions to performance gains, it is critical that these performance gains are achieved without actually *increasing* the absolute manufacturing cost. This means that researchers, when developing novel cathode formulations, must carefully consider several factors relating to materials selection, including the following:

- Abundance and supply/demand. How much of each component material exists in the world and how accessible is it? How much of each material might be required by the battery industry today and in the long term? Which other industries compete for these materials and in what volumes, today and in the future?
- Extractability. How costly is the raw material to extract and refine? Can this be done sustainably and in an environmentally sound manner?
- Geopolitics and ethical considerations. Is the raw material a conflict mineral? Do certain countries or companies control the supply of it? Is the material already within the supply

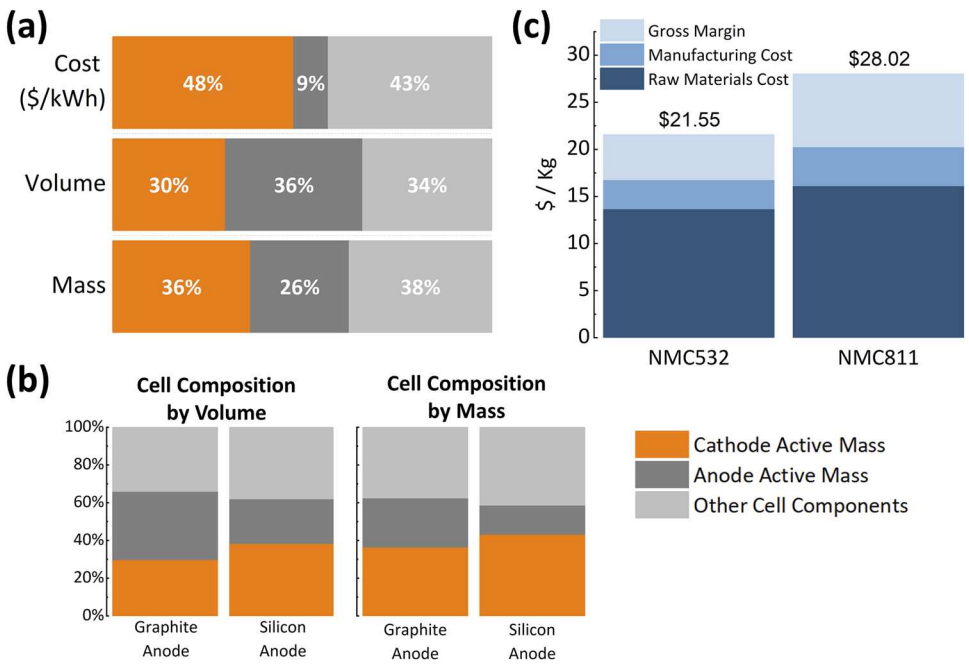

FIG. 1. Composition of the wet-electrolyte pouch cell. "Other" includes current collectors, separator, electrolyte, binders, cell casing, and other minor components of the cell. (b) Impact of introducing a high energy density anode on the composition of the cell by volume and mass. (c) Cathode active material price and cost structure for NMC532 and NMC811 based on manufacturer reports from China. Source Exawatt (2019 data).

chain, or can it be sourced locally on an economically viable basis?
- Quality. How much battery-grade material is available and at what price? Are the impurity levels acceptable, or even excessive (i.e., could materials costs be reduced by using a lower-grade material of acceptable quality)?
- Processability. Can the materials be processed cheaply into the cathode active material and ultimately into the cell?

Choosing the optimal cathode materials need not require avoiding expensive components entirely. As long as these materials are used in small enough quantities, e.g., as dopants to bulkier, cheaper base materials, the overall cost per kWh can be reduced even if the absolute cost increases slightly.

By 2019, the manufacturing cost of goods sold utilizing lithium-ion cells had already fallen below $85/kWh for the leading producers in China, which equates to a reduction of ~20% in two years. With the cathode already accounting for more than one-third of the cell cost and likely to account for closer to one-half with the emergence of high-performance anodes, the need for high-performance, affordable cathodes will only increase.

The cathode and anode are locked in a kind of technological arms race. Improvements to either electrode serve the ultimate goal of increasing the cell energy density and reducing battery pack cost, but disproportionate progress in one electrode increases the demand on the other. While anodic developments remain vital and welcome to the industry, they will not solve the fundamental challenge facing cell manufacturers. Improving the cathode becomes ever more important as the key lever to increase the cell energy density and reduce the cell and system cost.

III. STATE-OF-THE-ART CATHODE MATERIALS

Simon Clarke, Eddie Cussen, Serena Cussen, Viktoria Falkowski, Naresh Gollapally, Michael Hayward, Beth Johnston, Ziheng Lu, Xabier Martínez De Irujo Labalde, Kirstie McCombie, Beth Murdock, Chris Pickard, Louis Piper, David Scanlon, Nuria Tapia-Ruiz, Anthony West, Li Zhang, Xuan Zhi, Bonan Zhu

A. High nickel content layered cathodes

Layered transition metal oxides, of general formula $LiMO_2$, continue to dominate the commercial lithium-ion battery market. Such compositions, with the α-$NaFeO_2$ structure, consist of distinct transition metal and lithium layers where the Li ions can be removed and inserted during charge and discharge, respectively. The $LiCoO_2$ (LCO) structure,[1] utilized in the first commercialized lithium-ion batteries in 1990, is still widely in use 30 years later in cell phones and other portable electronics: a testament to their groundbreaking success. However, several issues have been identified with LCO: thermal runaway at higher states of charge mandates strict safety limits[2] that cap the practical capacities of LCO to ~140 mA h g^{-1}, and ethical and supply chain issues surround the mining practices of cobalt. These challenges have driven research in the direction of alternative and improved layered oxide compositions.

Substitution of the transition metal cations within these layered oxides has proven a pioneering strategy with the introduction of $LiNi_{1/3}Mn_{1/3}Co_{1/3}O_2$ (NMC111), where Ni^{2+}, Mn^{4+}, and Co^{3+} are distributed across the transition metal layer (Fig. 2).[3] Electrochemical activity arises from the redox behavior of Ni^{2+} to Ni^{4+} while Mn^{4+} remains electrochemically inactive but plays a vital role in structural stabilization. There is debate surrounding the electrochemical activity of the Co^{3+} cations, but Co also plays an important stabilizing role.[4,5] Under typical cycling conditions, NMC111 can deliver specific capacities of ~160 mA h g^{-1}. However, it is estimated that an energy density of ≥800 Wh kg^{-1} at the cathode level (corresponding to ≥350 Wh kg^{-1} at the cell level for state-of-the-art cell constructions) is required to meet the higher energy densities demanded by electric vehicle applications.[6] Thus, higher specific capacities at practical voltages are afforded by increasing the nickel content in these layered compositions with a particular interest in nickel-rich NMCs and NCAs, i.e., $LiNi_xMn_yCo_{1-x-y}O_2$ and $LiNi_xCo_yAl_{1-x-y}O_2$ (NCA) for $x \geq 0.8$, capable of delivering initial specific capacities ≥200 mA h g^{-1} at ~4.2 V vs lithium. Alongside these nickel-rich compositions, there is also a renewed interest in pristine $LiNiO_2$ (LNO), which can deliver the largest specific capacity of these layered oxides at practical working potentials.[7] However, specific challenges arise for such nickel-rich compositions, including synthetic complications and structural and thermal instabilities at high states of charge that drastically reduce their cycle life.

The challenges facing the application of higher nickel content layered oxides span from an increasing complexity presented by synthetic conditions at higher nickel content to structural and thermal instabilities initiated at higher states of charge (corresponding to larger degrees of delithiation). Upon moving to higher nickel compositions, reduced stability provides unique demands regarding synthesis and handling procedures particularly at scale. For example, the final calcination step requires an oxygen environment, expensive Li sources, such as LiOH, and stringent control of reaction times and temperatures depending on the desired composition. On an atomic

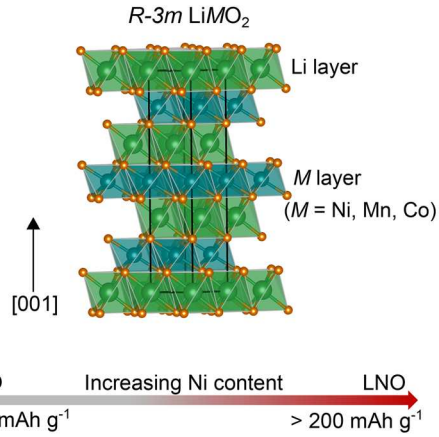

FIG. 2. Crystal structure representation of R-3m $LiMO_2$ layered oxide (M = Ni, Co, and Mn) showing the arrangement of Li and transition metal cations across separate layers. The specific capacities (at practical working potentials) improve upon increasing the Ni content.

level, synthetic challenges can also arise from cation mixing where the comparable ionic radii of Ni (0.69 Å) and Li (0.72 Å) can result in anti-site mixing across the layers. A similar off-stoichiometry is also observed during the synthesis of LNO, whereby structures of composition $Li_{1-z}Ni_{1+z}O_2$ are often obtained, with the excess Ni^{2+} ions occupying sites in the lithium layer. The presence of Ni^{2+} in the Li layer can block Li^+ ion diffusion pathways and cause local layer collapse during charge through cation shrinkage, which is manifested in a large irreversible capacity loss during the first cycle.[7]

The sensitive surface chemistry of these nickel-rich compositions presents additional requirements during handling and characterization. Surface residual lithium species, which may affect charge-transfer resistance or promote gas generation on cycling (e.g., Li_2CO_3 and LiOH), may persist via reactions with CO_2, H_2O, and O_2 and necessitate handling and storing under inert environments. These surface species may also influence chemical and structural observations drawn from surface sensitive analysis techniques.[8] Also associated with the increased surface reactivity are deleterious cathode–electrolyte reactions at high states of charge, which may lead to an increasingly complex surface reaction layer containing LiF, inorganic, and organic species.[9] Cycling to higher cut-off voltages also initiates surface reconstruction processes where the rhombohedral layered structure (*R*-3*m*) can irreversibly transform into spinel (*Fd*-3*m*) and/or rock salt (*Fm*-3*m*)-type surface phases. The decreased thermal stabilities arising from increased nickel content can also play a role through oxygen evolution from thermal lattice decomposition at highly delithiated states. As these processes generally take place at surfaces or interfaces, they are further intensified by the emergence of microcracks (and thus fresh surfaces) that are generated by abrupt and anisotropic expansion and contraction of the lattice at voltages above 4.2 V.[10] These evolving surface changes may result in a loss of active cathode material and increased charge transfer resistance upon cycling, which manifests in rapid capacity fade and drastically reduces the lifetime of these cathodes. In particular, the particle cracking associated with anisotropic lattice distortions at high states of charge can be regarded as a universal failure mechanism of Ni-rich layered oxide cathodes and must be overcome.[11]

Mitigating the degradation processes that occur in nickel rich layered oxides is paramount in realizing their full potential as high energy density cathodes. One strategy involves introducing electrochemically inactive dopant cations into the layered oxide structure. These dopants may be chosen to selectively substitute for either lithium or transition metal cations depending on the desired effect. For example, small amounts (~1–5 mol. %) of Mg^{2+} cations can be substituted into the lithium layer where they can provide a pillaring effect to enhance cycling stability. The Mg^{2+} ions successfully suppress the anisotropic lattice distortions occurring during cycling that lead to micro-crack generation.[12,13] Doping with Al^{3+} on the transition metal sites has also been widely reported in an effort to mitigate Ni migration and improve thermal stabilities.[14] Other dopants can also improve the surface chemistry of the cathodes while stabilizing the bulk structure; for example, small amounts of W^{6+} doped into LNO have been observed to promote a rock salt-type phase during synthesis, which segregates to the particle surfaces where it acts to passivate side reactions. Thermal and structural stabilities also increased, leading to much improved cycling performance.[15,16] A similar effect was also observed for Zr-doped materials.[17] A rich variety of further dopants, e.g., Na, Ca, Ti, Ta, and Mo, including co-doping of Mg–Ti, have been shown to improve the cycling properties of high nickel content cathodes.[18–21] Looking forward, a seemingly vast selection of potential future dopants exist, warranting insights from computational methods to guide further synthetic targets and technoeconomic analysis to ensure sustainability.

Implementing passivating surface layers on cathode particles to mitigate surface degradation processes is also commonly achieved through coating methods. An effective coating should be chemically and structurally stable during electrochemical cycling and should not impinge on the charge transport properties of the electrode. Popular coatings include metal oxides, for example, MgO, Al_2O_3, SiO_2, TiO_2, ZnO, SnO_2, and ZrO_2.[22] There is also an interest in binary metal oxides that contain lithium as effective coatings for nickel rich materials, e.g., Li_2SiO_3, $Li_4Ti_5O_{12}$, Li_2TiO_3, Li_2ZrO_3, Li_2MoO_4, and $Li_{0.5}La_{0.5}TiO_3$.[23] Wet coating methods using water or other solvents (e.g., ethanol) offer a cheap and scalable coating process, whereas techniques such as atomic layer deposition (ALD) offer excellent control over the film thickness, uniformity, and stoichiometry. ALD introduces cost and technological considerations so the process scalability must be considered.[24] Improved cycling stabilities of nickel rich NMCs and NCAs by coating with Al_2O_3 via an ALD process have been demonstrated.[25,26] Electrolyte chemistry also plays a significant role here due to the electrode–electrolyte interface and the corresponding high reactivity of the layered oxide toward the electrolyte at high state of charge (SOC).[27] Consequently, electrolyte composition is an additional factor that can be tweaked to promote more stable cycling. While typical carbonate based electrolytes can undergo oxidation when cycled above 4.3 V (leading to heat generation and parasitic reactions), fluorination strategies have been shown to both widen the electrochemical stability window and form a more stable and protective cathode–electrolyte interface (CEI) layer that ultimately improves cycling performances.[28,29] Additionally, developing ethylene carbonate free electrolytes for Ni-rich systems has also been shown to offer high voltage stability.[30] Furthermore, additives such as vinylene carbonate (VC) are popular and have been reported to suppress surface reconstruction in NMC811[31] and have also shown the ability to form a thermally stable CEI layer for NMC532 and NMC622 electrodes.[32] While only a few examples of electrolyte modification have been discussed here, the literature is rich with reports on further additives, improved lithium salts, and solvent blends.[33] Nevertheless, the effect on thermal stability, CEI formation and, suppression of unwanted interfacial reactions is clear, and the importance of designing tailored electrolyte compositions for specific applications cannot be overlooked. Further details on the influence of the CEI and interfaces are provided in Secs. IV B and IV C. Additional strategies to enhance cycling properties in these materials include core–shell or gradient-like structures, and advanced particle engineering routes to suppress particle cracking by obtaining, e.g., single crystal particles[34] or polycrystalline materials with specific grain crystallographic orientations.[35]

Development of single crystal layered transition metal oxides

Typically, polycrystalline arrangements of nickel-rich cathode materials are applied in current lithium-ion batteries consisting of agglomerated primary particles that form secondary assemblies.

When formulating an electrode from such structures, the pressure applied during calendering can cause secondary particle cracking, increasing the electrode surface area exposed to the liquid electrolyte. The resulting growth in the cathode–electrolyte-interface (CEI) may result in an increased charge transfer resistance. Additionally, during battery cycling, inter-granular fracture may disrupt Li-ion diffusion processes and result in the loss of active material leading to capacity fade.[36] The emergence of single crystal nickel-rich cathode particles is now opening up the possibility of greater resistance to crack formation during electrode processing and operation.

The random crystal orientation in polycrystalline assemblies results in anisotropic volume changes on charging. The absence of such stresses in single crystal materials may therefore reduce the likelihood of inter-granular fracture [Fig. 3(a)]. Considering the nickel-rich material $LiNi_{0.83}Co_{0.11}Mn_{0.06}O_2$, single crystal morphologies have shown excellent long duration cycling performance and thermal stability in half cells at 25 and 55 °C and full cells at 45 °C.[37] These observations are in addition to reduced Ni migration to the anode observed for single crystal NMC811 when compared to polycrystal NMC811.[38] However, intra-granular fracture is not entirely mitigated and does still occur when single crystal NMC particles are severely overcharged (e.g., to 4.7 V, >0.84 Li^+ extraction per NMC).[34]

Morphology may also play a role in suppressing gas evolution through a reduction in electrolyte side reactions, a concern around safe battery operation and storage. Figure 3(b) evaluates the influence of morphology on gas evolution when storing NMC811 single crystal particles obtained through flux synthesis at different states of charge. The reduced gas evolution correlates with the reduced surface area in the single crystal materials, since there are no internal pores and intergranular boundaries along the surface.[39] Micro-cracking has also been observed for single crystal Ni rich cathodes through plane gliding on charge, which is reversed on discharge.[40] Despite increased performance, synthetic challenges have limited the reports on single crystal materials to date.[41,42] However, the development of new synthetic approaches to single-crystal nickel-rich cathode materials could improve energy density, safety, and durability in lithium-ion batteries.[43]

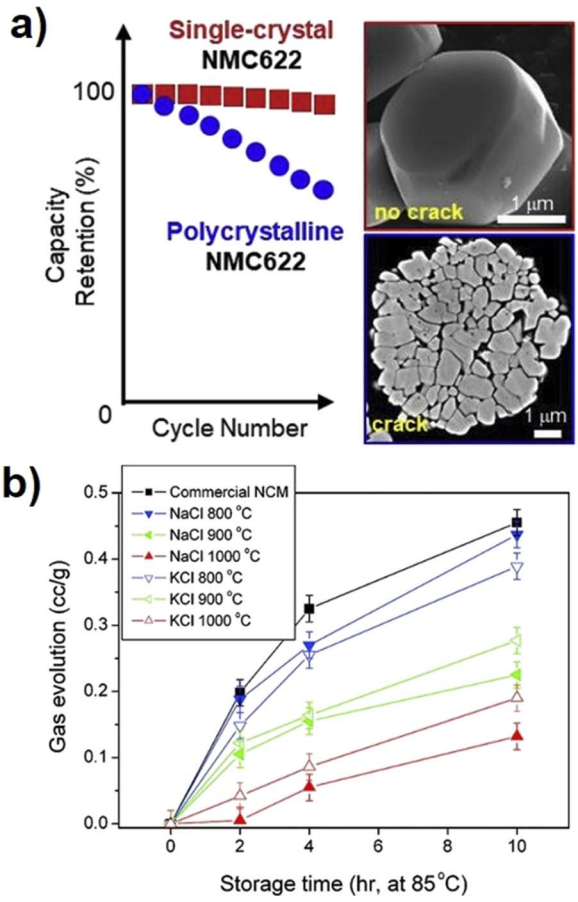

FIG. 3. (a) Cyclic performance and SEM image of single crystal and polycrystalline NMC cathodes after 300 cycles. Reprinted with permission from Qian *et al.*, "Single-crystal nickel-rich layered-oxide battery cathode materials: Synthesis, electrochemistry, and intra-granular fracture," Energy Storage Mater. **27**, 140–149 (2020). Copyright 2020 Elsevier. (b) Evolution of gas (cc/gram of NCM) from charged electrodes (4.45 V) with respect to storage time at 85 °C. Reproduced with permission from Y. Kim, ACS Appl. Mater. Interfaces **4**, 2329 (2012). Copyright 2012 American Chemical Society.

Concluding remarks

Owing to their successful history as cathodes, layered oxide materials remain the current cathode of choice for lithium-ion batteries, especially for automotive applications, with some low-cobalt and high-nickel compositions already primed for commercialization. To fully reap the benefits of these, efforts to mitigate and overcome deleterious degradation processes that impair such nickel rich compositions are essential. Strategies involving the introduction of electrochemically inactive, stabilizing cations into the structure and applying stable surface coatings have proved successful in prolonging the cycle life. A synergistic approach involving doping, coating, and sophisticated particle engineering is an attractive route for the cathodes of the future.

B. High capacity through lithium-excess layered transition metal oxides

Despite consistent year-by-year improvements in the energy density of NMC-based layered oxides, the target energy density of 500 Wh/kg at the cell level remains elusive as ultimately conventional layered cathodes are limited by both their lithium content and the extraction of one electron per transition metal ion. Li-excess layered oxide $Li_{1+x}TM_{1-x}O_2$ systems (Li-excess implies the molar ratio of Li over TM is larger than one by design) are promising candidates for higher energy density cells, where the capacity of the layered oxide can exceed that expected from conventional transition metal cation redox.[44] The excess capacity has been most frequently attributed to anion-redox processes involving O-dominated states after conventional transition metal redox up to 4+ has been achieved. Several mechanisms have been proposed to explain the excess capacity upon further Li^+ extraction for these materials,[45–48] ranging from localized electron–holes,[49,50] O–O dimers,[51] or trapped molecular O_2 with/without unconventional

$Mn^{4+/7+}$.[52,53] Currently, no single mechanism can explain all the observed phenomena.

Li-excess layered oxides are described as either a coherent nanocomposite of layered Li_2MnO_3 and $LiTMO_2$ (TM = Ni, Co, and Mn) or as a single-phase solid solution with transition metal and lithium uniformly mixed while preserving the global honeycomb ordering. The key difference between the two structure descriptions is the coherence length of Li_2MnO_3-like domains, which is much shorter in the solid solution model than that in the nanocomposite model. The variation in the coherence length of Li_2MnO_3-like domains in the published literature may originate from differences in synthesis methods and chemical composition.[54] Within the Li_2MnO_3-like motifs, the oxygen ions are coordinated by two transition metals and four Li, i.e., different from the coordination of oxygen by three transition metals in the classical layered oxide. This difference in oxygen coordination gives rise to unhybridized O-2p orbitals, termed an "orphan orbital" or a "Li–O–Li" environment.[49,50] As a result, there is a longstanding view that the Li_2MnO_3 component is the critical ingredient for both providing accessible excess Li^+ from the TM layer (in addition to interlayer) and promoting oxygen redox in the Li-excess layered oxide $Li_{1+x}M_{1-x}O_2$ systems.

The layered Li-rich oxides also display an activation "plateau" (absent for layered oxides) at around 4.5 V after the active transition metal ions have reached conventional 4+ oxidation limits.[55] This appears in the first cycle and is often absent in subsequent cycling. The activation plateau is suggestive of a two-phase reaction, but there is no conclusive *in situ* diffraction data indicating a two-phase co-existence in this region. Originally, the 4.5 V plateau was discussed in terms of the oxygen redox through comparison with Li_2MnO_3. Although oxygen redox is predicted computationally for Li_2MnO_3,[56] it has been shown experimentally that the 4.5 V "plateau" of Li_2MnO_3 does not correlate with oxygen redox and is instead associated with gas evolution.[51] The activation plateau instead reflects in-plane Li-TM ionic rearrangements upon charging that removes the initial "honeycomb" ordering, which can be recovered by a combination of annealing and relithiation of the cathode material.[57] An unanswered question is whether cation migration, in general, is crucial for enabling the redox process during the activation plateau or whether it is a side effect of this redox process. Recent *operando* studies of $Li[Li_{0.144}Ni_{0.136}Mn_{0.544}Co_{0.136}]O_2$ quantified the degree of Mn oxidation (beyond 4+) and extent of TM out of plane migration and concluded oxygen redox without requiring exotic Mn migration and oxidation.[58]

The Li-excess layered oxides are considered to display additional distinct redox mechanisms from conventional layered oxides. The literature on Li-excess materials is vague as to what is meant by reversible oxygen redox in this context; it is expected to be different to redox on the transition metals whereby electron extraction from the transition metals is accompanied by some degree of rehybridization between the M d-orbitals and O 2p orbitals. In addition to uncertainty over definition, there is a lack of direct probes capable of distinguishing oxygen redox from other irreversible reactions that occur in cathode materials, such as decomposition processes and side reactions with the (non-optimized) electrolyte. Of the few, resonant inelastic x-ray scattering (RIXS) has been increasingly used to quantify the metal and oxygen redox contributions.[59,60] O K-edge RIXS has proven to be a reliable method of detecting the emergence of spectroscopic signatures attributed to oxygen redox.[61] More recent high resolution RIXS studies have shown vibronic loss features from the elastic peak that equate with molecular oxygen,[53] meanwhile the rest of the loss-feature structure has components consistent with peroxide.[58,61] The origin of these features remains debated due to the absence of theoretical models adequately simulating the observed spectral signatures or conclusive structural probes confirming the assignments.

Various recent reports have shown that classical layered oxides do display similar spectroscopic "oxygen redox" signatures in O K-edge RIXS as observed universally in the Li-excess layered oxides (Fig. 4).[62–64] The emergences of the RIXS oxygen redox features at high states of delithiation (x_{Li} > 70%) coincide with increased degradation associated with the lattice collapse due to TM-O rehybridization in the layered oxides.[62,65] This suggests that (1) a similar underlying mechanism may exist for both systems and (2) oxygen redox may be related to electrolyte oxidation and increased degradation at the cathode–electrolyte interface. Interestingly, oxygen redox does not seem to result in bulk degradation issues, and as such, lessons on suppressing degradation in conventional layered oxides may translate to lithium rich materials. For example, optimized Li-excess NMC materials are presently able to deliver reversible capacities close to 320 mA h/g with over 90% Coulombic efficiency in the first cycle at room temperature with no obvious capacity decay after hundreds of cycles.[66] It is noteworthy that 450 Wh/kg specific energy at the cell level has been already demonstrated for Li-excess materials using 5 Ah pouch cells.[67] These results suggest that the bulk oxygen redox can be reversibly maintained through a combination of composition tuning, surface protection, electrolyte choice, and other engineering strategies.

C. High voltage through spinel materials

As discussed, the demand for high-energy density lithium-ion batteries has driven cathode research toward developing materials with increasing storage capacity (>200 mA h g^{-1}) and operating voltage (>4.0 V vs Li^+/Li). High-voltage spinel materials, with general formula $LiMn_{2-x}M_xO_4$ (M = Co, Cr, Fe, Cu, and Ni), have emerged as promising materials to meet future energy density requirements due to their high working voltages around 5 V vs Li^+/Li.[68] Among these, the $LiNi_{0.5}Mn_{1.5}O_4$ (LNMO) spinel has shown great promise owing to its high energy density (650 Wh kg^{-1}) provided by the two-electron $Ni^{2+/4+}$ redox couple operating at high voltage (≈4.7 V vs Li^+/Li), superior rate capability, and thermal stability.[69] Furthermore, LNMO offers a Co-free and, therefore, safe, cost-effective, and sustainable alternative to $LiCoO_2$ and NMC-type commercial materials, which provide lower energy densities (518 and 576 Wh kg^{-1}, respectively).

LNMO can crystallize into two cubic structures: the ordered ($P4_332$ space group) and disordered (Fd-3m space group) phases that differ on the site location of the Ni^{2+} and Mn^{4+} ions within the crystal lattice [Fig. 5(a)].[70] The disordered phase is obtained at temperatures above 700 °C, causing oxygen loss and the reduction of Mn^{4+} to Mn^{3+} ions, leading to a random distribution of the Ni and Mn cations over the 16d sites. Such oxygen vacancies also encourage the formation of a secondary rock salt phase ($Li_{1-x}Ni_xO$) resulting in the presence of both this nickel rich impurity and Mn^{3+} ions in samples that are fast cooled from 900 °C. Slow cooling,

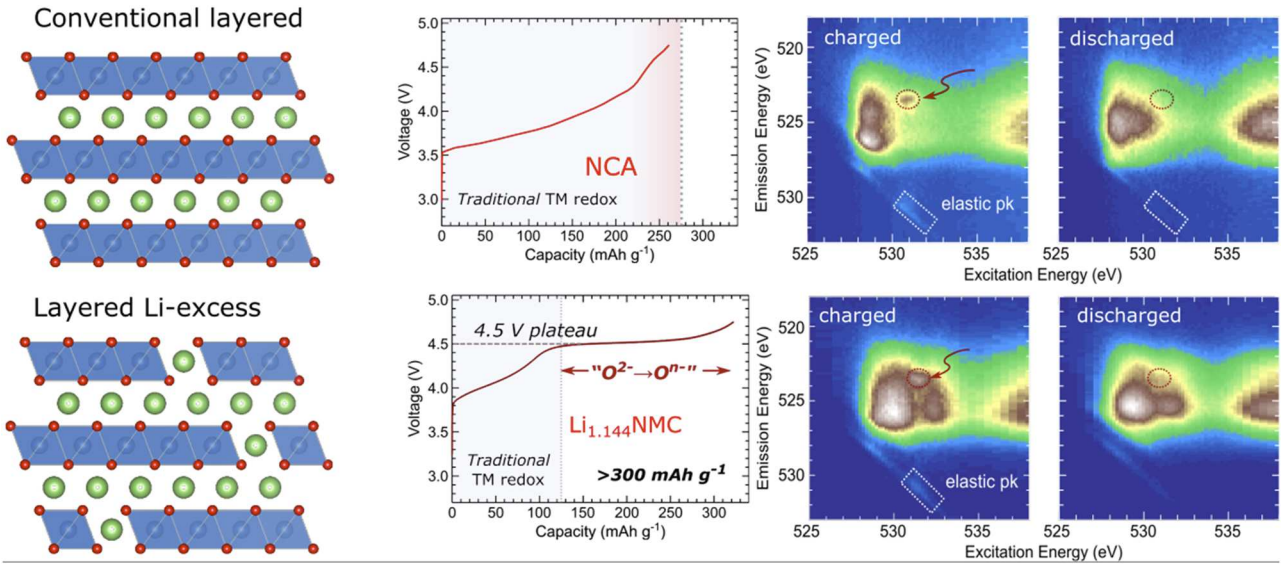

FIG. 4. Charge profile and RIXS features observed in the first cycle for a conventional layered transition metal oxide (top) and for a lithium rich layered NMC material (bottom). Adapted with permission from Lebens-Higgins *et al.*, Mater. Horiz. **6**, 2112 (2019). Copyright 2019 The Royal Society of Chemistry under Creative Commons Attribution CC BY 3.0 and reproduced with permission from Lebens-Higgins *et al.*, J. Phys. Chem. C **123**, 13201 (2019). Copyright 2019 American Chemical Society.

on the other hand, can effectively allow the dissolution of the rock salt phase. Such cooling is insufficient, however, for instigating long-range order, in which the Ni^{2+} and Mn^{4+} ions occupy the 4a and 12d sites, respectively. For such conversion, long annealing, at temperatures between 600 and 700 °C, is required.[71]

Clarity as to how ordering affects the electrochemical performance is not offered within the literature, with contrasting opinions presented throughout. The presence of increased impurity phase within disordered samples, compared to ordered samples, makes attributing any changes in performance to differences in long-range order difficult.[71] The disordering of the Ni^{2+}/Mn^{4+} ions and the presence of oxygen vacancies (and Mn^{3+} ions) often result in superior performance compared to the ordered phase in terms of cyclability and rate performance.[72] The enhanced cycling stability is attributed to a reduction in lattice strain of the (de)lithiated products, leading to a more solid-solution-like behavior [Fig. 5(b)], whereas the oxygen vacancies and Mn^{3+} ions are responsible for the improved Li-ion and electron mobility.[71] Micrometer-sized, ordered LNMO particles have shown impressive cyclability and high rate capability, suggesting that long-range ordering may not be a limiting factor.[73] The neutron pair distribution function (PDF) has shown identical local environments in both ordered ($P4_332$) and disordered (Fd-3m) LNMO samples below 5 Å and a *partially* ordered region up to 16 Å for the disordered LNMO sample, demonstrating that the disordered sample is comprised of Ni/Mn ordered and semi-ordered nano-domains. It is therefore suggested that the long-range order

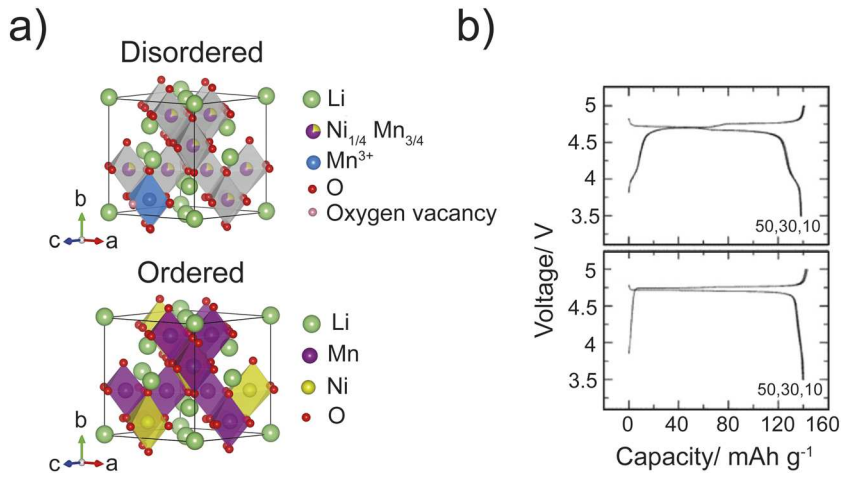

FIG. 5. (a) Schematic structures of ordered and disordered LNMO materials. (b) Charge/discharge curves of disordered (top) and ordered (bottom) LNMO at C/7 (20 mA g^{-1}). (b) is reprinted with permission from Kim *et al.*, Chem. Mater. **16**, 906 (2004). Copyright 2004 American Chemical Society.

may not have such a profound effect on the electrochemical performance, but instead the ordered domain size and boundaries may be more influential.[74]

Despite its great promise, there are still critical barriers to overcome for the commercialization of LNMO materials, including synthetic challenges, bulk and surface instabilities at high states of charge, and the absence of compatible high-voltage electrolytes. All these factors contribute to the reduced initial Coulombic efficiency, capacity decay, and subsequently increased cell impedance, especially at moderate temperatures and when used in full-cells with a graphite anode.

Spinel-type materials suffer from bulk and surface instabilities at high charge states, where their full capacity is attained. Here, competing reactions involving electrolyte decomposition of both solvent and salt take place. This occurs due to the anodic instability of commercial carbonate-based electrolytes above 4.5 V vs Li^+/Li.[75] The inorganic $LiPF_6$ salt decomposes into PF_5 and LiF, with the former further reacting with traces of water to form HF and POF_3 species.[76] On the other hand, the organic carbonate-based solvent reacts at the surface of LNMO to form a variety of organic compounds, e.g., species with carbonyl groups, oligomers, and alkyl carbonates.[77]

The oxidative decomposition of the electrolyte has shown to corrode the cell components[78] and, more importantly, leads to the rapid self-discharge of LNMO by inserting Li^+ ions from the electrolyte into the structure while reducing Mn^{4+} and Ni^{3+}/Ni^{4+} ions.[79] Subsequently, disproportionation reactions of type 2 $Mn^{3+} \rightarrow Mn^{4+} + Mn^{2+}$ occur, leading to the formation (and posterior dissolution) of Mn^{2+} ions.[80] This degradation mechanism is well known for $LiMn_2O_4$ cathodes[81] and in LNMOs is particularly critical in full-cells, given the limited Li supply.[82] Dissolved Mn^{2+} ions not only translate into active material loss but also trigger the migration of Mn ions into empty tetrahedral Li sites at high states of charge to form the Mn_3O_4 spinel phase on the surface of LNMO, which is also soluble in the electrolyte.[83] Furthermore, transition metal (TM) migration to empty octahedral sites at subsurface regions leads to the formation of rock salt-like structures with subsequent oxygen evolution (Fig. 6).[83]

O_2, together with CO and CO_2 evolved from the decomposition of the organic solvent,[77] contributes to the swelling and ultimate failure of the cell.[84] Additionally, CO_2 can be reduced at the anode by reacting with Li to form Li_2CO_3, aggravating the capacity decay.[85] TM dissolution occurs independent of the Ni/Mn site order, and it is highly dependent on several factors, such as temperature, storage time, and state of charge.[80] Ni and Mn dissolution leads to the formation of LiF, MnF_2, NiF_2, and polymerized species on the cathode surface, increasing the cell impedance.[80] At the anode surface, on the other hand, dissolved Mn and Ni ions are reduced to form Mn and Ni particles while obstructing the diffusion of Li^+ ions into the structure, promoting the formation of a thick solid-electrolyte interface (SEI) layer.[80]

Finally, optimization of the synthesis methodology by controlling the level of Ni/Mn disorder and the amount of redox-inactive rock salt $Li_xNi_{1-x}O$-like impurity is necessary, given their strong correlation with the electrochemical performance.[86]

Advances related to bulk and surface structure control and electrode/electrolyte stabilization are needed for high-voltage spinels to expand their presence in the lithium-ion battery market. Numerous

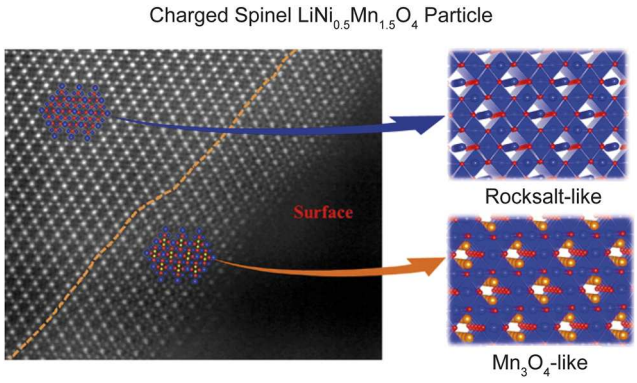

FIG. 6. Schematic representation showing the structural complexity of LNMO. HRTEM studies show that during cycling between 3.5 and 4.9 V, a Mn_3O_4-like phase forms on the surface of LNMO together with a rock salt-like phase on the subsurface. Reprinted with permission from Lin *et al.*, Chem. Mater. **27**, 292 (2014). Copyright 2014 American Chemical Society.

reports have been published on the use of doping strategies to improve the electrochemical performance of LNMO.[87,88] Elemental doping effectively solves the formation of rock salt phases during synthesis, improving the overall cycling performance.[88] Furthermore, the site location of these dopants has a direct effect on the properties of LNMO. For example, dopants located on the Li 8a site, such as Na^+[89] and Ti^{4+},[90] improve the charge transfer and, more importantly, alleviate the problem on TM dissolution. On the other hand, dopants on the 16d octahedral sites, such as Fe^{3+}, Cr^{3+}, Co^{3+}, Al^{3+}, Cu^{2+}, and Mg^{2+}, enhance the electronic conductivity as well as thermal and structural stability of LNMO.[88,91] Oxygen substitution with more electronegative anions, e.g., F^- ions, has been shown to minimize TM dissolution during cycling due to structure stabilization.[92]

The modification of the surface properties in LNMO has been shown to also stabilize the LNMO/electrolyte interface. Several works have described the importance of surface orientation, showing strict correlation between this parameter and the electrochemical performance observed in the LNMO particles studied.[93] Furthermore, surface-doping has been claimed to be more effective than bulk-doping to alleviate TM dissolution. In $LiNi_{0.5}Mn_{1.2}Ti_{0.3}O_4$, the formation of a titanium–oxygen-enriched cathode–electrolyte interface (CEI) layer plays an important role in stabilizing the surface of LNMO.[94] Surface coatings may also provide a more stable electrode/electrolyte interface by minimizing TM dissolution, electrolyte oxidation, and other side reactions. These include the following: (1) electronic-conductive coatings, which improve the charge-transfer kinetics of LNMO, particularly at high rates (e.g., carbon coatings and[95] polymer coatings);[96] (2) ionic-conductive coatings that allow for superior Li^+ ion diffusion through the use of Li^+ ion conductive materials (e.g., Li_3PO_4,[97] $Li_4P_2O_7$,[98] and Li_2SO_3,[99]); and (3) acid-protective coatings that aim to defend against HF corrosion of the LNMO cathode (e.g., SiO_2,[100] TiO_2,[90] and Al_2O_3).[101] Hybrid coatings provide a combination of the aforementioned advantages. For example, Li_3PO_4–TiO_2 shows the hybridization of an ionic- and electronic-conductive coating, providing enhanced ionic and electronic conduction as well as minimizing TM dissolution.[102]

Aside from the optimization of LNMO materials and their interface, a major leap forward in this technology will occur after developing suitable and safe electrolyte formulations with high anodic stability that form a stable SEI layer on the anode. To date, literature reports have focused on modifying the current state-of-the-art electrolytes by adding additives[103] or sacrificial salts[104] that provide a stable CEI layer by becoming oxidized at the cathode surface prior to the electrolyte. Furthermore, novel liquid solvents, such as ionic liquids,[79] sulfone-[105] and nitrile-based electrolytes,[106] and solid-electrolytes,[107] have been considered. Concentrated electrolytes, such as concentrated LiFSA/carbonate ester mixtures,[108] are gaining attention due to their unique solvation chemistry in which anions take precedence over solvent molecules. This allows greater flexibility in solvent choice, opening possibilities for solvents previously disregarded. Nevertheless, these electrolytes are still far from providing LNMO with optimal battery performance and, thus, require further refining.[109]

Concluding remarks

High-voltage spinels are a promising high-energy density cathode alternative to be used in future EVs and hybrid EVs. To date, the lack of in-depth studies on high-voltage advanced electrolytes has driven research toward solving issues related to the stabilization of the cathode (bulk and surface) and electrolyte as well as their interphase. These issues directly compromise the long-term cycling performance of LNMO/graphite full-cells at moderate temperatures (i.e., in "real" conditions), preventing their use in future applications.

Multiple strategies such as elemental substitution, surface engineering, and the use of electrolyte additives, among others, have proved successful in improving the cycling stability in full-cells. It is anticipated that a combination of these strategies will lead to further improvement in performance. Furthermore, a better understanding of the surface degradation reactions and their dependence on the cathode and the anode choice must be sought to minimize capacity decay. Finally, corrosion of cell components and their effects on electrochemical performance represent an understudied research area that will require further attention.

D. High capacity through disordered rock salts

Disordered rock salt (DRX) materials have only relatively recently been considered as potential cathodes. They offer the possibility of significant increases in capacity (>300 mA h g^{-1}), operation at high voltages, and high energy densities up to 1000 Wh kg^{-1}.[110] Their structures have a disordered arrangement of Li and transition metal atoms on the same cation sites within a cubic α-$LiFeO_2$ structure. Many studies on ordered layered rock salt materials followed the commercial introduction of $LiCoO_2$, with particular attention to the factors that control Li diffusion kinetics.[111,112] The energy barriers for Li hopping increased significantly in the presence of disorder and, including the effects of channel blocking, lead to loss of performance and reduced cyclability. However, a report of high specific capacity, 253 mA h g^{-1}, combined with good cyclability in the disordered rock salt Li_2VO_3,[113] led to a re-examination of the effects of cation disorder. Similarly, $Li_{1.211}Mo_{0.467}Cr_{0.3}O_2$, has shown good reversible cycling behavior, providing 265 mA h g^{-1} capacity, despite transforming to an apparently disordered rock salt after ten cycles. The broad accessibility and compositional variability of these materials is typified by the cation-disordered rock salts, $Li_{1.3}Nb_{0.3}M_{0.4}O_2$ (M = Mn, Fe, Co and Ni), which showed facile Li migration through a percolation network and large reversible capacity.[114]

When looking at the development of DRX materials, the abundance, broad geographical availability, and low cost of manganese make Mn-based disordered rock salts highly attractive targets as cathode materials. Their high capacity originates from a combination of both cation and anion redox contributions. In disordered $Li_4Mn_2O_5$ for instance, the initial capacity of 355 mA h g^{-1} is far higher than the theoretical capacity from the transition metal redox contribution alone, which would be 245 mA h g^{-1} (Mn^{3+}/Mn^{4+} and Mn^{4+}/Mn^{5+}). As with the Li-rich systems discussed earlier, x-ray absorption spectroscopy (XAS) and resonant inelastic x-ray scattering (RIXS) measurements have demonstrated the significant oxygen redox contribution of these materials.[115–118] The activation of oxygen redox presents both an opportunity and a challenge. Established materials such as $LiCoO_2$ and $LiFePO_4$ operate with localized oxidation of Co^{3+} and Fe^{2+}, respectively, to accompany de-intercalation of Li^+. In these classic examples, the role of the oxide or phosphate sublattice is to provide a passive framework that largely retains the Li^+ sites as vacancies that are well-matched for Li^+ re-insertion during battery cycling. Although, as noted above, oxygen involvement has been observed at high states of charge in such classical systems as well,[64] the presence of oxide redox enhances capacity but at the cost of activating the chemical reactivity of oxide ions. Many of the challenges, and opportunities, associated with disordered rock salts arise from understanding, limiting, and controlling the oxygen redox contribution.

Inducing cation disorder within a material can pose significant experimental challenges. One approach, high energy ball milling, can transform ordered monoclinic Li_2MnO_3 into a disordered rock salt structure [Fig. 7(a)] that shows a reversible capacity of 250 mA h g^{-1} at 3 V [Fig. 7(b)].[119] The nature of the disorder continues to attract scrutiny, and recent reports showed that, although the average structure of nanosized Li_2MnO_3 is cubic, the local structure is composed of short-range ordered layers.[120] The short range ordering in these materials has a deleterious impact on the performance of the cathode; mitigation approaches include attention to material compositional design as well as an improved synthetic pathway.[117,121]

There appear to be at least three routes to the synthesis of disordered rock salt structures. The first is via ball milling ordered structures of the same composition, such as has been achieved with Li_2MnO_3. The second is by rapid quenching from above the temperature of a possible order–disorder transition so as to preserve the disordered material at ambient temperature, as achieved with $Li_{1.25}Nb_{0.25}Mn_{0.5}O_2$.[121] The third uses mechanochemical synthesis in which, following Ostwald's law of successive reactions, the first product is frequently entropy-stabilized and either fully or partially disordered but metastable; the kinetic stability of the product is obviously essential to its usefulness. This method offers great scope for compositional tuning to optimize properties while keeping a watchful eye on product stability. The choice of milling media is important. The use of tungsten carbide and stabilized zirconia media appears to avoid problems of Fe contamination associated

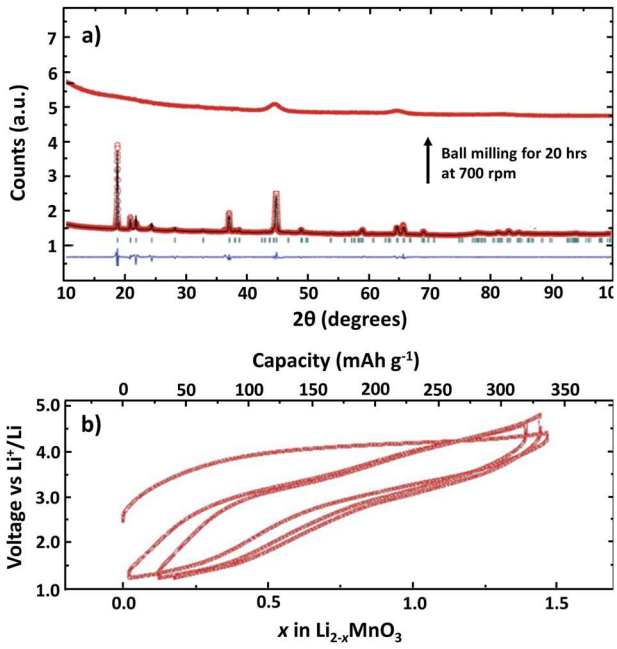

FIG. 7. (a) The powder x-ray diffraction pattern obtained for Li_2MnO_3 as prepared by the solid state reaction after 20 h of highly energetic ball milling. (b) Galvanostatic charge/discharge data obtained for Li_2MnO_3 at a rate of 1 Li^+ per formula unit in 20 hours (11.5 mA h g^{-1}) cycling to 4.4, 4.6, and 4.8 V on the first three cycles. Reproduced with permission from Freire *et al.*, J. Mater. Chem. A **5**, 21898 (2017). Copyright 2017 The Royal Society of Chemistry under Creative Commons Attribution CC BY 4.0.

with steel media; control of atmosphere within closed jars permits control of oxidation states; and milling time may be important, given the relative reactivities of the reagents and the metastability of the products.

To achieve both high capacity and high cycling stability, it is necessary to activate the oxygen redox but limit the scope for further oxidation to form molecular O_2, which can escape the lattice, leading to irreversibility and loss of capacity. Considered at the battery level, O_2 loss presents the risk of gas evolution with the associated mechanical, containment, and safety problems.

The apparent stabilization of disordered rock salt structures by d^0 transition metal cations may be due to their ability to accommodate large octahedral distortions with a low energy cost due to the absence of crystal field splitting energy. The presence of d^0 elements in the structure has been proposed to minimize oxygen redox processes, and a large majority of disordered rock salts reported to date contain d^0 dopants, most commonly, Ti^{4+}, V^{5+}, Nb^{5+}, and Mo^{6+}.[110] A possible cause of enhanced cycling stability comes from the ability of the d^0 cations to coordinate various partially oxidized oxygen anions. The examination of the related compositions $Li_{4+x}Ni_{1-x}WO_6$ showed that the presence of reversible oxygen redox was facilitated by the coordination of the peroxo species $(O_2)^{2-}$ to the W^{6+}, d^0 cation.[122]

The substitution of Mn by various transition metals has been screened using density functional theory (DFT).[123] From the results, niobium was selected as the best dopant giving superior properties compared to those with 3d dopants. The authors successfully prepared phase-pure $Li_{1.95}Mn_{0.95}Nb_{0.05}O_3$ and demonstrated that Nb doping increased the reversible capacity while also impeding decay of the discharge potential.

A major challenge is to find suitable preparative routes to deliver materials that combine reversible oxygen redox and associated additional capacity compared with that obtained from Mn redox activity alone. As a note of caution, high capacity has been observed where the introduction of excess lithium led to the formation of a composite whose high capacity was delivered by the presence of Li_2O, trapped in vacancy clusters on the cathode surface.[124] Such extrinsic capacity may be useful, but careful characterization is vital to avoid pitfalls of mis-assigning capacity to targeted phases where an impurity or undetected secondary phase is responsible.

One route to combine oxygen and transition metal redox is to manipulate the latter via judicious doping of the anion lattice. Li_2VO_2F prepared by ball milling shows that the disordered oxyfluoride can deliver a higher capacity than the analogous oxide Li_2VO_3.[125] Significantly, the lithium content and fluorine content of the DRX structure should not be considered in isolation.[126]

The complexities and open questions that remain over redox active oxygen have been outlined in relation to lithium excess systems in Sec. III B, what is clear, particularly in relation to the disordered rock salt structures, are the high reversible capacities that may be achieved and the new opportunities that exist to build on these discoveries. A better understanding is needed of the compositional or structural parameters that favor oxygen redox, whether the holes that are generated on charging are small polarons located on either individual oxygens, short chain catenated peroxo species, or large polarons associated with transition metal *d*–oxygen 2p hybridized orbitals and band structure. The need to limit oxidation to one electron per oxide ion is essential.

Control of transition metal oxidation states by aliovalent cation doping is a very well-established doping strategy. Aliovalent anion doping, with replacement of O^{2-} by $halide^-$ or N^{3-} ions, is much less well investigated but has already achieved considerable success, as shown by the synthesis of Li_2MnO_2F, and has much scope for further development.

The role of disorder in structures is complex with highly disordered phases showing unexpected high Li^+ conductivity and high capacity. Further, by careful choice of material processing conditions, it is possible to control both the size of the disordered rock salt particles and the domain size of ordered regions within the rock salt sublattice. The role of simulation and experimental probes below the Bragg diffraction limit [total scattering PDF analysis, nuclear magnetic resonance (NMR), extended x-ray absorption fine structure (EXAFS), and simulation] is essential for an improved understanding of the effect of these different length scales on the resulting electrochemical properties.

Concluding remarks

The capacity of disordered rock salts can greatly exceed that of current commercial cathodes. The potential capacity of 460 mA h g^{-1}, realized in Li_2VO_2F, offers the promise of energy densities exceeding 1000 mA h g^{-1} that could double the energy stored in commercial batteries.[96] Achieving this performance safely over the lifetime of a commercially viable battery is the key

challenge, and kinetically limiting the oxygen redox is likely to be an important strategy in addition to thermodynamic control. Significant opportunities for improvement are provided by the range of cation and anion dopants that can be introduced into the structure. In addition to using the classic solid state approach of adding aliovalent cation dopants to manipulate charge balance, it is also necessary to incorporate knowledge from coordination chemistry to consider bonding to partially oxidized oxygen species and help stabilize oxygen redox.[122] Many of the above factors attest to the importance of both cation and anion disorder within the rock salt crystal structure. We are fortunate that these discoveries are proceeding in tandem with major advances in our understanding of local structure through advanced experimental techniques and modeling capabilities.

E. Sustainable alternative chemistries

Committing to sustainability, the requirements for current cathode research extend beyond the development of cheaper, lighter, and safer cathodes with superior electrochemical performance. Important aspects such as low-energy synthesis routes and the use of earth-abundant, non-toxic, and recyclable materials are increasingly coming into focus.

The $LiCoO_2$/C cell technology still provides the backbone of cathode research; however, due to the issues implied with this system, the emphasis of recent efforts has been on non-traditional electrode materials complying with sustainability demands. Notably, compounds displaying reaction mechanisms that diverge from conventional intercalation-based cathodes that exclusively rely on the electrochemistry of their redox-active TM cation centers, e.g., the redox couple Co^{3+}/Co^{4+} in LCO, have attracted attention. The additional utilization of anion redox mechanisms in cathode materials provides higher capacities, given that more Li can be removed and inserted per formula unit of the cathode material. Here, the anions (mostly oxygen) also participate in redox processes by forming dimers of the anion species like the oxo- (O^{2-}) to peroxo-like $(O_2)^{n-}$ transformation observed in Li_2IrO_3 or in $Li_2Ru_{1-x}Sn_xO_3$ or the (S^{2-}) oxidation to $(S_2)^{2-}$ in Li_2FeS_2 upon cycling.[51,127–131]

Compounds that exhibit reversible conversion reactions with lithium have also been considered as another interesting alternative, offering higher theoretical capacities than intercalation-based systems. Unlike intercalation, conversion based lithiation/delithiation involves complete structural disintegration and rearrangement, passes through several intermediate phases, and can be expressed as $TM_xX_y + zLi \rightleftarrows xTM^0 + yLi_{(z/y)}X$ or $zLi + X \rightleftarrows Li_zX$, where Li is lithium, TM is the transition metal, and X is the anionic species.[132,133] Transition metal fluorides are regarded as the most promising conversion materials as they offer good operating voltages, e.g., 3.55 V vs Li/Li^+ in CuF_2, and high gravimetric capacity as found for FeF_3 (712 mA h g^{-1}).[134,135] Lithium–chalcogen reactions are also considered as conversion systems and can be described as $zLi + X \rightleftarrows Li_zX$. Based on naturally abundant, low-cost, and environmentally benign resources, LiS and LiO_2 with their high theoretical capacities (1166 and 1168 mA h g^{-1}) and potentials (2.28 and 2.96 V vs Li/Li^+) are the most promising candidates for chalcogen-based conversion cathodes.[136,137] Recently, another material class showed conversion-type electrochemical reactions with lithium. Transition metal carbodiimides, such as FeNCN, show good cycling properties and excellent capacity retention.[138,139] These promising materials and concepts display the potential that arises through the expansion of the chemical systems under investigation and going beyond traditional cathode chemistry.

As promising as these new cathode systems seem, they still have some challenges to overcome to be considered suitable to industry. These materials have to meet many demands: hinging on redox-active elements with high elemental abundance, offering high performance, good cyclability, low cost, and low volume expansion, and their synthesis should be scalable and, at best, environmentally friendly.

A major challenge of oxide-based electrode materials utilizing anionic redox is the loss of oxygen from the structure at high potentials caused by the irreversible formation of O_2, as with the lithium rich and DRX materials described previously. The evolution of the volatile component leads to structural degradation of the cathode, electrolyte oxidation, and can cause a thermal runaway and the release of toxic and flammable compounds.[140–142] In the case of sulfide cathode materials, the anionic redox is more reversible but as a trade-off limits the voltage.[143]

Conversion processes with materials such as FeF_3 and CuF_2 can offer vast capacities; however, their reactions involve complete structural disintegration and rearrangement during cycling, which can result in volume changes and active material loss through incomplete conversion reactions. While metal halogen bonding in metal halide cathodes enables the significant increase in the working potential, the ionicity of these bonds results in poor electrical conductivity.[13,144,145]

An in-depth understanding of the challenges present in these different systems, and optimizing methods to overcome these, is fundamental to the design of new cathode materials. The steps involved between the theoretical concept, synthetic realization, and optimization at a lab scale and routes toward its industrial implementation are vast and complex as represented within this work and in the scale of the wider field.

With an idea of how the desired product should look like, the realization may involve sophisticated multistep-approaches to yield the desired structure or control the oxidation state of specific elements. For example, the layered modification of $LiMnO_2$ could not be obtained by direct synthesis routes, but it was possible by a cation-exchange reaction in previously synthesized layered $NaMnO_2$.[146]

When moving from research stage studies to considerations of introducing new compounds as cathodes, the cost and abundance of the raw materials and the feasibility of scale-up play an important role. In addition, the geopolitical concentration of elements is not to be neglected, especially if there is a global dependence on the supply from one or a few countries. Conventional cobalt containing cathodes suffer from comparably low abundance, high costs, and the reliance on supplies from the Democratic Republic of Congo associated with the element. Recycling is unlikely to provide significant short-term supply, hence fostering the search for and in-depth investigations of Co-free alternatives. On the other hand, the supply of the inexpensive elements, including Fe, Mn, Ni, O, F, and S, can meet the future demands; thus, cathodes mainly consisting of such abundant elements are coming increasingly into focus.[147,148]

Research-laboratory synthesis usually yields materials in small quantities and with minimal restrictions in terms of synthetic methods. Due to the possible variability in the compounds when prepared in large batches, morphological optimization are crucial considerations as even the most promising material cannot be used commercially if high-volume manufacturing is not possible or too costly. This relates directly to the $/kWh metric examined earlier.

Structural degradation is an issue that all electrode materials face over time. However, with studies that reveal its causes and provide new insights into why some materials exhibit superior structural integrity and reversibility, the first life performance of electrode materials is continually improving.

Great advances have been achieved to overcome the irreversible O_2 release after anion redox when the battery is operating at the desired high voltages. As indicated with the DRX materials, stabilization of the oxide can be achieved by suppressing the anion-transition metal charge transfer by adding d^0 elements in the cation sublattice (i.e., Ti^{4+}, Nb^{5+}, or Ta^{5+}) or the substitution of O^{2-} by F^- within the anion sublattice.[149,150] Furthermore, there is evidence that the different intermediate oxygen species, such as the peroxides and superoxides, are stabilized at high voltages without O_2 evolution in some 4d and 5d transition metal oxides.[128,129,131] Such results are encouraging when looking to exploit anion redox processes. However, the cost and additional mass of 4d and 5d elements make them unattractive as the main components in a cathode material. Mixed anion systems are also highly suited to stabilize the anionic redox and maintain high working potentials. Oxysulfides, such as the anti-perovskite material Li_2FeSO, show promising behavior. In this material, Fe shows redox activity at low states of charge, whereas at higher states of charge, the sulfur is responsible for the redox reaction, with oxygen remaining as O^{2-} during cycling.[151–153] Even if this class of material exhibit lower voltages than pure oxide-based cathodes, the advantage of such low-cost and environmentally friendly compounds offering longer life spans of batteries cannot be ignored.

The high energy consumption that is often associated with the preparation of current state-of-the-art cathode materials is another main issue that cannot be neglected, especially when thinking about the additional demand associated with conversion from conventional fuels to electric vehicles. Using low-temperature processes, such as hydrothermal synthesis and multistep approaches like ion-exchange, can open the doors to a more sustainable era. Beyond that, the use of multistep synthesis can give us access to an assorted range of new materials even out of the thermodynamic equilibrium with a tailored control of the crystal and electronic structure. For instance, within the $LiFeO_2$ composition, topochemical manipulation triggers the formation of metastable structures with an enhanced cyclability in comparison with the most stable disordered material obtained by the conventional ceramic route.[154,155] Aside from the crystal structure tailoring, topochemical methods allow transition metal oxidation states to be controlled, which could be a promising tool for the next generation of cathodes. In particular, avant-garde post-synthetic topotactical reduction processes could put novel redox pairs into play by stabilizing unusual low oxidation states such as Ni^+ in $LaNiO_2$ to tune the corresponding electrochemical window.[156] These developments also contribute to the realization of the scale-up of materials that could not be obtained cost effectively and in a high volume so far, making them more commercially attractive.

Precise manipulation of the materials offered by these novel approaches can also be complemented by the multiple possibilities of additional computational input. *Ab initio* calculations can support synthetic approaches by identifying new stable compositions and predicting their crystal structure, as detailed in Sec. III F.

Concluding remarks

The exploration of alternative cathode chemistries offers major benefits going beyond sustainability and lowering the production cost. By expanding the field of material classes considered as potential electrode materials, we see and learn from unique features in their (de)lithiation processes that occur during battery cycling. These insights, which can be supported by additional computational input, can finally guide the development of better cathode materials in general. As we move away from traditional battery materials, however, we recognize the need to make advances in the synthetic approaches used, as the preparation of such materials is often challenging, and structural optimization is required to fully exploit the potential of these structures.

F. Searching for new materials through crystal structure prediction

The elemental composition of cathodes is critical to the overall performance of lithium-ion batteries (LIBs). The history of cathode development shows that advances in performance have been fueled by the experimental discovery of new materials or material systems.[157] There are many possible selection criteria for cathode materials. Key among them are the energy density, reliant on the amount of Li available for cycling and the average working voltage, and the rate capability, which is limited by the Li diffusion barrier within the material. The widespread utilization of first-principles methods, in particular, density functional theory (DFT) calculations,[158] combined with ever-increasing computing power has allowed computational chemists to study these systems at the atomistic level and give an accurate explanation of the mechanisms behind the performance-critical processes, such as charge transfer, lithium diffusion, and phase transition. In a complementary manner, the atomic structure of the underlying material is an essential input for computational studies, which are typically obtained experimentally via characterization techniques, such as powder x-ray/neutron diffraction, and electron microscopy. This is, of course, only possible if the materials have already been synthesized.

Methods of first-principles crystal structure prediction have been developed to allow prediction of the structure of unknown materials with little or no experimental data. They have been applied to a wide range of fields[159] but represent a virtually untouched frontier for cathode materials. A few studies successfully reproduced experimentally known phases of cathode materials.[160,161] We have excluded the discussion of the screening approach based on existing databases and the relevant species-substitution approaches[162] as they are interpolative and dependent on the underlying databases and therefore bias toward currently known phases. This limits their applicability in unexplored regions of the composition and phase space. In fact, despite the success of applying DFT to assist the understanding of cathode chemistries, e.g., anion redox, successful cases of identifying new cathodes from computation has been limited. This is partially because of the limited compositional and structural space are examined.

Structure prediction is typically based on basin/minima hopping,[163,164] genetic algorithms,[165] particles swarm optimization,[166] and random searching,[167,168] with the last being our choice for the FutureCat project. The *ab initio* random structure searching (AIRSS) approach[167,168] is a straightforward method that explores the distribution of basins of the potential energy surface (PES) by generating random "sensible" structures based on sound physical and chemical considerations, such as the number density of atoms, species-wise separations, and space group symmetries. Making no attempt to *learn* the PES, the search is insensitive to the precision and accuracy of the underlying energy evaluations (e.g., DFT calculations) and can be trivially parallelized. Symmetries can be exploited to gain further speedups in DFT calculations by several folds, and the reduction in the degrees of freedom will further accelerate the convergence of the local relaxations. Accurate, but costly, calculations, possibly involving high levels of theory, only need to be performed for a small number of selected low-energy structures. In addition, very often it is not only the ground state structure that is of interest but also metastable polymorphs, which are also encountered in the search. The results of exploratory searches can be used to provide guidance for experimental works. In fact, the AIRSS method can be interpreted as a *computational synthesis* of materials in that the generated random structures resemble those at extremely high temperatures, i.e., the atoms are extremely energetic and are well-mixed. Therefore, an AIRSS search is similar to an experimental trial to synthesize a material by quenching (relaxing) it after heating at extremely high temperatures (which results in randomly generated structures), as illustrated in Fig. 8. Given enough trials, one can find a structure that is thermodynamically stable. On the other hand, searching can be tailored based on existing experimental findings and support cases where the atomic structures are only partially resolved.[169] The use of AIRSS for the prediction of novel cathode structures has recently been demonstrated.[170] Specifically, efficient sampling of the PES could be achieved by constraining the interatomic separations, cell volumes, and space group symmetries. The method was successfully benchmarked against a number of known cathode materials, including $LiCoO_2$, $LiFePO_4$, and $Li_xCu_yF_z$, to demonstrate the efficiency. The search was then expanded to novel potential cathode architectures, avoiding expensive transition metals, such as Co. This approach has seeded low energy structures in the family of Li–Fe/Mn oxalates and Li–Fe oxysulfides.[170,171]

Transition metal (TM) intercalation cathodes typically contain three or more elements: Li, TM ions, and anions, and there can be four or more elements for polyanion-based materials as well as those with mixed cation/anions. The complexity of the PES increases with the number of elements under consideration. Magnetism, originating from the transition metal ions, also poses additional challenges as the degrees of freedom in spin induce additional local minima on the PES. Unlike atomic positions, the electronic spins are not fully controllable in the calculations. Hence, the PES can be ill-defined, as multiple solutions of the electronic structure become possible for a given structure. Fortunately, it may be sensible to decouple the spin and positions, since quite often the energy differences between various spin configurations are relatively small. Standard DFT calculations usually give poor descriptions of transition metals due to the self-interaction error associated with localized electrons. A popular approach to address this is to apply the +U correction,[172] but it should be noted that the value of the U has to be chosen carefully. An alternative approach is to use hybrid functionals such as HSE06;[173] however, this leads to orders of magnitude increases in the computational cost.

Another shortcoming of crystal structure prediction is that, as the name suggests, it only considers crystalline solutions. The existence of a periodic solution does not always mean the material will be crystalline. On the other hand, a random search does produce disordered-like structures at higher energies, although the unit cells are relatively small. In reality, many cathode materials exhibit certain degrees of site-occupancy disordering, such as the disordered rock salt materials.[110] The ensemble of the produced structures may give clues about the ordered/disordered nature of the target material. The role of disorder in cathode structures is examined in detail in Sec. V B.

The vast size of the chemical space poses another challenge for discovering new cathode materials. The number of possible compositions increases combinatorially with the increasing number

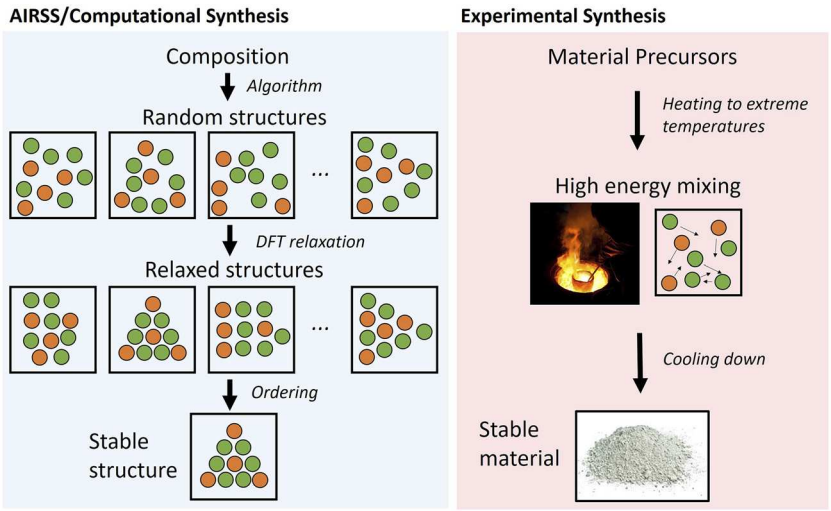

FIG. 8. Comparison between an AIRSS search of a composition and an experimental synthesis of a material.

of elements, and the computational and time cost for an exhaustive exploration quickly becomes prohibitively high.[174] It is often necessary to limit the search space based on expected oxidation states, theoretical cycle capacity, and cost of the raw materials. Constructing pseudobinary/pseudoternary systems can be a viable option to mitigate the *curse of dimensionality*. Choosing the right system to explore is crucial, and selecting such systems remains reliant on the domain knowledge of the researchers.

Obtaining the crystal structure is just the first step toward a comprehensive understanding of a material. There is also a lack of accurate descriptors for cathode performance purely based on atomistic models. For example, the real energy density of a cathode depends on the number of Li that can *reversibly be removed* (per f.u.) and its corresponding voltage. Such a value is relevant not only to the oxidation states of the TM ions but also to the structural stability after the Li atoms have been removed, which is difficult to capture efficiently using atomistic models. Beyond that, the rate capability of the cathode relies on several factors beyond the Li energy barrier, such as the percolative property of Li diffusion paths, which is not easy to quantify accurately.

Recent progress in a range of materials research communities can be utilized to help meet the challenge of predicting novel cathode materials. For instance, the development of better exchange–correlation functionals improves the accuracy of DFT calculations.[175,176] While density functional theory is still the go-to method for atomic-level predictive modeling, it suffers from its inherent cubic scaling nature. Methods of constructing interatomic potentials or forcefields using machine learning have been developed to tackle this problem.[177,178] Using first-principles calculations as the training data, these forcefields are capable of achieving the same level of accuracy with orders of magnitude lower computational costs. Pioneering works have demonstrated that the resulting potentials can be used for predicting new crystal structures.[179] Building such potentials from scratch, however, is still not a trivial process, so developing robust and automated fitting workflows could help access these state-of-the-art techniques. The local environment descriptors, originally introduced for these potentials, turned out to be invaluable tools for analyzing a large number of structures routinely generated during structure prediction.[180]

The development of efficient and standardized searching protocols will help improve search efficiency. Since intercalation type cathode materials are predominately ionic, a significant part of the total energy comes from the long-range Coulomb interactions. While classical interatomic potentials may not be transferable enough for predicting entirely new phases, they do capture a significant portion of the underlying interactions. It may be possible to use them for removing structures that are not "sensible" and deemed to end up with high energies.

The success of structure prediction undoubtedly relies on the identification of the promising chemical space to explore in the first space. Existing computational material databases, such as the Materials Project[181] and the Open Quantum Material Database,[182] are useful tools for researchers to quickly identify the explored and underexplored regions, acting as *entry points* for new studies, and providing data to build property-driven machine learning models.[183] The development of simple and physical descriptors, such as site-specific electrostatic energies[184] and specific "structure units,"[185] would also help to tease out the underlying structure–property relationships to provide a fundamental understanding of existing and new cathode systems.

It is also worthwhile to point out the limitations of the crystal structure prediction methods for cathode materials, which is also the direction for future theoretical development in this area. First, as mentioned previously, the composition needs to be defined prior to the search and has a significant impact on its success. Therefore, a suitable approach to determine the best possible composition is needed. Second, the (de)lithiation process during electrochemical cycling is often far from the structural equilibrium for the composition. As such, DFT may not fully capture the properties of the cathode material during cycling. While not an intrinsic flaw in the crystal structure prediction methods, this has an effect on the screening of candidate materials following a structural search. To resolve this challenge, it is important to either develop new computational schemes to capture the charge and discharge properties of a material more accurately or the threshold for success should be loosened to avoid the elimination of suitable candidates for experimental exploration. Finally, it should also be noted that the current methods are limited to the atomic scale. This means that materials with large spatial features cannot be predicted using crystal structure methods, e.g., gradient structure NMC materials such as those covered in Sec. IV A. In this context, multi-scale methods need to be incorporated and coupled to the current approach.

Concluding remarks

The development in structure prediction and first-principles methods has made it possible to discover new materials before they even come into existence. While there are challenges ahead for applying it to cathode materials, the development of new methodologies and technologies from the wider research community will continue to benefit this field. In the near term, the computational cost will remain the bottleneck for scaling up its application in complex materials systems. Search algorithms that are inherently parallel, such as AIRSS, will receive the full benefit of the upcoming transition to "exascale" multi-core massively parallel computing platforms. Identifying promising chemical systems is also crucial for searching to succeed. Crystal structure prediction offers a unique opportunity to dramatically enhance the breadth and rate of materials discovery, providing novel compositions and fundamental understanding to both complement and direct experimental work.

IV. CATHODE MODIFICATION AND OPTIMIZATION STRATEGIES

Nirmalesh N. Anthonisamy, Rebecca Boston, Hugo Bronstein, Serena Cussen, Venkat Daramalla, Michael De Volder, Siân Dutton, Beverley Inkson, Judith MacManus-Driscoll, Debasis Nayak, Alisyn Nedoma, Seungkyu Park, Laura Wheatcroft

A. Enhancing lifetime through gradient and core–shell structures

As previously discussed, there exist numerous cathode materials that display high capacities but for which remaining challenges

exist around structural degradation, thermal instability, and/or reaction with the electrolyte. These processes can lead to capacity fade, often including oxygen evolution at the cathode/electrolyte interface, which has implications for the longevity and safety of the battery. As a first line of defense, surface coatings may be employed to curtail these processes. Such coatings can be applied through simple sol–gel or hydrothermal methods, although it can be challenging to provide conformal coatings via these methods. By comparison, superior ultrathin nano-level coatings can be obtained using state-of-the-art chemical vapor deposition (CVD) and atomic layer deposition (ALD) techniques.[186] Scalability then becomes a challenge to overcome. In light of this, core–shell and concentration-gradient structures have emerged as an efficient alternative in tackling degradation issues.

The choice of synthetic pathway can facilitate the introduction of a core–shell or concentration-gradient arrangement to cathode particles. Co-precipitation of multi-component Ni-rich materials (e.g., NMC811) from solution via a continuous stirred tank reaction (CSTR), for example, affords an approach that combines the necessity of atomic-level mixing of constituent elements with the potential to generate core–shell and concentration-gradient structures due to its potential to fabricate unique highly dense, spherical precursors. Importantly, a CSTR permits large-scale production of cathode materials facilitating material advancement from lab to industry. Hydroxide, carbonate, or oxalate metal precursors can be used, with hydroxides playing a particularly important role in achieving core–shell and concentration-gradient materials. In the case of hydroxides, the solubility product constant (K_{SP}) of $Mn(OH)_2$ is two orders higher than that of $Ni(OH)_2$ and $Co(OH)_2$.[187] Therefore, ammonia is used as a complexing agent to achieve the required atomic distribution of nickel, manganese, and cobalt ions. The pioneering works of Zhou *et al.*[187] and Lee *et al.*[188] have established the growth mechanism of secondary spherical particles in the presence of ammonia as follows: (i) the reaction begins with the metal-ammonia complex formation (ii) of which the ammonia ions are gradually replaced by hydroxide ions via anion-exchange reaction and (iii) then due to coalescence and Ostwald-ripening the primary nanocrystals self-assemble into micrometer-sized spherical hydroxide precursor. The surface free energy reduction is the key driving force that benefits the growth of larger particles at the cost of smaller particles through dissolution and recrystallization.

Core–shell materials are typically designed in such a way that a high-capacity (Ni-rich or Li-rich), less stable material is at the core, with a thermally stable (Mn-rich) material as the shell. The main requirements for a successful core–shell structure are high density, low layer inter-diffusion, good inter-layer adhesion, and compatible rates of expansion/contraction during (de)intercalation. High density of both the core and shell is critical to ensure mechanical stability along with high energy density, as any voids equate to lost active material.[189] The core–shell materials can be broadly classified into two types: (i) pairs with similar crystal structure and chemical composition (layer–layer, spinel–spinel, olivine–olivine, etc.) and (ii) either dissimilar crystal structure or chemical species (layer-spinel, layer-olivine, oxides-phosphates, etc.). An ideal shell material should be versatile enough to overcome those shortcomings of the core including, lattice-oxygen evolution, transition metal dissolution at the surface promoting secondary phase formation, and impedance growth at the interface in a fully de-lithiated state. Therefore, the choice of shell material largely depends on the type of challenges one wishes to address with the core material.

For example, in 2005, Sun *et al.* demonstrated that the thermal stability of Ni-rich high capacity NMC811 can be substantially improved by coupling it with a Mn-rich $LiNi_{0.5}Mn_{0.5}O_2$ shell. The core–shell material exhibited reduced heat generation of 2261 J/g at 250 °C at a charged state to 4.3 V in contrast to 3285 J/g at 180 °C found for the pristine material.[189] Consequently, the cycling stability of the core–shell material was considerably higher than the pristine materials (98% vs 81%) after 500 cycles. In another work, Liang *et al.* showed that at high voltages (4.5 V), it is possible to alleviate the layered to rock salt-like phase transformation in $LiNi_{0.5}Mn_{0.3}Co_{0.2}O_2$ (NMC532) by shielding this with a layer of sodium superionic conductor (NASICON) type-$NaTi_2(PO_4)_3$ shell material.[190] This shell has proven effective against HF attack, which would give rise to the dissolution of electroactive elements from the surface regions. With 5% Mn-rich $Li_{0.65}Mn_{0.59}Ni_{0.12}Co_{0.13}O_\delta$ (LMNCO) on NMC811, a nearly one order of magnitude decrease in interfacial charge transfer resistance was reported by Dong *et al.*[191] As a result, the core shell material delivered a remarkable capacity of 150 mA h/g at 5C rate (1C = 200 mA/g) with 83.4% retention after 500 cycles. A novel double shelled material $(Li\{[(Ni_{0.8}Co_{0.1}Mn_{0.1})_{2/7}]_{core}[(Ni_{1/3}Co_{1/3}Mn_{1/3})_{3/14}]_{shell1}[(Ni_{0.4}Co_{0.2}Mn_{0.4})_{1/2}]_{shell2}\}O_2)$ was tailored by Hou *et al.* in which one of the shells ($[(Ni_{1/3}Co_{1/3}Mn_{1/3})_{3/14}]_{shell1}$) improves the rate capability and the other ($[(Ni_{0.4}Co_{0.2}Mn_{0.4})_{1/2}]_{shell2}$) contributes to the cycling stability of the hybrid structure. The double shelled material displayed superior electrochemical performance in comparison to the homogeneous compound with the same average composition $[Li(Ni_{0.5}Co_{0.2}Mn_{0.3})O_2]$.[192]

Structural or chemical mismatch between the core and the shell could lead to voids between the two components, hindering Li^+ ion diffusivity and electron transport. Additionally, such voids may generate chemical pressures leading to compositional variations that can form a blocking layer, shielding the core entirely. Concentration-gradient materials may be applied to try to overcome these challenges, where the transition metal cation concentration varies radially from an area of higher to lower concentration. In the case of nickel-rich cathodes exhibiting concentration-gradients, one can experimentally visualize that a Ni-rich solution 1 is pumped into the reactor to form the core, after which a more Ni-poor solution 2 is pumped into solution 1 and simultaneously the mixture is injected into the reactor to give rise to a concentration-gradient. This strategy was demonstrated by Sun *et al.* in 2009 by synthesizing the $LiNi_{0.8}Mn_{0.1}Co_{0.1}O_2$ core and $LiNi_{0.46}Co_{0.23}Mn_{0.31}O_2$ surface composition by pumping 0.08:0.46:0.46 of Ni–Mn–Co molar solutions (solution 2) into 0.8:0.1:0.1 molar solution (solution 1) resulting in a constant core and concentration-gradient shell. This concentration-gradient cathode material delivered a high specific capacity of 200 mA h/g in contrast to 142 mA h/g exhibited by the pristine material after 50 cycles within a 3.0–4.4 V voltage range at 55 °C.[193] Interestingly, the authors reported a shrinking in the core and an expansion in the shell during the subsequent high temperature calcination process, which may be attributed to the inter-diffusion of the transition metal cations. To resolve this and further boost the electrochemical traits of concentration-gradient materials, a new full concentration gradient (FCG) material was proposed

where the Ni and Mn concentration varies continuously resulting in a Ni-rich core and Mn-rich shell and an average composition $LiNi_{0.75}Mn_{0.15}Co_{0.10}O_2$. Owing to the FCG nature and needle-like nanostructure, the material exhibited a high specific capacity of 215 mA h/g and excellent capacity retention of 90% after 1000 cycles.[194] In 2015, Sun *et al.* further extended this concept by introducing two slopes of transition metal ion concentration within the particle (termed TSFCG). The synthesis of these TSFCG is achieved by sequential addition of two Mn-rich solutions [solution 2—molar ratio 0.68:0.11:0.21(Ni–Co–Mn) and solution 3—molar ratio 0.51:0.20:0.29 (Ni–Co–Mn)] at regular intervals to the Ni-rich core solution [solution 1—molar ratio 0.8:0.05:0.15 (Ni–Co–Mn)]. The materials obtained by this approach delivered a high specific capacity of 200 mA h/g and superior cycling stability of 88% for 1500 cycles in a full-cell configuration.[195] Efforts to simplify the process of introducing concentration-gradients include work by Song *et al.* who proposed an alternative approach by first preparing a double-shelled precursor material followed by tuning of the subsequent calcination temperature or duration to promote the inter-diffusion of transition metal cations, yielding an internal concentration gradient.[196]

Concluding remarks

A recent study on pinpointing the major degradation mechanism governing the capacity loss in NMC811 has discussed in detail the formation of the fatigue phase in aged electrodes. The active-bulk lattice planes of the layered structure pinned to the surface-reconstructed rock salt-like NiO that constrain lattice dynamics during Li^+ extraction is responsible for the generation of this fatigue phase, particularly at high states of charge (SOC >75%).[197] These findings further emphasize the significance of developing novel core–shell or concentration-gradient structures to mitigate these processes. Although they can be challenging to produce, core–shell and concentration-gradient structures offer a route to the use of high capacity, but oft-times unstable, compositions. As the Li-content of NMC is pushed higher, there is a general trend to lower stability, and so core–shell or concentration-gradient structures may represent a means to exploit these high Li compositions while minimizing decomposition. Similarly, new compositions may not be immediately compatible with existing electrolytes, and so the means to provide a passivating but still electrochemically active surfaces may become increasingly important. Using first principle calculations, Mou and Yao also showed that by appropriate choice of core and shell material, one could exploit the high Li diffusivity originating from the difference in Gibbs free energy, which opens up an enticing new avenue of material design for fast-charging requirements.[198]

B. Enhancing performance through hierarchical structuring of electrodes

As set out in Sec. III, cathodes materials are achieving ever higher operating voltages and gravimetric energy densities. However, to be commercially viable, the optimization of the cathode particles described needs to go hand in hand with optimizing the electrode structure in order to improve the overall electrochemical performance. For this, several additional factors need to be considered to achieve competitive electrode level performance. This includes how these materials behave during the shear mixing of the electrode slurry and slot die coating on a roll-to-roll tool. First, transition metal oxide cathodes tend to have intrinsically low electronic conductivities (10^{-10}–10^{-8} S/m),[199] which can cause non-uniform charge distributions in the electrode. To alleviate potential inhomogeneous states of charge, the optimization of electrode composition and material design, such as coating with conductive polymers or carbonaceous substances, as well as methods to incorporate advanced conductive additives to the electrodes has been intensively researched.[200–205] Furthermore, certain newly developed cathode materials consist of particles with low packing densities, resulting in reduced overall volumetric energy densities, despite advances in the gravimetric energy density.

For many electrode materials, a popular strategy for enhancing electrical conductivity is coating the surface with a conductive carbon layer. However, for a number of materials, this process is not well suited. This is because the pyrolysis reactions generally used to create carbon coatings tend to scavenge oxygen from the cathode material, forming CO_2.[200] These reactions typically degrade the cathode performance. To address this challenge, there is a substantial amount of work invested in the development of carbon coating methods for advanced cathodes at a relatively low temperature (<600 °C).[203,206] Another key challenge involves coating uniformity. Many cathodes consist of secondary aggregates of nano-sized primary particles, and most carbon coating methods will only coat the outer surface of the secondary particles. As a result, electron transport to primary particles located in the center of secondary particles often remains problematic.[207]

Both the conductive additives and binders required for most cathodes to perform effectively do not take part in the charge storage process, so excessive use of these materials leads to a decrease in the overall energy density of the cell. In addition, the large surface area of certain additives can lead to side reactions with the electrolyte. Conversely, too little conductive additive or binder can lead to insufficient electric conductivity and poor mechanical integrity. This contributes to a complex optimization process, which not only affects the volumetric capacity but also has a significant impact on rate performance and cycling stability. The latter is illustrated in Fig. 9, which shows an example of capacity fade for a spinel structured $LiMn_2O_4$ cathode with cycling [Fig. 9(a)] and electrochemical impedance spectroscopy (EIS) spectra [Fig. 9(b)] when varying the binder and conductive additive compositions.[208]

In an idealized model, every individual particle has the same state of charge (SOC) at any given time during the cell operation. However, these conditions are rarely met due to the presence of inhomogeneity in the conductive network as discussed above as well as heterogeneity in the particle size distribution, electrolyte exposure, phase transitions, and electrolyte decomposition products.[209,210] The variations in lithium-ion access and electrical contact result in macroscale SOC inhomogeneities across the entire electrode during cycling. For example, the primary particles located in the center of secondary particles have comparatively large electric resistance, lacking direct contact with the conductive additives. Furthermore, the chemical environment of the primary particles

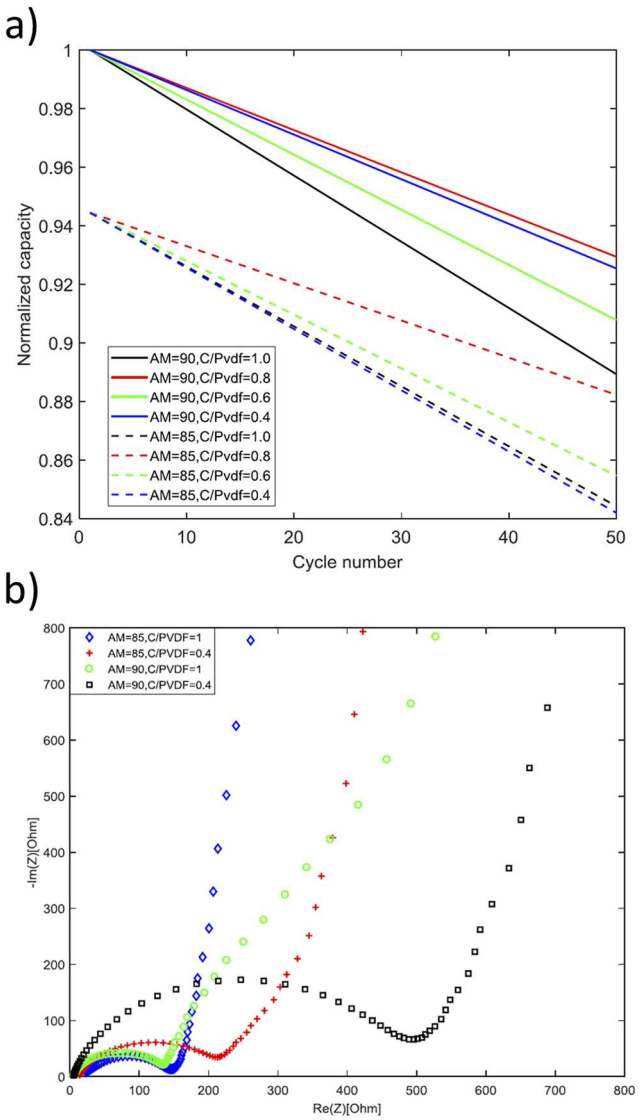

FIG. 9. (a) Normalized capacity as a function of cycling for $LiMn_2O_4$ and (b) EIS spectra with different electrode composition. The electrode composition presents the active material (AM), e.g., 90% for AM = 90 and the ratio of conductive material and binder for C/PVDF.

varies from the secondary particle core to surface, leading to further nanoscale SOC inhomogeneity. These different sources of SOC variability are problematic as they are difficult to control and quantify while significantly impinging on the electrode performance and contributing to degradation.

Substantial academic and industrial effort is being exerted toward addressing the challenges described. For instance, recently reported oxidative chemical vapor deposition (oCVD) techniques using 3,4-ethylenedioxythiophene (EDOT) monomers and vanadium oxytrichloride ($VOCl_3$) oxidant vapors at 90 °C have shown the ability to coat ultraconformal conductive poly(3,4-ethylenedioxythiophene) (PEDOT) skins on the surface of primary or secondary particles.[211] Material structuring techniques, such as spray drying, are also being developed for cathode films to improve the packing density of nanoparticles.[212,213] A particular challenge with some of the more advanced material organization techniques is that they are not compatible with conventional electrode mixing and coating methods. In a limited number of examples, advanced material structuring has been demonstrated through techniques such as continuous roll-to-roll coating.[214] Looking forward, key developments will rely on new hierarchical electrode designs that revisit how we pack materials more densely in electrodes without compromising the electron and ion transport.

Concluding remarks

During the development of new cathode materials, the focus is often on measuring the intrinsic properties of the materials in thin electrodes using large amounts of conductive additives. While this allows characterization of the inherent material properties, there is a significant risk that these materials fail at a later stage when testing against industrial requirements. The high areal loadings, high volumetric densities, and low quantities of conductive additive and binder required in commercial applications are often difficult to achieve with new materials. For example, a novel cathode material that is unable to form a dense packing structure may see a reduced volumetric capacity at the electrode level even if the specific performance of the material is improved. The same is true for materials that require excessive amounts of conductive additive or binder to operate reliably. Therefore, both the development of new cathode materials and their coating in electrodes needs to be judiciously co-developed. Finally, these efforts need to be orchestrated with optimization of the material morphology. In the case of nano-sized materials, issues in volumetric performance and possible side reactions with the electrolyte necessitate techniques to pack these materials into secondary structures, allowing for efficient coating with high areal loading and packing density. Ultimately, though, micrometer sized, single crystal cathode particles offer even higher volumetric densities and these are therefore playing a key role in the further development of advanced cathodes. The significance of single crystal particle morphologies is further underlined in Sec. V E. By optimizing synthetic approaches to fabricate large single crystals materials and efficient techniques to assemble dense secondary structures, the performance and lifetime of these materials can be enhanced, along with minimizing the reliance on non-active electrode components.[38]

C. Understanding the role of interfaces

As discussed Sec. III, achieving a high energy density and high operating voltage is key to cathode development, aiming for real terms improvements in $/kWh. Performance improvements within the material often come at the cost of reduced stability and an increase in detrimental side reactions. Investigations into high nickel content in the layered cathodes and through spinel materials show that it is particularly important to mitigate the challenges these classes of materials suffer during cycling to achieve

high performance. Significantly, the surface of nickel-rich compositions is very sensitive to the atmosphere and an increase in charge-transfer resistance is often observed during cycling. This is particularly due to structural instability and formation of non-electroactive species through side reactions that occur at the electrode–electrolyte interface. In addition, metal dissolution at a high operating voltage (>4.7 V), capacity fade at elevated temperature, and Li^+-consumption at the SEI in high voltage spinel cathodes are other problems that need to be addressed.[215] Li extraction/insertion in Ni rich cathode materials also causes a strong anisotropy in crystal structure leading to chemo-mechanical degradation and bulk fatigue at the surface.[197] Spinel-type materials also suffer from bulk and surface instabilities at high charge states, issues common to the majority of cathode materials.

The interface between the electrode and electrolyte is one of the vital components of the battery and must remain stable enough for safe operation and to avoid performance degradation. A functioning CEI structure provides an unimpeded passage for Li^+ charge transfer from the electrode to the electrolyte. The electrode/electrolyte interaction can suffer from parasitic reactions in the case of liquid electrolytes and the formation of a space charge layer in the case of solid electrolytes.[216,217] Surface coatings (or also known as surface stabilization or surface coating/modification in the wider scientific literature) are a promising solution to address these challenges. An interface layer or coating acts as a bridge or "pseudo electrolyte" between the electrode and electrolyte and protects from any unwanted reactions in the battery cell.[218] Cathode coatings offer a number of beneficial target properties that include improvements to the structure, morphological stability, Li-ion transport, and thus electrochemical performance (cycling performance and rate performance at high current densities) of battery electrodes. The coating can prevent unwanted side reactions and act as a scavenger for any HF, reducing the acidity of non-aqueous electrolytes. Similarly, the coating can mitigate/protect or suppress the metal dissolution (TM/Li-migration) from the cathode. Such improvements can allow for higher performance and operation with an increased cut-off voltage.

There are numerous inorganic materials explored and experimentally tested as interfacial coatings on different classes of cathode materials in the scientific literature. These include (i) single element interfaces, such as carbon[219] and titanium,[220] (ii) binary oxides ZrO_2,[221] ZnO,[222] TiO_2,[223] and Al_2O_3,[224] (iii) composite oxides,[225] and (iv) even some battery electrodes[226] and electrolytes ($Li_4Ti_5O_{12}$, $LiNbO_3$, Li_3PO_4, and LiPON).[227,228] Each of these materials offers different functionalities and challenges depending on the particular cathode chemistry, other battery-cell components, and coating method. This is a very active area, with several review articles and perspectives available in the literature, along with many research articles.[228–232] Herein, we lay out the experimental design principles to form an effective artificial CEI. This is important while selecting or screening the right materials. An ideal interfacial coating should be chemically and electrochemically inactive, offering the following properties:

(i) Homogeneous microstructure with good mechanical and thermal stability—to facilitate adequate Li-ion transport, diffusion (electron—ion conduction media) across the electrode–electrolyte, and good coverage of the cathode particles.
(ii) Good adhesion between the liquid (solid)-electrolyte and cathode/anode electrodes.
(iii) Low-interfacial resistance, long-term stability, and safety during the operation of batteries at standard operating and elevated temperatures.
(iv) Adaptable with the specific battery chemistry-industrial manufacturing process coating technology and from thermal budget to final battery packaging.
(v) Must not directly or indirectly participate in any adverse chemical reactions with either the cathode or the electrolyte components (salts, solvents, and additives).
(vi) Ideally, the cathode–electrolyte (CEI) interface should be formed *in situ* during the first cycles (like SEI formation)—acting as a passivation layer with adequate Li-ion transport.
(vii) Contribute to rather than detract from the performance indicators required of next generation sustainable cathode materials, such as high capacity with structure/morphological stability at high current densities, long cycle life, low cost, and safe operation.

An appropriate film that can satisfy all ideal requirements stated above is yet to be achieved. What is clear is that the artificial CEI can alleviate some of the performance issues raised previously; however, this usually comes at the expense of a different property or significant increases in the non-active mass within the cell. A promising recent coating example, $LiAlF_4$, has been examined as a coating on NMC811.[218] However, the performance of NMC811 could yet offer further improvements by reducing the effect of bulk fatigue at the surface. Alongside the stability of the cathode, coatings that enable high voltages in liquid electrolyte cells will benefit layered materials, high voltage spinels, disordered rock salts, and numerous new cathode chemistries.

Apart from coating methods, electrolyte modification by different additives can be vital for stable CEI formation. Vinylene carbonate (VC) has been found to reduce the surface reconstruction of layered NMC811 to rock salt during high voltage cycling.[31] Similarly, triphenylphosphine oxide has been shown to enhance the electrochemical performance of graphite/NMC811 full cells as an electrolyte additive.[233] Alternatively, cathode surface treatment can have a significant impact on CEI formation. For instance, Li-rich NMC materials have been treated with CO_2 to generate oxygen defects in the cathode surface (20 nm).[234] These defect sites reduce the gas evolution during the first cycles, inhibiting the side reactions that normally form a thick, resistive CEI layer. Such oxygen vacancies also appear to aid bulk anion redox. When examining possible artificial CEI materials, numerous suitable materials must often be screened. The interfacial layers must be tuned to the specific behavior of the cathode material (nickel rich layered materials, disordered rock salts, spinels, and multi-anion cathode materials), with optimization of the structure, morphology, and thickness of the coating. A suitable coating must also be tuned to be compatible with the underlying cathode particle size and morphology, aiming to enable high ion conduction, high capacity, thermal stability, a stable structure, and high cut-off voltage at high current rates.

To understand and develop suitable cathode coatings, a fundamental understanding of the interactions that occur at the buried cathode/CEI interface is required. This can be approached in

two distinct manners—through computational simulations of the interfaces or through the synthetic development of ideal cathode interfaces for advanced characterization. An AIRSS approach, as described previously, can provide structural models along with in-depth DFT calculations; however, for such studies, a sound synthetic model is initially required as such complex interfacial interactions may stray from the thermodynamic minima.

Ideal cathode interfaces for such investigations can be produced through formation of epitaxial or highly calligraphically oriented cathode thin film electrodes. Enabling the study of anisotropic distortions or structural transitions (nickel rich layered materials), isotropic volume changes (disordered rock salts), or diffusion properties through specific crystallographic planes (spinels). Such thin film cathode materials offer an ideal substrate to study coating interactions, detailed ion transport behavior, and structural and electrochemical properties. A combined understanding of such films both computationally and experimentally will help to advance progress toward optimization of cathode coatings.

Concluding remarks

In order to understand the material's intrinsic characteristics and resolve the associated challenges, it is essential to study the electrochemical behavior of binder and additive-free electrodes. Again, to understand the role of the interface between the electrode and electrolyte and modify the surface strategically, thin-film fabrication of the electrodes is the way out. The interface study and engineered modification of surfaces can enable measurement of the fundamental properties of the system in isolation and offer improved cycling performance. To understand the effect of different coating materials in enabling enhanced cycle stability and safer operation of the electrode materials, it is often important to apply advanced and developing characterization techniques to these challenging interfaces. Some example techniques that are being developed are highlighted in Sec. V D.

D. Understanding the interplay between morphology and performance

Recently, there has been increased understanding of the influence that electrode microstructure, and particle morphology across the length scales, has on cell performance. For example, electrode performance is influenced by particle size and pore distribution heterogeneities leading to proposals for graded-microstructure design.[235] Elongated, radially orientated primary particles have been found to make NMC secondary assemblies more crack resistant,[236] and cathode–electrolyte interphase distribution has been found to be influenced by the chemistry and distribution of the binder.[237]

Greater understanding of complex degradation processes, how they are affected by morphology or microstructure, and morphology changes in high energy density cathode materials has required the use of advanced microscopy techniques. Figure 10 outlines various electron, ion-beam, and x-ray microscopy techniques used in Li-ion battery research, highlighting their lateral resolutions and typical electrode morphology features that lie within the respective length scales. Depth resolution has also been highlighted for surface sensitive techniques.

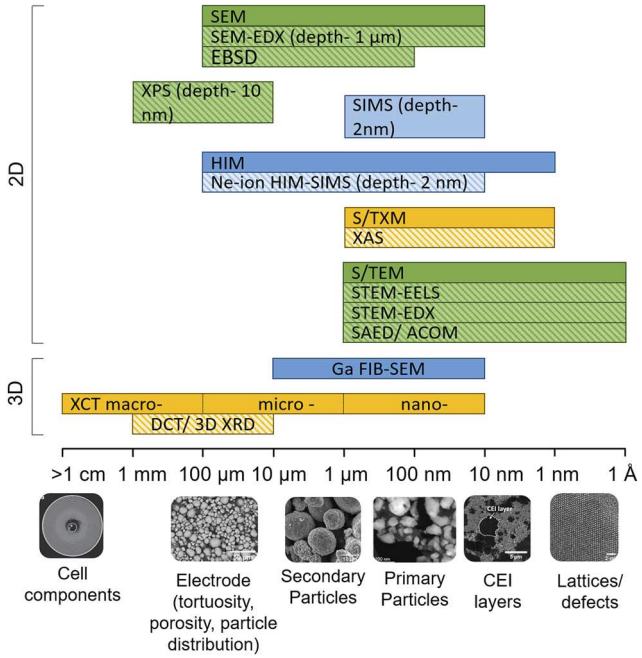

FIG. 10. Lateral resolution of different electron (green), ion beam (blue), and x-ray microscopy (yellow) techniques compared with standard cathode morphology components.[238,239] Solid colors represent microscopy techniques, with striped colors representing the associated chemical or structural characterization techniques. Electron microscopies represented: scanning electron microscopy (SEM), energy dispersive x-ray spectroscopy (EDX), electron backscatter diffraction (EBSD), x-ray photoelectron spectroscopy (XPS), scanning/transmission electron microscopy (S/TEM), electron energy loss spectroscopy (EELS), selected area electron diffraction (SAED), and automated crystal orientation mapping (ACOM). Ion-beam microscopies represented: secondary ion mass spectrometry (SIMS), helium ion microscopy (HIM), HIM-SIMS, and gallium ion focused ion beam scanning electron microscopy (Ga FIB-SEM). X-ray microscopies represented: scanning/transmission x-ray microscopy (S/TXM), x-ray absorption spectroscopy (XAS), x-ray computed tomography (XCT), diffraction computed tomography (DCT), and 3D x-ray diffraction (3D XRD). Cell components XCT image reproduced with permission from Finegan *et al.*, Nat. Commun. **6**, 6924 (2015). Copyright 2015 Nature Communications under Creative Commons Attribution CC BY 4.0.[240] CEI layer image reproduced with permission from Wheatcroft *et al.*, ACS Appl. Energy Mater. **3**, 8822 (2020). Copyright 2020 Author(s), licensed under Creative Commons Attribution CC BY 4.0.

Recent advances in technique development of some of those outlined in Fig. 10 have led to improved resolution of different electrode features. Some of the recent developments in resolution and correlation with chemical or structural techniques are highlighted here.

X-ray computed tomography (XCT) has been widely used for imaging the 3D structure of electrodes. However, segmenting the carbon/binder domain (CBD) from nanometer scale pores within the CBD is challenging due to the low attenuation coefficient of the CBD.[241] Recently however, methods to differentiate pores from binder have been developed to overcome this challenge. Contrast between CBD and pores has been enabled by correlating focused ion beam-scanning electron microscopy (FIB-SEM) imaging of CBD-rich regions with XCT and[242] nano-CT of CBD phases with

micro-CT[235] and by using contrast enhancing nanoparticles in the CBD.[243] Accurate analysis of porosity could greatly improve understanding of electrolyte penetration into electrodes and consequent optimization of electrode structures.

Understanding surface layers and how underlying morphology effects their growth is important for degradation studies. Electron backscatter diffraction (EBSD) has recently been applied to lithium-ion battery electrodes to understand grain boundary orientations on electrode surfaces.[244,245] Electrode EBSD has potential applications for understanding preferential lithiation and CEI growth on different electrode regions. The importance of the local environment on CEI growth has also led to CEI characterization using region-of-interest secondary ion mass spectrometry (SIMS) chemical mapping,[246,247] and helium ion microscopy (HIM)-SIMS.[248] Both techniques provide chemical, positional, and thickness information, but the quantification of thickness can be challenging.

Overall, there have been a number of developments in imaging electrode microstructures, which aid understanding of degradation processes and improved microstructure development.

A major challenge for cathode microscopy techniques is the development of *in situ* and *operando* techniques. So far, Sec. IV D has demonstrated the versatility of microscopy techniques for characterizing electrode morphology. *In situ* and *operando* techniques are beneficial as they enable characterization of transient phenomena and reduce atmosphere induced sample damage. The goal here is to characterize the material in its representative environment as found in a bulk cell (*in situ*) and under working conditions (*operando*). As with the previously examined techniques, *in situ* imaging techniques should aim to be representative of the real cell and minimize technique induced sample damage.

Ideally, the materials used in the real cell should be used in any *operando* characterization. However, the ultra-high vacuum requirements of electron, ion beam, and soft x-ray microscopy limit the choice of electrolyte. Typical organic electrolytes (such as LP-30) are unstable under high vacuum; hence, *operando* cells that require electrolyte exposure to the vacuum are limited to ionic liquid and solid-state electrolytes.[249,250]

The geometry of *quasi-operando* cell setups for nano-scale microscopy [scanning/transmission electron microscopy (S/TEM) and some scanning/transmission x-ray microscopy (S/TXM)] can potentially alter diffusion pathways and make quantitative electrochemistry challenging.[251] Due to the requirement for micropatterning, Pt electrodes are often used as quasi-reference electrodes; however, these may cause measured or applied potentials to drift.[251,252] Nano-wire architectures are also used with a solid-electrolyte that can adjust diffusion pathways.[249] Similarly, surface sensitive techniques, such as SEM, SIMS, and x-ray photoelectron spectroscopy (XPS), cannot use traditional electrodes due to surface sensitive imaging requirements.

Beam damage is a major issue that must be mitigated for all microscopy techniques. X rays do not typically affect cathode materials, but the incident x-ray beam can cause heating of the electrolyte (at high kV or high flux) and subsequent bubble formation. For electron and ion beam microscopies, heating is also an issue, but radiolysis (particularly in high energy S/TEM) can cause beam induced precipitation in the electrolyte due to reduction by the incident electrons.[253]

A number of strategies have been developed to overcome the vacuum requirements of electron and ion beam microscopy experiments. Electron microscopy *in situ* cell designs can be classified as open cell, where the components are exposed to high vacuum, and closed-cell where the components are sealed from the vacuum allowing non-vacuum stable electrolytes to be used. The different open- and closed-cell designs for SEM and TEM experiments are detailed in Fig. 11.

Open-cell designs [Figs. 11(a), 11(b), 11(d), and 11(e)] consist of cells using high vapor pressure electrolytes, such as ionic liquids,[249,250] and solid-state battery set-ups often prepared by thin-film deposition techniques and FIB sectioning.[254] Open cell setups allow for low beam doses to avoid beam damage to organic liquid electrolytes,[253] and also, open cells experience no impact on resolution through thickness issues, and thus, image quality is not compromised. Solid-state battery setups have been used for high-resolution interfacial studies and electron energy loss spectroscopy (EELS) oxidation state mapping in the TEM.[254] The use of a metal grid with an ionic liquid cell electrolyte has enabled surface sensitive analysis with techniques such as SEM.[250,255] Ionic liquids have also enabled *in situ* XPS experiments.[256]

Closed-cells are designed using electron transparent windows, such as SiN_x, to seal the electrolyte away from the vacuum, enabling the use of standard electrolytes [Figs. 11(c), 11(f), and 11(g)]. Closed-cells have been developed for both SEM and TEM based experiments, studying the lithiation mechanisms of $LiFePO_4$ with energy filtered TEM[257] and Li dendrite formation in SEM.[258]

In situ TEM cells require unusual closed-cell geometries due to electron transparency requirements [Fig. 11(f)]. Recently, a lithium–gold alloy has been reported[252] as a more stable reference electrode than Pt, which relies on Li^+ ions from the electrolyte.[259] A sandwich cell with a Li metal anode has also been designed [Fig. 11(g)], but the cell relies on exposed nano-rods at the edges for electron transparency.[260]

Luckily, hard x-ray experiments do not have the same vacuum limitations as experienced in electron microscopy. Here, *operando* x-ray microscopy cell geometries can mimic real cells, such as Swagelok setups, or coin cells containing Kapton windows for x-ray transparency.[261,262]

Concluding remarks

The development of advanced microscopy techniques is enabling improved resolution of multiple components in the complex 3D structure of lithium-ion battery cathodes. The improvements in imaging are already having an impact in optimization of microstructure and understanding of complex degradation mechanisms. The holy grail for microscopy would be to establish *operando* techniques allowing transient information to be gained without sample damage associated with removal from the cell. Numerous different *in situ* cells have been developed for SEM, TEM, and x-ray microscopy, providing information on morphology and chemical changes during cycling. Some of the developed techniques, such as solid-state open *in situ* electron microscopy cells, do not severely compromise the capability of the instrument due to beam damage during sampling. However, further developments to *in situ* cell design are required to take full advantage of imaging technique

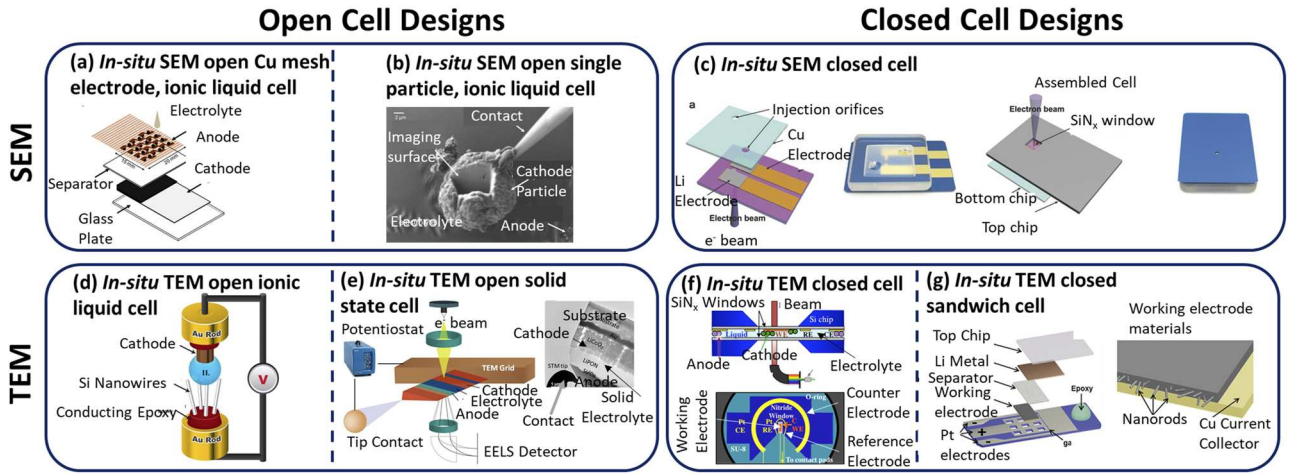

FIG. 11. Examples of open and closed cell *in situ* TEM and SEM designs. (a) Open cell *in situ* SEM cell design consisting of active material particles on a copper mesh in a sandwich cell geometry with an ionic liquid electrolyte, reproduced with permission from Chen *et al.*, Sci. Rep. **6**, 36153 (2016). Copyright 2016 Author(s), licensed under Creative Commons Attribution CC BY 4.0. (b) Open cell *in situ* SEM cell with an active material particle cathode suspended on an ionic liquid electrolyte and lithium titanate anode[263] [reproduced with permission from Miller *et al.*, Adv. Energy Mater. **3**, 1098 (2013). Copyright 2013 Wiley-VCH Verlag GmbH and Co. KGaA, Weinheim]. (c) Closed cell *in situ* SEM design utilizing SiN_x observation windows[258] [reproduced with permission from Rong *et al.*, Adv. Mater. **29**, 1606187 (2017). Copyright 2017 Wiley-VCH Verlag GmbH and Co. KGaA, Weinheim]. (d) Open cell *in situ* TEM cell using Si nanowires and an ionic liquid electrolyte,[249] reprinted with permission from Gu *et al.*, Nano Lett. **13**, 6106 (2013). Copyright 2013 American Chemical Society. (e) Open all solid state cell *in situ* TEM cell created using a FIB sectioning,[254] reprinted with permission from Wang *et al.*, Nano Lett. **16**, 3760 (2016). Copyright 2016 American Chemical Society. (f) Closed cell *in situ* TEM cell in a three-electrode configuration using an organic liquid electrolyte,[257] reprinted with permission from Holtz *et al.*, Nano Lett. **14**, 1453 (2014). Copyright 2014 American Chemical Society. (g) Closed cell *in situ* TEM cell in a sandwich geometry with a Li metal anode.[260] [Reproduced with permission from Xu *et al.*, Small **16**, 1906499 (2020). Copyright 2020 Wiley-VCH Verlag GmbH and Co. KGaA, Weinheim.]

while minimizing beam damage, improving cyclability, and without limiting material choice.

V. ADVANCES IN THE CHARACTERIZATION OF CATHODE MATERIALS

Peter Baker, Samuel Booth, Serena Cussen, Norman Fleck, Harry Geddes, Andrew Goodwin, John Griffin, Abby Haworth, Stephen Hull, Ziheng Lu, Innes McClelland, Gabriel Pérez, Helen Playford, Joe Stallard

A. Structural analysis

Investigation of the structural changes that the cathode experiences during battery operation is paramount to understand their role in the performance and stability of the device and, consequently, to improve the cathode design to develop more capable and lasting batteries. Due to their arguably unmatched ability to provide atomic-scale information (averaged over the sample volume) with high detail and accuracy, diffraction techniques have been the go-to methodologies to study the structure of cathodes. Specifically, x-ray and neutron diffraction have been effectively used as complementary techniques to study complex cathode structures due to the distinct physical interactions between each probe and the motifs within the unit cell of a given crystal structure. While x rays interact almost exclusively with the electron cloud of atoms, neutrons can interact with the atom's nucleus to provide structural information or the atom's electron cloud to provide information on the magnetic properties of the sample.

In the simplest type of diffraction experiment, the cathode sample of interest is investigated before and after applying some environmental and/or operational conditions to it. A slightly more sophisticated variation of this study involves the use of *in situ* temperature and pressure modifiers, such as furnaces, cryostats, or diamond anvils, that are compatible with the experimental setup, allowing the collection of the diffraction pattern while such conditions are applied. However, these experiments are unable to provide crucial information about the structural changes that the cathode experiences during battery operation. For such information, one must look to electrochemical control through *in situ* or *operando* type diffraction experiments. Herein, we define *in situ* as analysis of the material within its controlled test environment, for instance, an electrochemical cell at a set voltage, and *operando* defines a subset of *in situ* measurements conducted under operational conditions, for instance, during continuous charge/discharge cycling. Both the environmental and operational conditions that the cathode experiences in its intended real application are reproduced as closely as possible while the structure is examined. This requires the design and fabrication of *in situ*/*operando* cells that closely replicate the electrochemical stimulus provided in a standard battery cell while ensuring meaningful diffraction data from the cathode. This can pose an engineering challenge when it comes to required modifications of the cathode

geometry or composition, materials requirements for the inspection windows, and stability under vacuum. These conditions must be tempered against those of a suitable electrochemical cell; in the case of cathode materials, which are often poor electronic conductors, the window should ideally function as the current collector to ensure that the reaction of interest is occurring at the point of inspection.[264] Despite the strict requirements of the cell, *in situ*/*operando* diffraction experiments provide a unique route toward mechanistic understanding of processes occurring at high states of charge or on repeat cycling. Therefore, there is significant interest in the further optimization of existing cell designs, along with the development of novel cells to enable access to additional unexplored techniques or refined combinatorial measurements—for instance, scattering in conjunction with spectroscopy.

Evidently, obtaining a high-intensity and high-resolution diffraction pattern is crucial for the correct analysis of the cathode structure. In the first instance, this requires the collection of a significant number of probe-cathode interactions. For x-ray experiments, bench top experiments using soft x-ray sources have been around for a significant amount of time, and there exist several suitable *in situ* cell designs. Synchrotron sources by comparison offer significant enhancements in flux and therefore detection time, resolution, and more flexible cell design due to the higher penetration depth of the x rays. Tunable x-ray energies allow for resonant diffraction measurements, and the development of specialist detectors also enhance the possible Q-space range that can be gathered, which is hugely significant for total scattering analysis. However, beam damage to the cell's materials must be considered due to the highly energetic x rays.

Neutrons are naturally highly penetrating; however, the typical incident flux at a neutron source is significantly lower than that of x-ray sources, especially synchrotron sources. This increases the duration of the experiment and often requires the use of large samples in the range of cm^3. For cathode materials, this can offer a significant challenge. In addition to this, to fully exploit the advantageous isotopically dependent scattering of neutrons, labeling techniques such as deuteration are often required, especially when determining the location of some atoms within the cathode. Deuteration is also needed to reduce the level of incoherent neutron scattering from highly hydrogenous materials in the cell. Regardless of the purpose for deuteration, the synthesis of deuterated materials can be complex and expensive.

In addition to the previous considerations, cells need to be easily assembled/disassembled, highly reproducible for further electrochemical testing, and adaptable to the specific instrumentation in which they will be used. As synchrotron facilities continue to invest in upgrades, the significance of limitations in measurement time diminish, with more and more techniques reaching time resolutions that can examine fast charge/discharge processes to understand the implications of higher power operation on battery cathode materials.

The most effective approach to address the challenges previously described has been to focus on the design of an *in situ*/*operando* cell. Cells for x-ray diffraction can be designed for either soft or hard x rays and for reflection or transmission mode (Fig. 12). One of the most popular designs, due to its widespread applicability, is the "coin cell" whose designated probing area has one (for reflection mode) or two (for transmission mode)

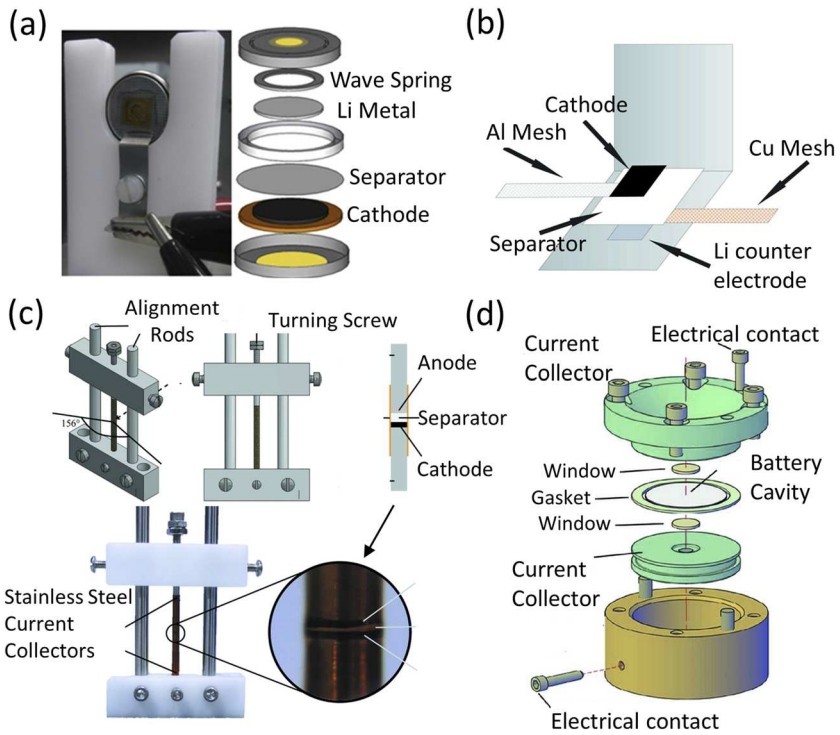

FIG. 12. (a) A coin cell, along with its schematic representation, mounted on a specially designed holder for the powder diffraction beamline at the Australian Synchrotron. [Reprinted with permission from Brant *et al.*, "Comparative analysis of *ex situ* and *operando* X-ray diffraction experiments for lithium insertion materials," J. Power Sources, **302**, 126–134 (2016). Copyright 2016 Elsevier.] (b) Schematic representation of a coffee bag cell before sealing. (c) Schematic representation of the cylindrical RATIX cell. (d) Schematic representation of the AMPIX cell. Reproduced with permission from Rosciano *et al.*, J. Synchrotron Radiat. **14**, 487 (2007). Copyright 2007 IUCr, reproduced with permission from Liu *et al.*, J. Appl. Crystallogr. **49**, 1665 (2016). Copyright 2016 IUCr and reproduced with permission from Borkiewicz *et al.*, J. Appl. Crystallogr. **45**, 1261 (2012). Copyright 2012 IUCr Author(s), licensed under the Creative Commons Attribution CC BY 4.0.

x-ray-transparent windows.[265] Coin cells owe their popularity to their low cost, simple assembly, and good sealing: therefore, there are many variations of this type of cell. For instance, for the detection window, beryllium is highly toxic and is often replaced with a different material, such as a Kapton film (polyamide),[266] which is highly transparent to x rays and chemically inert. As a non-conductive material, the applicability of the response in this region of the cathode must be considered carefully. This can be mitigated by reducing the window size, adding a conductive mesh, or increasing the amount of conductive additive in the cathode. With flexible inspection window materials, it is often also a challenge to provide the uniform stack pressure required for consistent electrochemistry.[264] For large inspection windows, measurements in different regions within the window or *ex situ* measurements of the cathode afterward are good practice to ensure uniformity of response. The AMPIX cell, developed by researchers at the Advanced Photon Source in the US, uses a glassy carbon inspection window to ensure uniform electrochemistry through the cathode.[264,267] Radial cell designs, such as the RATIX cell, developed at the APS and DRIX cell developed at the Diamond Light Source can help to reduce the measured background or isolate individual cell components.[268,269] When larger cathode areas are required or to minimize unwanted scattering from non-cathode materials, a pouch or "coffee bag" cell design is often employed.[270] To avoid cell damage from the highly energetic hard x rays, intermittent sampling or different region probing is often utilized as good practice.

For neutron diffraction experiments, the increased sample mass requirements mean that smaller cell types are less suited to such measurements. Cylindrical and pouch cells designs have been applied, however, additional factors in neutron measurements have also motivated the development of specialized cells. In neutron experiments, to minimize incoherent scattering, it is common to use deuterated electrolytes and fluorinated separators.[271] The wider range of neutron transparent materials means that it is often easier to maintain good electrochemical performance, utilizing inspection windows that act as the current collector, for instance, Ti–Zr alloy or Al.[272] Additionally, time-of-flight diffractometers available at pulsed neutron sources, such as the ISIS Neutron and Muon Source in the UK, allow the collection of the diffraction pattern at fixed scattering angles. This fixed geometry makes it possible to define a scattering volume strictly within the sample by collimating the incident and scattered beam and, thus, eliminate Bragg peaks from surrounding components (Fig. 13). The key drawback for *in situ* neutron experiments, as touched on before, is the very high sample mass requirements. This can be hard to achieve in a planar cathode electrode, and thus, there is significant room for further optimization in this area.

Concluding remarks

In situ/*operando* diffraction techniques can provide detailed and accurate information about the crystal structure of the cathode during battery operation, provided the experiment, especially the cell, is carefully designed to obtain reliable information. However, even when the ideal experimental conditions for an *in situ*/*operando* diffraction experiment are met, many candidate next generation cathode materials offer complex structures that are not possible to resolve through conventional diffraction alone. This is due to the disordered nature of the crystal structure of some cathodes, with the likely presence of cation and anion disorder increasing with the complexity of the cathode chemistry and processing conditions. In such cases, other experimental techniques, such as neutron/x-ray imaging, and data analysis techniques, such as atomic pair distribution function (PDF), should be considered. Regardless of the chosen technique, the same considerations for the *in situ*/*operando* experimental design should be taken for high quality data collection.

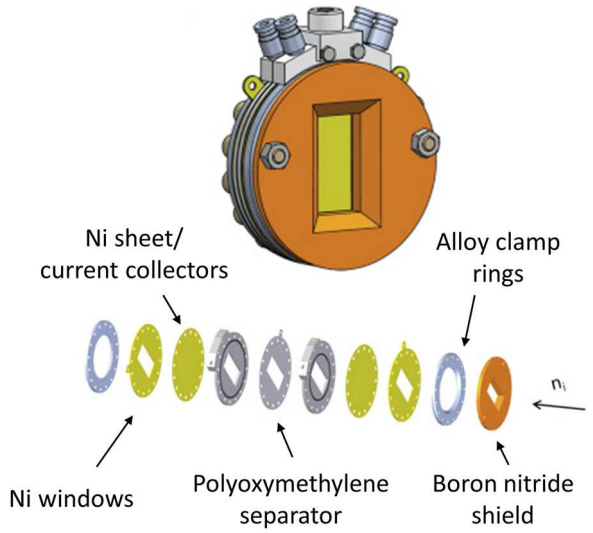

FIG. 13. Diagram of an *in situ* cell used in the POLARIS diffractometer at the ISIS neutron spallation source. Reprinted with permission from Biendicho *et al.*, "New *in situ* neutron diffraction cell for electrode materials," J. Power Sources **248**, 900–904 (2014). Copyright 2014 Elsevier.

B. Understanding the role of disorder

The structural and compositional complexity of cathode materials presents clear challenges for characterization. Many of these difficulties are exacerbated in the presence of disorder—not least because classical crystallographic approaches are inadequate in such cases. Instead, local structure probes, such as NMR and total scattering, are increasingly relied upon in order to provide accurate structural descriptions of cathode materials. Moreover, a complete understanding of the cathode function means characterizing the dynamic processes involved in cycling: the complex phase evolution that occurs during lithium insertion and removal.

In situ and *operando* measurements are designed to replicate as closely as possible the native operating environment in a working battery. Doing so helps identify and track the key phase transformations that occur during battery cycling—including the presence and role of transient phases otherwise hidden from *ex situ* characterization. An excellent example of the state-of-the-art in this respect is the discovery of transient Li_xFePO_4 ($0 < x < 1$) solid solutions that are present during rapid cycling of the commercially important $LiFePO_4$–Li battery. These transient phases subsequently relax to a mixture of stoichiometric phases when charge/discharge is stopped,

giving the false impression that lithium (de)intercalation is a two-phase process.[273] *In situ* synchrotron x-ray powder diffraction patterns played a central role in identifying the importance of these non-equilibrium phases [Fig. 14(a)].

At the same time, there is an increasing realization of the importance of exploiting multiple experimental and computational approaches to develop realistic atomic-scale models of compositionally and structurally complex cathode materials. A recent study of the $Li_xMn_{2-x}O_{2-y}F_y$ disordered rock salt family serves as a topical example. In Ref. 274, Lun *et al.* drew together x-ray and electron diffraction, neutron total scattering, ^{19}F NMR, electron microscopy, voltammetry, x-ray absorption spectroscopy, density functional theory calculations, and Monte Carlo simulations to characterize the local Li, Mn, O, and F arrangements as a function of composition and then to link these distributions to charge capacity. Combinatorial studies such as this currently rely on *ex situ* measurements—often employing different cell environments; ideally, each measurement would be performed under identical conditions.

Complete structural characterization of disordered cathodes involves understanding lithium insertion/extraction mechanisms, which, in turn, requires determining how charge state affects both atomic structure within individual cathode materials and also the relative amounts of different phases. The ubiquity of amorphous and nanoparticulate phases is a clear challenge in this regard, demanding the use of local probes to identify intermediate phases and track their evolution. For example, *operando* x-ray PDF data have been used to identify the different phases present in an iron oxyfluoride electrode during cycling and then to determine the corresponding phase fractions as a function of lithium content [Fig. 14(b)].[275] The PDF analysis, in combination with *ex situ* NMR, showed that the structure of the recharged electrode is different to that of the pristine electrode, even though the discharge capacity is nearly fully recovered upon recharge. The recharged electrode is a complex mixture, comprised of an oxide-rich rock salt phase and fluoride-rich rutile phase. Despite this mechanistic insight, it is still difficult to determine accurate three-dimensional models of the structures of such complex mixtures.

What is becoming increasingly clear is that very rich crystallographic information is required to develop such models for disordered materials. This insight comes from the use of single-crystal diffuse scattering measurements (either x-ray or neutron) of disordered cathode materials that have revealed the presence of highly structured scattering that is extremely difficult to measure in powder samples. In the case of Prussian blue analogs, for example, this scattering characterizes the disordered vacancy networks—these dictate the mass transport pathways (Fig. 15).[276] Likewise in disordered rock salts, the non-random arrangements of transition-metal ions give rise to qualitatively similar scattering.[277] In both cases, there appears to be scope to design and engineer defect networks with specific storage or transport properties. However, the characterization of these disordered networks appears to rely heavily on access to 3D datasets. Since functioning cathode materials are almost universally obtained in powder form, *in situ* and *operando* measurements give one-dimensional data only: a clear challenge to be addressed.

From an experiment design viewpoint, a parallel ongoing challenge is to ensure that complementary *operando* measurements are meaningfully related. Despite best efforts, *operando* and *in*

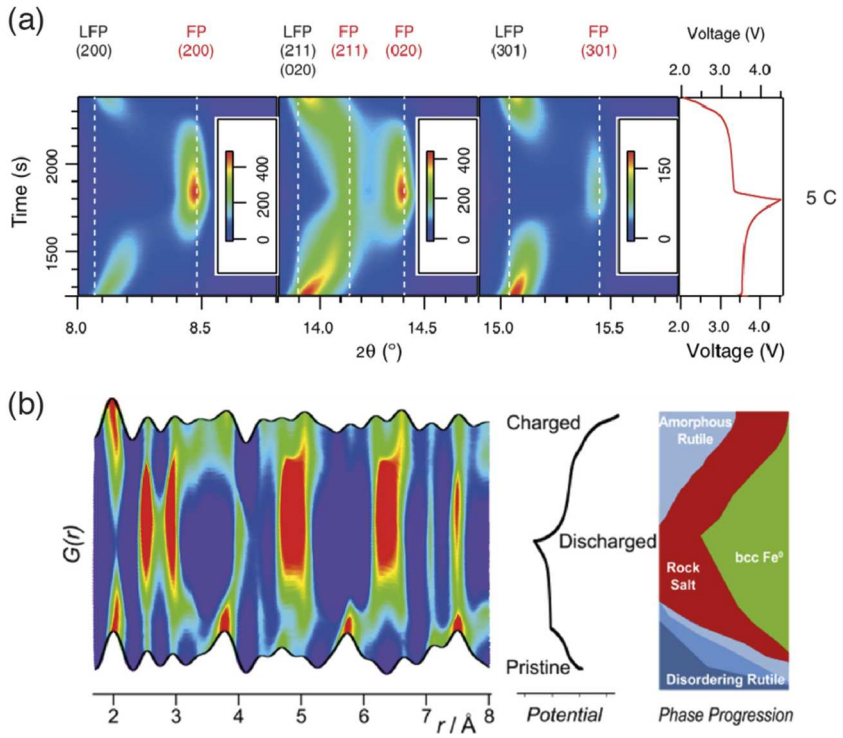

FIG. 14. *In Situ* XRD and *operando* PDF measurements. (a) *In situ* XRD pattern during fast cycling between $LiFePO_4$ (LFP) and $FePO_4$ (FP). The electrochemical reaction proceeds via an intermediate solid solution, which is evident in the diffraction pattern between the LFP and FP states. Dashed lines indicate the peak positions of the $LiFePO_4$ and $FePO_4$ phases.[273] Reprinted with permission from Liu *et al.*, Science **344**, 1252817 (2014). Copyright 2014 AAAS. (b) *Operando* PDF data during charge and discharge for an iron oxyfluoride electrode (left); evolution of Fe phases during cycling (right) determined from analysis of *operando* PDF data.[275] Reprinted with permission from Wiaderek *et al.*, J. Am. Chem. Soc. **135**, 4070 (2013). Copyright 2013 American Chemical Society.

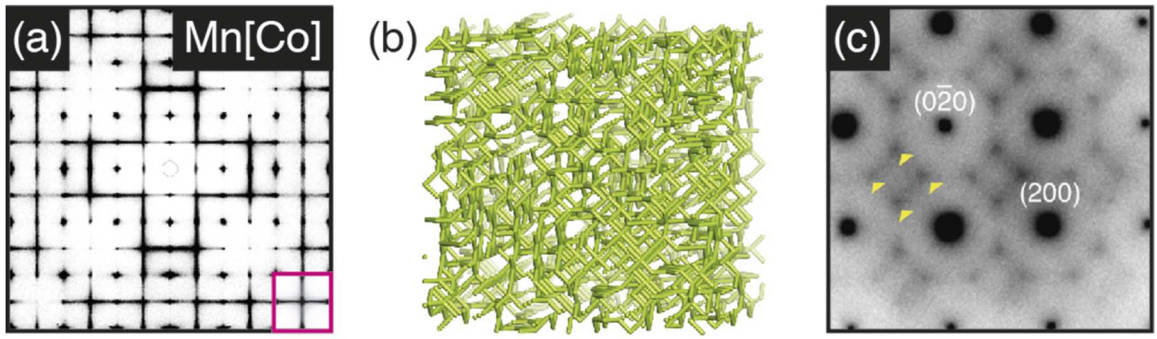

FIG. 15. Single-crystal diffuse scattering measurements of disordered cathodes. (a) Reconstructed single-crystal diffuse scattering for Mn[Co] Prussian blue analog in the (hk0) scattering plane; the bottom-right corner is the averaged diffuse scattering patter in the (hk0) plane. (b) Representative pore network for the Mn[Co] Prussian blue analog in (a), determined from Monte Carlo simulation.[276] (c) Experimental electron diffraction pattern of $Li_{1.2}Mn_{0.4}Zr_{0.4}O_2$ (LMZO) along the zone axis (100). Reproduced with permission from Ji *et al.*, Nat. Commun. **10**, 592 (2019). Copyright 2019 Author(s), licensed under Creative Commons Attribution CC BY 4.0.

situ experimental setups are never perfect and the physical region being probed in any one measurement is not necessarily indicative of the cathode as a whole.[267] As a consequence, due care must be taken when interpreting measurements, perhaps increasingly exploiting computational approaches to draw together measurements that pertain to different length scales. An additional complexity is the relevance of cathode history at the time a given measurement was taken. These various considerations form a significant part of the impetus for developing multiprobe measurement capability.

A good example of such technique development is the combination of *operando* x-ray diffraction and x-ray absorption spectroscopy possible at the B18 beamline at the Diamond Light Source (UK). This beamline has been used, for example, to study long- and short-range structure and electrochemical behavior of a $NiFe_2O_4$/carbon nanotube composite.[278] The bridge to mesoscopic length scales seems all the more tractable given the development of x-ray diffraction computed tomography (XRD-CT).[279–281] By collecting diffraction patterns for a sample in a large number of different orientations and positions, it is possible to obtain a three-dimensional map of diffraction patterns at some fundamental resolution. XRD-CT can track microstructural changes *in situ* while providing a spatially resolved picture of the sample, without the need for a specially designed battery cell.[282] Moreover, this approach has even been extended to PDF computed tomography, which allows the short-range structure and spatial distribution of disordered/complex phases to be determined in a single mixture.[283]

With continually developing experimental techniques and the increasing efficiency with which data can be collected for complex multicomponent systems—including cathodes—there is a growing need for multivariate data analysis techniques that can deconvolute these datasets. Multivariate techniques aim to describe a collection of experimental measurements in terms of fewer components. Principal component analysis (PCA) is perhaps the mostly widely used multivariate technique and has been applied to PDF data obtained for battery materials;[275,284] however, the difficulty of interpreting PCA analyses of experimental measurements, including PDFs, is well recognized.[284] An important development is the application of novel analysis approaches—including non-negative matrix factorization (NMF)—to the interpretation of complex datasets.[285] Our own experience is that NMF can help characterize otherwise unexpected intermediates that arise during cathode cycling—without *a priori* knowledge of their composition or structure.

Finally, as characterization techniques for disordered cathodes develop, it is important that these techniques dovetail with advances in computation. Disordered cathodes are complex, dynamic, multicomponent systems, and so atomistic models are necessarily large. Here, machine learning approaches are helping develop effective potentials with the accuracy of *ab initio* calculations. The reduction in computational expense is dramatic, giving access to large configurations that capture quantitatively both structure and dynamics as probed experimentally, as previously achieved in monatomic systems, such as hard carbon for anode materials (Fig. 16).[286]

Concluding remarks

We are fortunate that as our appreciation for the compositional and structural complexity of cathode materials matures, so too is it that the tools used in their characterization—experimental, analytical, and computational alike—are also developing extremely quickly. That ultimate goal seems ever closer: namely, of developing self-consistent spatially resolved multi-scale models of cathode materials and their variation during battery operation. This represents no small challenge. Not only are cathodes comprised of multiple components, but also those components may be nanoparticulate or amorphous; even the crystalline phases often contain non-trivial compositional or structural disorder. Not only are the materials complex, but so too are the datasets obtained during experimental measurements. For this reason, we attach particular weight to the importance of developing robust data analytical methodologies—such as NMF—that allow this complexity to be reduced in a systematic and model-independent fashion.

C. Establishing diffusion properties

Key to the function of insertion-type cathode materials, especially for high power performance, is the migration of ions through

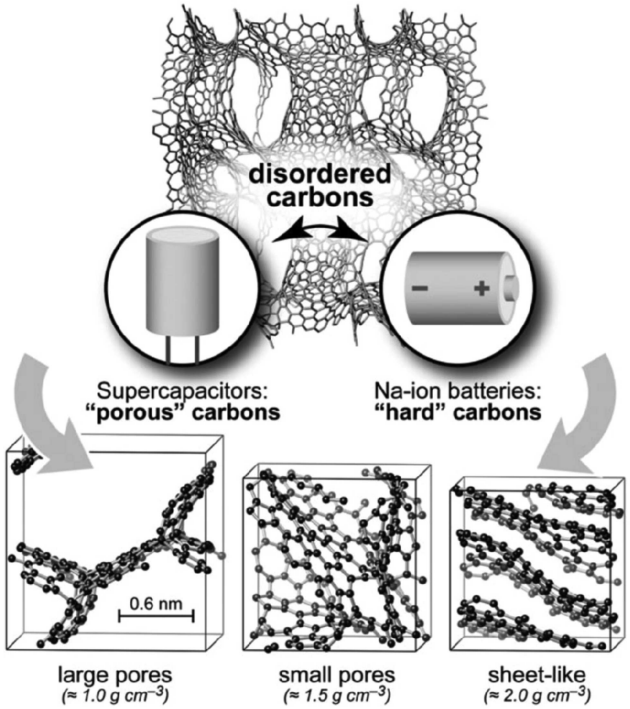

FIG. 16. Machine learning approaches for modeling disordered electrodes. Examples of pore structures in disordered carbons, determined from a combination of machine learning and DFT.[286] Different pore sizes are seen experimentally and are each suited to different applications. Reproduced with permission from Deringer *et al.*, Chem. Commun. **54**, 5988 (2018). Copyright 2018 The Royal Society of Chemistry and Author(s), licensed under Creative Commons Attribution CC BY 3.0.

the solid-state structure. In general, diffusion processes within the solid cathode material are significantly slower than liquid-state diffusion in the electrolyte. Therefore, in the development and optimization of cathode materials, it is important to be able to quantify and understand the solid-state diffusion processes that govern charge and discharge mechanisms.

Some of the most well-established methods for quantifying solid-state diffusion are based on electrochemical measurements, such as electrochemical impedance spectroscopy (EIS)[287,288] and galvanostatic intermittent titration technique (GITT).[289] These techniques have the advantage that they can be carried out using standard electrochemical equipment and directly relate the ion diffusion to the measured current and voltage. However, they also rely on some assumptions about the structure and properties of the electrochemical cell, which must be modeled as an equivalent circuit in order for the diffusion coefficient to be extracted.

An alternative approach to studying solid-state ion diffusion is to utilize a direct structural probe that is sensitive to ionic motion. One such technique is nuclear magnetic resonance (NMR), which is sensitive to solid-state dynamics over a wide range of time scales. Ionic motion on the millisecond–microsecond timescale can be investigated and quantified through two-dimensional exchange experiments[290] or changes in the position or shape of spectral resonances due to motional averaging of magnetic interactions. Faster nanosecond timescale processes can be quantified by measuring changes in the longitudinal spin relaxation (SR) time, which is sensitive to fluctuations of the local magnetic field on the timescale of the Larmor frequency (i.e., $\sim 10^9$ s^{-1}).[291]

Another complementary approach is muon spin relaxation (μSR),[292] which measures the spin polarization of muons implanted into the material of interest via the detection of their positron decay products. In systems where ion dynamics are present on the microsecond timescale, they cause fluctuations of the local magnetic field experienced by the muon modulating the spin polarization, which can be interpreted in terms of a rate constant for the ion hopping process.

From both NMR and μSR, the diffusion coefficient is not obtained directly but can be determined from the precise rate constant for ion hopping that is obtained. Furthermore, variable-temperature measurements of the rate constant enable an activation energy to be obtained for the dynamic process. This can then be correlated with, e.g., diffraction structures and theoretical simulations to determine ion migration pathways.

As efforts continue to increase the capacity and decrease the cost of the cathode, it remains important to ensure that new materials retain a high diffusion rate throughout the accessible charge window. This relies on understanding processes ranging from atomic scale hopping between sites, through grain boundaries and interfaces within the particles, to the interfaces formed with the electrolyte, all as a function of the charge state of the cathode.

At the atomic scale, recent measurements have started to uncover how different ion hopping processes can occur within the same material. One of the early kinetic Monte Carlo studies of $LiCoO_2$[293] identified two hopping mechanisms, Tetrahedral Site Hop (TSH) and Oxygen Dumbbell Hop (ODH), with the latter having a larger energy barrier to motion. The presence of two distinct process in Ni-rich NCA materials has recently been identified with *ex situ* μSR measurements,[294] with a fourfold difference in energy barriers in excellent agreement with the prediction. The lower-energy barrier process is less clearly evident in $LiCoO_2$ and lower Ni-content materials. An open question is whether particular transition metal combinations act to favor the TSH process and thereby improve the diffusion properties at the atomic scale.

Another area where further understanding can be derived at the atomic level is in cathode phases that only form during the charging or discharging process. The development of *operando* cells for NMR and μSR allow these to be investigated. Questions that are relevant in this area are often related to the structure including accessible pathways and distortions on changing site occupancy.

Understanding ionic motion at grain boundaries and interfaces is considerably more challenging since they represent small volumes within the cell or material but can be the dominant restrictions on the motion of ions within a cell. There are two approaches to this challenge. Since bulk probes, such as impedance spectroscopy, are sensitive to the greatest restrictions to motion within the cell, differences with the results of local probe measurements are likely to be due to grain boundaries or interfaces. The alternative is to artificially expose or replicate the interface to use surface sensitive local probes, appropriate for controlled interfaces such as those in core–shell nanoparticles, or increasing its size to

increase signal contribution, which can work for cathode–electrolyte interfaces.

Since individual probes of diffusion are generally unable to obtain a full picture of a material or its behavior within a cell, it is vital to combine multiple techniques within a study and also use theoretical modeling to understand how different pieces of information reflect the full picture.

In situ and *operando* measurements with local probes are well-suited to coupling with techniques that provide bulk measurements; for instance, where impedance spectroscopy can be carried out at the same time. Developments in this area will focus on improving the signal from *in situ* cells and enabling faster *operando* measurements.

For NMR spectroscopy, a number of *in situ* cell designs exist, with the plastic bag cell and plastic capsule cells being the most popular [Figs. 17(a) and 17(b)]. These cells are based on a conventional layered battery structure but are adapted to fit within the ~10 mm diameter NMR detection coil and also feature free standing electrodes and mesh current collectors to allow penetration of radiofrequency pulses into the sample.[295] Compared to the diffraction cells described above, *in situ* NMR cells typically offer limited rate performance due to the thicker electrodes used, and difficulties in maintaining consistent pressure in the cells. Another ongoing challenge is to make these cell designs compatible with variable-temperature conditions while maintaining sufficient signal sensitivity and battery performance.

For μSR, *in situ* cells are at an earlier stage in their development but are already being applied to questions in cathodes and solid-state electrolytes.[296] Similar to the neutron diffraction cell described above, the coin cell design is ideally suited to the experimental geometry [Fig. 17(c)]. Specific layers in the cell can be investigated through control of the muon implantation depth and choice of the layer thicknesses. Advantages over NMR include the ability to use different metal foils as current collectors and the ease of variable temperature measurements. Cells used for NMR are typically <10 mm, limited by the detection coil diameter, those typically used for x-ray measurements are in the range 10–20 mm, cells for both muon (~20 mm) and neutron (~40 mm) are both sized to ensure a large fraction of the beam is incident on the active material. All these techniques are amenable to cells with a coin cell geometry, with some other geometries used in special cases.

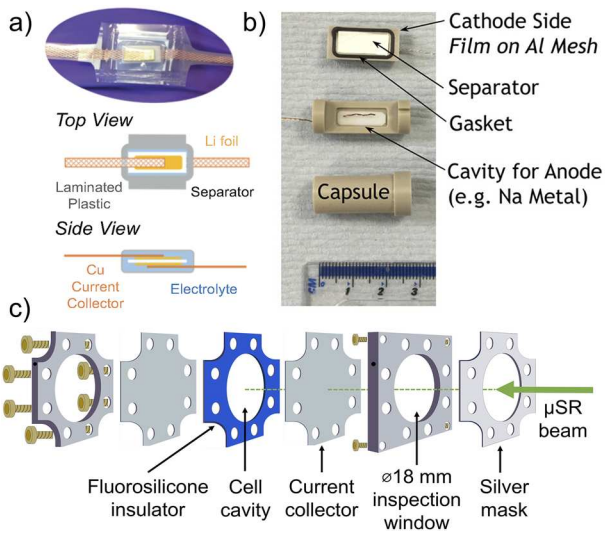

FIG. 17. (a) NMR bag cell. (b) NMR capsule cell. [Adapted with permission from Pecher *et al.*, Chem. Mater. **29**, 213 (2017). Copyright 2017 American Chemical Society and Author(s), licensed under Creative Commons CC BY 4.0.] (c) μSR cell.

Diffusion measurements on novel cathode materials need to work hand-in-hand with theoretical modeling to maximize the information derived from them. Further work on specific materials to identify diffusion pathways, estimate energy barriers, and understand defects will improve the understanding of new materials. More general questions about how the ionic motion affects the probes used to investigate it may also be able to increase the information derived from particular experiments, whether that is in terms of how correlated the ionic motion is or whether different pathways can be better distinguished in the data.

Concluding remarks

Consistent measurements of diffusion using multiple techniques are now well-established and ready for use in understanding new cathode materials. However, a key consideration is that the choice of technique will necessarily depend on the material properties and the relevant diffusion time scales. Recent work combining multiple techniques has provided a more complete picture of how ions move on different length and time scales in materials.

In situ and *operando* measurements with local probes are developing rapidly to probe materials at intermediate stages of charge but challenges remain in optimizing the cell design, and ensuring that the cells compatible with these techniques provide a realistic model of commercial cells.

Finally, as the theoretical and experimental understanding of diffusion in cathode materials improves, this information can hopefully be used to inform rational materials design, among the numerous other inputs to that process.

D. Characterization of interfaces

As discussed in Sec. IV C, the CEI layer, either artificially added to protect the surface of the cathode, or formed *in situ* through reaction with the electrolyte, can be critical to maintaining high performance or safety of the cell during operation. The low volume fraction of the CEI layer and the buried nature of the interface with the cathode make it highly challenging to measure using the bulk techniques described above. Here, we highlight some key areas of technique development in this field being used to target the interface specifically to glean fundamental insights both computationally and experimentally.

1. Using DNP NMR spectroscopy to probe surfaces and interfaces in batteries and battery materials

Fully understanding structures and processes at interfaces is crucial to the advancement of battery research. However, these can be challenging to probe as they make up a small proportion of the sample and are often complex and disordered in nature.

As solid-state NMR spectroscopy is a versatile, non-destructive technique with no requirement for long-range order, it has the potential to provide valuable insight into such interfaces. Unfortunately, intrinsic sensitivity limits can prove challenging to overcome. Recently, dynamic nuclear polarization (DNP) has emerged as a powerful technique for sensitivity enhancement in NMR experiments. In DNP, polarization is transferred from an unpaired electron to surrounding nuclear spins at cryogenic temperatures. This technique is extremely promising for studying surfaces and interfaces, which, without enhancement, may be impossible to observe using conventional NMR spectroscopy. Hence, it has recently gained interest in a number of research areas.[297–299]

Typically, unpaired electrons are introduced to the system via a solution of organic radicals, e.g., TOTAPOL,[300] which is added to the powdered solid sample. As the radical is external to the sample of interest, the polarization spreads from the surface of the particles into the bulk. As a result, DNP experiments can provide surface-selective enhancement. For example, the first three surface layers of CeO_2 nanoparticles can be probed using ^{17}O MAS-DNP NMR experiments.[301] Additionally, DNP experiments have been used to study the solid electrolyte interphase (SEI) layer that forms on reduced graphene oxide and silicon anodes.[302,303] However, despite its promise, DNP has its limitations. Most notably, the addition of the radial solution may alter the system, which may be problematic for reactive or unstable samples such as battery electrodes. Recently, alternative approaches have been developed, such as introducing paramagnetic ions as dopants into the bulk of the sample, allowing polarization to be transferred directly to neighboring nuclei. Using this approach, ^{17}O MAS-DNP NMR data have been acquired for anode materials, including $Li_4Ti_5O_{12}$ and $Li_2ZnTi_3O_8$, without costly isotopic enrichment.[304,305] Recently, DNP has allowed observation of the interface between the SEI that is deposited onto lithium metal anodes during cycling. The selective enhancement of this interface was achieved by utilizing the metallic electrons with the lithium metal as the polarization source.[306] The increased sensitivity afforded by DNP is extremely encouraging and provides an exciting opportunity to probe cathode-related interfaces, which, in turn, is promising for the advancement of battery research.

2. The application of total scattering measurements to interfaces in cathode materials

Pair distribution function (PDF) methods are well suited to studying nanostructures such as interfaces. The PDF is essentially a weighted histogram of interatomic separations and is sensitive to both short- and long-range correlations. PDFs of multicomponent systems are usually considered in terms of the individual component PDFs.[284] This is the basis of the widely used "differential PDF" approach that has been used to study host–guest systems, surface structures, and thin films.[307–312] Yet, this interpretation remains an approximation because it assumes that the interface contribution can be neglected. In a recent proof-of-concept study, non-negative matrix factorization (NMF) has been used to extract the interface contribution to the PDF—the iPDF.[313] This approach allows for the structure of the interface to be studied directly from the iPDF and is not restricted to surface structures (i.e., buried interfaces can be studied). There is scope for these approaches to be applied to the study of interfaces in cathode materials, such as coatings/thin films, and also buried interfaces, such as CEI.[314,315]

3. Low energy muons to probe variations in Li diffusion properties

Much as Li diffusion in the bulk of cathode materials can be probed used muon spectroscopy (Sec. V C), the ionic motion in thin films can be probed using low energy muon spectroscopy. To make low energy muons a conventional, "surface," a muon beam of energy ~4 MEv is slowed down in a cryogenic moderator and then reaccelerated to 1–20 keV using electric fields.[316] This reduces the implantation depth from 100(50) μm in the conventional experiment to a controllable 10–200 nm with a spread of depths around half the implantation depth.

By reducing the implantation depth, a whole new range of problems can be addressed if they can be replicated in the form of thin films. Boundaries between different cathode materials, the cathode–electrolyte interface, and thin film batteries can be investigated at specific depths within the structure and are amenable to investigation with low energy muons.

4. AIRSS structure prediction and machine learning approaches to complex interfaces

Despite the continued success and development of novel techniques to probe the interfaces, no current method is able to give a full picture of the structure of the interface, especially when it comes to the atomic scale. In this context, computational methods can facilitate the understanding of the structure of the complex interfaces. A few tools to date have been developed or are being developed in this context.

(a) DFT for interfacial thermodynamics: Despite the complex nature of interfaces, the interfacial reaction product is usually reflected by the thermodynamic equilibrium. Since thermodynamic properties of materials can be calculated using first principle methods such as DFT, by considering large number of possible reaction products, one can locate the most likely interfacial structure. This method has been widely used in the area of solid-state batteries, cathode coating, and electrolyte–cathode interfaces. By screening a large number of possible reaction products, the material with the applicable thermodynamic electrochemical window can be selected. However, it is important to note that such an approach relies solely on thermodynamics and fails to account for the kinetic aspects that are often crucial in determining the local structure.

(b) Molecular dynamics simulations: The local structure of an interface is highly dependent on the kinetics of the interfacial reactions, so molecular dynamics simulations can be applied to mimic the atomic motion at the interface. This technique assumes that the atomic nuclei are Newtonian particles and that their motion can be modeled using Newton's equations. For example, Fig. 18, shows the *ab initio* molecular dynamics simulations of a Mn oxide|electrolyte interface and the decomposition process of the solvent.[317] However, the complexity and the large spatial and temporal scales can limit the

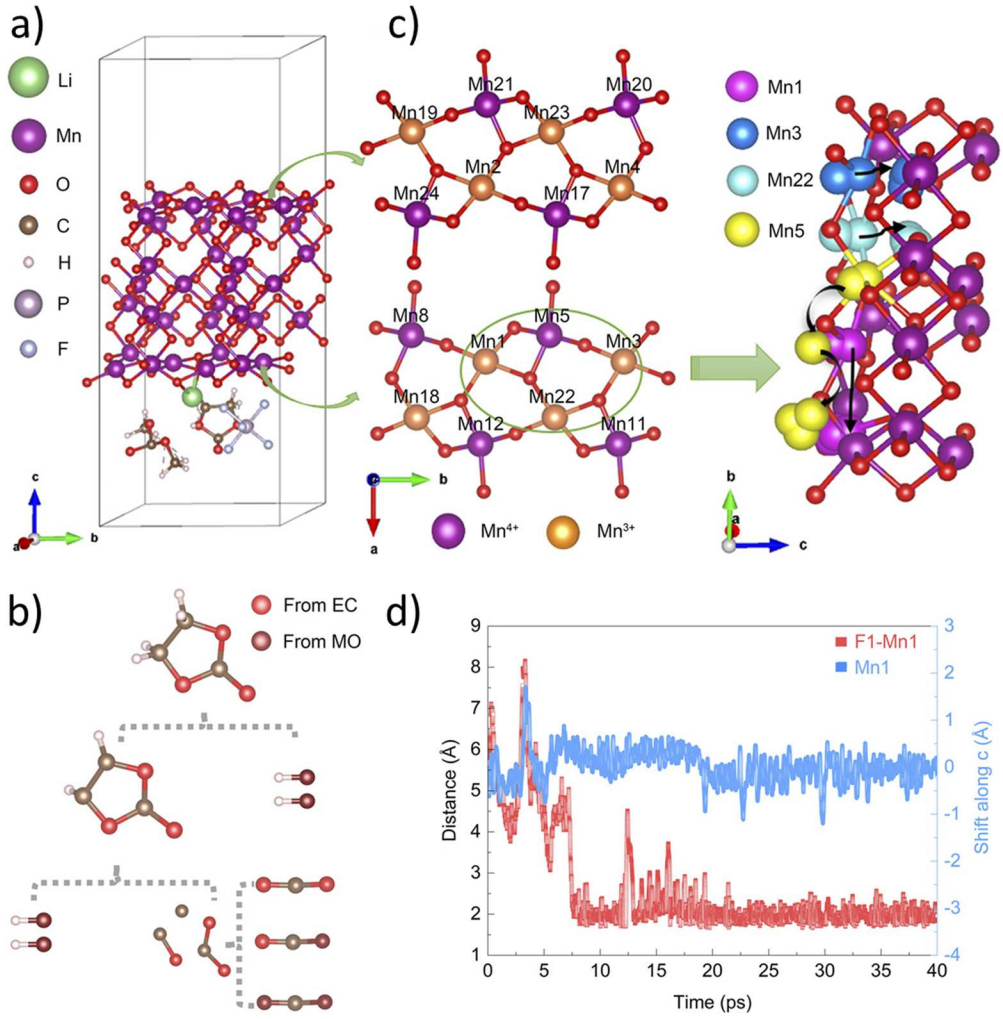

FIG. 18. The dissolution processes of Mn in Mn oxides based on *ab initio* molecular dynamics (AIMD). (a) The cathode–electrolyte interface model includes Mn oxide's (110) slab and electrolytes (EC, DMC, and $LiPF_6$). (b) The stepwise oxidative decomposition process of EC molecules. (c) Mn ions with different valence states at the interface layer. Synergistic movement of Mn^{4+} (Mn5) and its surrounding Mn^{3+} (Mn1, Mn3, and Mn22). (d) Interaction between F^- from $LiPF_6$ and surface Mn ion. F^- has negligible effect on Mn dissolution. Reprinted with permission from Zhou *et al.*, J. Phys. Chem. Lett. **11**, 3051 (2020). Copyright 2020 American Chemical Society.

accuracy. Usually, the accuracy of molecular dynamics simulations are highly dependent on the description of the interatomic potentials. To achieve a reasonable result for complex interfaces, density functional theory usually needs to be used as an engine to evaluate the forces. This limits the simulation cell to hundreds of atoms and the simulation time to hundreds of picoseconds. Machine learning-based approaches have been developed to resolve such issues.

(c) Crystal structure predictions: While molecular dynamics simulations offer a method to sample the interface structure. The phase space is usually not well sampled due to the limited simulation time and the choice of simulation temperature. In this context, direct sampling of the interfacial structure within a much broader structural space is possible via crystal structure prediction methods such as *ab initio* random structure searching (AIRSS) described in detail in Sec. III F.[167,168] The AIRSS approach can be applied to interfaces between cathode materials and surface coatings, for example, the interface between the spinel LNMO and alumina (Al_2O_3) (Fig. 19). The different local structures can have significantly different energies, and this can be a useful method to promote candidate structures. The determination of the actual solution needs to be determined in combination with experimental characterization of the real system.

(d) Machine learning and new advancements: As mentioned previously, both molecular dynamics simulations and crystal structure predictions are methods to sample potential atomic structures of interfaces. However, both methods are bottlenecked by the accuracy and efficiency of the force engines,

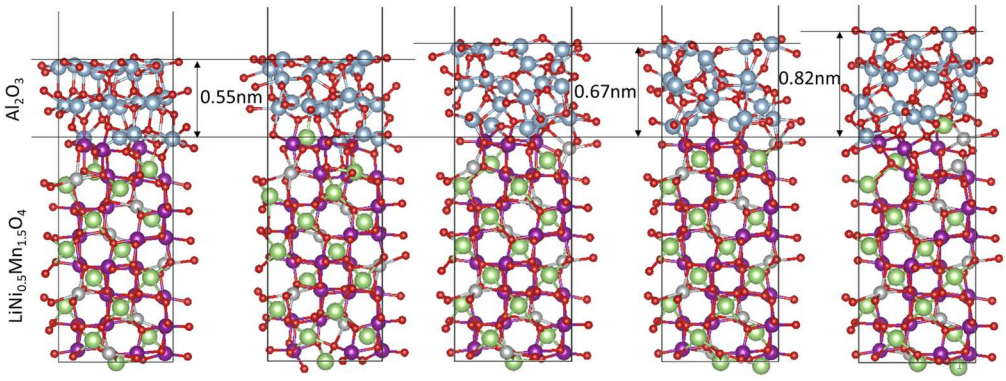

FIG. 19. AIRSS search results on the interfacial structure between Al_2O_3 and $LiNi_{0.5}Mn_{1.5}O_4$.

with DFT not currently efficient enough to handle the large scale models required to describe an interface. One way to resolve this issue is to train machine learning forcefields.[318] Using a number of different models, such as neural networks, one can mimic the highly non-linear solution of quantum mechanical DFT using a set of explicit functions that are much faster to evaluate. Using such a method, one can efficiently model systems up to millions of atoms.[319,320] This area is relatively new, but it does show significant promise with exciting applications likely in the near future.

E. Mechanical strength properties and testing

Substantial research efforts are presently directed toward new cathode materials that are capable of enhancing LIB performance and extending their service life. Mechanical phenomena such as cathode particle fracture have been observed using advanced microscopy techniques[321] and are thought to be relevant to cathode performance and degradation.[322] Micromechanical models of cathode particles that aim to predict the stress state within them over the charge cycle[323,324] have been developed to aid the advancement of new cathode architectures and employ measured values of cathode material mechanical properties as inputs. The dependence of the cathode mechanical properties upon microstructural features, such as primary particle size and internal porosity,[324,325] has also been investigated with mechanical tests. The effects of the state of charge and multiple charge/discharge cycles upon the hardness, modulus, and fracture strength of cathode particles have also been quantified[326,327] with experiments. The accurate measurement of cathode mechanical properties is thus important in the pursuit of new cathode materials and architectures.

Experimental techniques used to measure the mechanical properties of cathode materials include indentation testing, biaxial flexure, and particle compression. Indentation tests are performed by pressing a pyramid-shaped diamond tip into the sample surface with a specified load. After the removal of the indentation tip from the sample surface, the area of the indentation mark left by the indentation tip is used to determine the hardness. The Young's modulus may be calculated from measurements of the contact stiffness between the sample and indentation tip,[328] and measurements of fracture toughness are derived from the lengths of cracks that grow from the corners of indentations made with pyramid-shaped tips.[329] Two methods have been used to characterize the fracture strength of cathode materials: biaxial flexure tests have been performed on macroscopic sintered specimens,[325] and uniaxial compression tests on polycrystalline secondary particles have provided an estimation of secondary particle fracture strength.[327] Together, the testing techniques described above allow for the measurement of mechanical properties within individual primary particles, secondary particles, and macroscopic specimens.

Together, these testing techniques allow for the measurement of mechanical properties within individual primary particles, secondary particles, and macroscopic specimens. The measured mechanical properties of cathode active materials are within the range of other brittle ceramics. The Young's modulus, hardness, and fracture toughness of polycrystalline NMC532 secondary particles are 143 ± 11 GPa, 8.3 ± 1.3 GPa, and 0.10 ± 0.03 MPa $m^{1/2}$, respectively.[326] The measured fracture strength of NMC111 secondary particles is below 300 MPa.[327] This strength is less than 1/30th of their hardness, as their low toughness of about 0.1 MPa $m^{1/2}$ leads to brittle behavior.[326] Measurements reported in the literature for the olivine cathode material $LiCoPO_4$[330] and layered $LiCoO_2$[331] inform that their mechanical properties lie within an order of magnitude of those measured for ternary $NMC_{x,y,z}$ samples.

The mechanical properties of NMC secondary particles have been measured as a function of their state of charge and charge–discharge history, revealing that their Young's modulus, hardness, fracture strength, and fracture toughness all decrease upon delithiation and as a consequence of electrochemical cycling.[326,327] Finite element simulations suggest that this softening within the secondary particles may decrease the internal stresses that develop within them during charge and discharge.[323] Images of polycrystalline secondary particles from cathodes subjected to electrochemical cycling have revealed the development of fractures within and between primary particles,[263] and dislocation networks are observed in secondary particles subjected to multiple charge/discharge cycles.[324] A full understanding of the origin of softening during delithiation and after cycling is yet to be obtained—softening may arise due to the formation of internal cracks or, alternatively, may arise as a consequence of variation in

the composition of the primary particles brought about by delithiation or other processes. Experiments that measure the mechanical properties of primary particles or single crystal cathode particles as a function of their state of charge are now needed to provide inputs for models that can determine the cause of softening measured after delithiation or after the application of multiple charge–discharge cycles.

When examining the influence of cycling on cathode materials, a key property in many current cathode materials, including the atomic lattices of olivine and layered cathode materials, is their anisotropy. The anisotropy gives rise to anisotropic strains within the lattices during cycling, yet the effects of the anisotropy upon the mechanical properties of the primary particles are largely unexplored. Recent measurements have shown that the fracture toughness of $LiCoO_2$ primary particles varies depending on the direction of testing relative to the lattice orientation,[331] yet the anisotropic moduli, hardness, and yield strengths of the layered and olivine cathode material lattices are yet to be measured at the time of writing. Observations of fracture within primary particles[332] have led to suggestions that mechanical cracking may still occur within single crystal cathode architectures; the characterization of elastic constants within single crystals of anisotropic cathode materials is now needed to provide inputs to models for the prediction of stresses during electrochemical cycling. Indentation testing techniques have been developed to measure the properties of anisotropic crystals[333] with indentation and could be applied to olivine and layered cathode materials across the states of charge.

In addition to experimental measurements of mechanical properties, predicting mechanical damage within cathode particles relies upon the development of models that capture the physical origin of stress brought about in charge and discharge. At the basis of these models lie assumed relationships between state of charge, diffusivity, and mechanical properties.[323]

Early predictive models for the stress state within cathode particles assumed that diffusion could be modeled accurately without consideration of mechanical stresses and that the stresses simply followed from the distribution of charge and resultant lattice strain. More recently, coupled relationships between diffusivity and stress have since been adopted for use in simulation,[323] and the variation of lithium-ion mobility with the state of charge has been measured for NMC811 cathodes.[334] The effect of any variation in cathode material modulus, hardness, and toughness with the state of charge remains to be studied. At present, assumed relationships between the distribution of stress, state of charge, and diffusivity within cathode particles lack experimental confirmation, offering an opportunity to scientists for further experimental study and characterization. Such experiments may rely upon new methods for sample preparation and require mechanical tests on cathode particles to be performed within the cell environment.

To date, *in situ* experimental techniques capable of measuring stress and strain during charge and discharge have been developed to study the mechanical properties of porous cathode composites, coated upon foil substrates to form electrodes. By measuring the bending of the electrode structure, strains in the cathode composite due to swelling can be deduced.[335] Considerable scope remains for the development of experimental tests capable of measuring and applying stresses at the particle level within the *in situ* environment; these, in turn, may rely upon the development of new sample fabrication techniques and experimental methods.

Concluding remarks

Mechanical tests have revealed that polycrystalline cathode particles are elastic brittle in tension and that their modulus, hardness, fracture toughness, and fracture strength all vary with electrochemical cycling and their state of charge. It remains to identify the origin of softening upon delithiation and cycling and to further the development of predictive models for cathode particle fracture that are of use to cathode designers. Anisotropy in the mechanical properties of primary particles, the variation in their mechanical properties during cycling, and the relationships between the state of charge, diffusivity, and mechanical stress are all topics for future experimentation. Test methods exist for the characterization of anisotropic crystals and for pre-charging specimens prior to measurement of their mechanical properties, whereas measurement of the relationships between stress, state of charge, and diffusivity may require the development of new experimental techniques capable of imposing a combination of mechanical and electrochemical loads.

VI. CONCLUSIONS AND OUTLOOK

Li-ion cells are likely to remain the dominant battery technology in the short to medium term, with further promising alternatives, such as Li-metal, solid-state, and Na or Mg cells, requiring more development. For the progression of Li-ion performance, cathode materials improvements are needed to achieve targets such as EV ranges in excess of 300 miles and high-rate capability for rapid recharging to 80% capacity and to achieve cost parity with ICE vehicles. Alongside performance developments, much can still be done in terms of the sustainability of the raw materials required, improved yields and lower energy processing through alternative synthesis routes, and improved recyclability and use of recycled raw materials.

As the materials and processes reach maturity causing a bottoming out of the cost of the cathode, further developments will be driven through materials that are competitive in terms of price but where the performance wins out. In terms of present day, lithium iron phosphate (LFP) cathodes have been able to reach a point where the costs have been minimized for a performance that nears the theoretical capacity of the cell. While further improvements in materials costs and processing can be achieved, performance quickly becomes the key driver in terms of $/kWh. Further increases in the Ni content of layered transition metal oxides are likely to provide the majority of performance increases in the next five years, with a key focus on the removal of Co to improve supply chain stability and cost and to address challenges in material abundance. This supply chain can be tempered by recycling of first-generation electric vehicle batteries to reduce the new raw materials requirements. Beyond LNO, further energy density improvements can be sought through Li-rich species, along with transitions to Mn based disordered rock salts or spinels. The increased abundance and reduced toxicity of Mn, coupled with the high initial energy densities reported, offer significant promise. In both cases, a full understanding of the anion redox contribution and methods to stabilize this approach will be key.

The development of brand-new materials classes will require much greater time for computational and experimental effort, along

with advanced characterization techniques, such as those discussed within this piece in order to gain the fundamental understanding needed to optimize performance. However, the chemical space available remains largely underexplored, and advances in knowledge and understanding, along with computational and characterization improvements, will continue to contribute to progress in this area. As demonstrated, the development of next generation cathodes encompasses numerous disciplines and involves considerations of materials across length scales, including local structure, morphology of the primary and secondary particles, and electrode consolidation. There remain further complexities for optimized battery performance and life cycle at the full cell and pack level, including thermal stability for safe operation and good recyclability of the components, which must also be considered. With the current focus on batteries in science and industry, along with the density of researchers involved, it is likely that numerous viable technologies will emerge, offering solutions that can be targeted to the specific application to aid in decarbonization and the removal of fossil fuels from our energy systems.

ACKNOWLEDGMENTS

This work was supported by the Faraday Institution projects FutureCat (Grant No. FIRG017) and Degradation (FIRG001). I.M.C. acknowledges the ISIS Neutron and Muon facility for a Facility Development Studentship. We acknowledge present collaborators: Dr. Anita Blakeston, Jiayi Cen, Ryan Emmett, Lavan Ganeshkumar, Dr. Gareth Hinds (NPL), Dr. Xiao Hua, Katja Kress, Adam Lovett, Suraj Mahato, Sarah McKinney, Dr. Nina Meddings (NPL), Dr. Glen Murray, Liam Nagle-Cocco, Elinor Noble, James Nohl, Dr. Juyeon Park (NPL), Chirag Patel, Dr. Stephen Price (Finden Ltd.), Dr. Cornelia Rodenburg, Dr. Enrique Sanchez Perez, Xiaoqun Shi, Katherine Steele, Josie-May Whitnear, and Aysen Zerey.

AUTHORS' CONTRIBUTIONS

S.G.B. and A.J.N. contributed equally to this work.

DATA AVAILABILITY

Data sharing is not applicable to this article as no new data were created or analyzed in this study.

REFERENCES

[1] K. Mizushima, P. C. Jones, P. J. Wiseman, and J. B. Goodenough, Solid State Ionics **3–4**, 171 (1981).
[2] T. Ohsaki, T. Kishi, T. Kuboki, N. Takami, N. Shimura, Y. Sato, M. Sekino, and A. Satoh, J. Power Sources **146**, 97–100 (2005).
[3] N. Yabuuchi and T. Ohzuku, J. Power Sources **119–121**, 171–174 (2003).
[4] Y. W. Tsai, B. J. Hwang, G. Ceder, H. S. Sheu, D. G. Liu, and J. F. Lee, Chem. Mater. **17**, 3191 (2005).
[5] N. Yabuuchi, Y. Makimura, and T. Ohzuku, J. Electrochem. Soc. **154**, A314 (2007).
[6] W. Li, E. M. Erickson, and A. Manthiram, Nat. Energy **5**, 26 (2020).
[7] M. Bianchini, M. Roca-Ayats, P. Hartmann, T. Brezesinski, and J. Janek, Angew. Chem., Int. Ed. **58**, 10434 (2019).
[8] L. Mu, Z. Yang, L. Tao, C. K. Waters, Z. Xu, L. Li, S. Sainio, Y. Du, H. L. Xin, D. Nordlund, and F. Lin, J. Mater. Chem. A **8**, 17487 (2020).
[9] F. Lin, I. M. Markus, D. Nordlund, T.-C. Weng, M. D. Asta, H. L. Xin, and M. M. Doeff, Nat. Commun. **5**, 3529 (2014).
[10] L. Liang, W. Zhang, F. Zhao, D. K. Denis, F. u. Zaman, L. Hou, and C. Yuan, Adv. Mater. Interfaces **7**, 1901749 (2020).
[11] H. Li, A. Liu, N. Zhang, Y. Wang, S. Yin, H. Wu, and J. R. Dahn, Chem. Mater. **31**, 7574 (2019).
[12] Q. Xie, W. Li, and A. Manthiram, Chem. Mater. **31**, 938 (2019).
[13] H. Li, P. Zhou, F. Liu, H. Li, F. Cheng, and J. Chen, Chem. Sci. **10**, 1374 (2019).
[14] M. Guilmard, L. Croguennec, D. Denux, and C. Delmas, Chem. Mater. **15**, 4476 (2003).
[15] U.-H. Kim, D.-W. Jun, K.-J. Park, Q. Zhang, P. Kaghazchi, D. Aurbach, D. T. Major, G. Goobes, M. Dixit, N. Leifer, C. M. Wang, P. Yan, D. Ahn, K.-H. Kim, C. S. Yoon, and Y.-K. Sun, Energy Environ. Sci. **11**, 1271 (2018).
[16] H.-H. Ryu, G.-T. Park, C. S. Yoon, and Y.-K. Sun, J. Mater. Chem. A **7**, 18580 (2019).
[17] C. S. Yoon, U.-H. Kim, G.-T. Park, S. J. Kim, K.-H. Kim, J. Kim, and Y.-K. Sun, ACS Energy Lett. **3**, 1634 (2018).
[18] H. Xie, K. Du, G. Hu, Z. Peng, and Y. Cao, J. Phys. Chem. C **120**, 3235 (2016).
[19] M. Chen, E. Zhao, D. Chen, M. Wu, S. Han, Q. Huang, L. Yang, X. Xiao, and Z. Hu, Inorg. Chem. **56**, 8355 (2017).
[20] T. Weigel, F. Schipper, E. M. Erickson, F. A. Susai, B. Markovsky, and D. Aurbach, ACS Energy Lett. **4**, 508 (2019).
[21] L. Mu, R. Zhang, W. H. Kan, Y. Zhang, L. Li, C. Kuai, B. Zydlewski, M. M. Rahman, C.-J. Sun, S. Sainio, M. Avdeev, D. Nordlund, H. L. Xin, and F. Lin, Chem. Mater. **31**, 9769 (2019).
[22] C. Li, H. P. Zhang, L. J. Fu, H. Liu, Y. P. Wu, E. Rahm, R. Holze, and H. Q. Wu, Electrochim. Acta **51**, 3872 (2006).
[23] M. K. Shobana, J. Alloys Compd. **802**, 477 (2019).
[24] X. Meng, X.-Q. Yang, and X. Sun, Adv. Mater. **24**, 3589 (2012).
[25] W. Zhu, X. Huang, T. Liu, Z. Xie, Y. Wang, K. Tian, L. Bu, H. Wang, L. Gao, and J. Zhao, Coatings **9**, 92 (2019).
[26] D. Mohanty, K. Dahlberg, D. M. King, L. A. David, A. S. Sefat, D. L. Wood, C. Daniel, S. Dhar, V. Mahajan, M. Lee, and F. Albano, Sci. Rep. **6**, 26532 (2016).
[27] D. Aurbach, K. Gamolsky, B. Markovsky, G. Salitra, Y. Gofer, U. Heider, R. Oesten, and M. Schmidt, J. Electrochem. Soc. **147**, 1322 (2000).
[28] L. E. Downie, S. R. Hyatt, and J. R. Dahn, J. Electrochem. Soc. **163**, A35 (2016).
[29] Y. Lee, T. K. Lee, S. Kim, J. Lee, Y. Ahn, K. Kim, H. Ma, G. Park, S.-M. Lee, S. K. Kwak, and N.-S. Choi, Nano Energy **67**, 104309 (2020).
[30] W. Li, A. Dolocan, J. Li, Q. Xie, and A. Manthiram, Adv. Energy Mater. **9**, 1901152 (2019).
[31] J. Li, H. Liu, J. Xia, A. R. Cameron, M. Nie, G. A. Botton, and J. R. Dahn, J. Electrochem. Soc. **164**, A655 (2017).
[32] W. J. Lee, K. Prasanna, Y. N. Jo, K. J. Kim, H. S. Kim, and C. W. Lee, Phys. Chem. Chem. Phys. **16**, 017062 (2014).
[33] K. Xu, Chem. Rev. **104**, 4303 (2004).
[34] G. Qian, Y. Zhang, L. Li, R. Zhang, J. Xu, Z. Cheng, S. Xie, H. Wang, Q. Rao, Y. He, Y. Shen, L. Chen, M. Tang, and Z.-F. Ma, Energy Storage Mater. **27**, 140 (2020).
[35] Z. Xu, Z. Jiang, C. Kuai, R. Xu, C. Qin, Y. Zhang, M. M. Rahman, C. Wei, D. Nordlund, C. J. Sun, X. Xiao, X. W. Du, K. Zhao, P. Yan, Y. Liu, and F. Lin, Nat. Commun. **11**, 83 (2020).
[36] J. Kim, H. Lee, H. Cha, M. Yoon, M. Park, and J. Cho, Adv. Energy Mater. **8**, 1702028 (2018).
[37] X. Fan, G. Hu, B. Zhang, X. Ou, J. Zhang, W. Zhao, H. Jia, L. Zou, P. Li, and Y. Yang, Nano Energy **70**, 104450 (2020).
[38] H. Cha, J. Kim, H. Lee, N. Kim, J. Hwang, J. Sung, M. Yoon, K. Kim, and J. Cho, Adv. Mater. **32**, 2003040 (2020).
[39] Y. Kim, ACS Appl. Mater. Interfaces **4**, 2329 (2012).
[40] Y. Bi, J. Tao, Y. Wu, L. Li, Y. Xu, E. Hu, B. Wu, J. Hu, C. Wang, J.-G. Zhang, Y. Qi, and J. Xiao, Science **370**, 1313 (2020).
[41] J. Zhu and G. Chen, J. Mater. Chem. A **7**, 5463 (2019).
[42] H. Li, J. Li, N. Zaker, N. Zhang, G. A. Botton, and J. R. Dahn, J. Electrochem. Soc. **166**, A1956 (2019).

[43]J. Langdon and A. Manthiram, Energy Storage Mater. **37**, 143 (2021).
[44]Z. Lu, D. D. MacNeil, and J. R. Dahn, Electrochem. Solid-State Lett. **4**, A191 (2001).
[45]S. Hy, H. Liu, M. Zhang, D. Qian, B.-J. Hwang, and Y. S. Meng, Energy Environ. Sci. **9**, 1931 (2016).
[46]A. Grimaud, W. T. Hong, Y. Shao-Horn, and J.-M. Tarascon, Nat. Mater. **15**, 121 (2016).
[47]M. Okubo and A. Yamada, ACS Appl. Mater. Interfaces **9**, 36463 (2017).
[48]B. Li and D. Xia, Adv. Mater. **29**, 1701054 (2017).
[49]K. Luo, M. R. Roberts, R. Hao, N. Guerrini, D. M. Pickup, Y.-S. Liu, K. Edström, J. Guo, A. V. Chadwick, L. C. Duda, and P. G. Bruce, Nat. Chem. **8**, 684 (2016).
[50]D.-H. Seo, J. Lee, A. Urban, R. Malik, S. Kang, and G. Ceder, Nat. Chem. **8**, 692 (2016).
[51]M. Sathiya, G. Rousse, K. Ramesha, C. P. Laisa, H. Vezin, M. T. Sougrati, M.-L. Doublet, D. Foix, D. Gonbeau, W. Walker, A. S. Prakash, M. Ben Hassine, L. Dupont, and J.-M. Tarascon, Nat. Mater. **12**, 827 (2013).
[52]M. D. Radin, J. Vinckeviciute, R. Seshadri, and A. Van der Ven, Nat. Energy **4**, 639 (2019).
[53]R. A. House, G. J. Rees, M. A. Pérez-Osorio, J.-J. Marie, E. Boivin, A. W. Robertson, A. Nag, M. Garcia-Fernandez, K.-J. Zhou, and P. G. Bruce, Nat. Energy **5**, 777 (2020).
[54]A. S. Menon, S. Ulusoy, D. O. Ojwang, L. Riekehr, C. Didier, V. K. Peterson, G. Salazar-Alvarez, P. Svedlindh, K. Edström, C. P. Gomez, and W. R. Brant, ACS Appl. Energy Mater. **4**, 1924 (2021).
[55]W. E. Gent, K. Lim, Y. Liang, Q. Li, T. Barnes, S. J. Ahn, K. H. Stone, M. McIntire, J. Hong, J. H. Song, Y. Li, A. Mehta, S. Ermon, T. Tyliszczak, D. Kilcoyne, D. Vine, J. H. Park, S. K. Doo, M. F. Toney, W. Yang, D. Prendergast, and W. C. Chueh, Nat. Commun. **8**, 2091 (2017).
[56]H. Chen and M. S. Islam, Chem. Mater. **28**, 6656 (2016).
[57]Y. Li, M. J. Zuba, S. Bai, Z. W. Lebens-Higgins, B. Qiu, S. Park, Z. Liu, M. Zhang, L. F. J. Piper, and Y. S. Meng, Energy Storage Mater. **35**, 99 (2021).
[58]M. J. Zuba, A. Grenier, Z. Lebens-Higgins, G. J. P. Fajardo, Y. Li, Y. Ha, H. Zhou, M. S. Whittingham, W. Yang, Y. S. Meng, K. W. Chapman, and L. F. J. Piper, ACS Energy Lett. **6**, 1055 (2021).
[59]W. Yang and T. P. Devereaux, J. Power Sources **389**, 188 (2018).
[60]W. E. Gent, I. I. Abate, W. Yang, L. F. Nazar, and W. C. Chueh, Joule **4**, 1369 (2020).
[61]Z. W. Lebens-Higgins, J. Vinckeviciute, J. Wu, N. V. Faenza, Y. Li, S. Sallis, N. Pereira, Y. S. Meng, G. G. Amatucci, A. Van Der Ven, W. Yang, and L. F. J. Piper, J. Phys. Chem. C **123**, 13201 (2019).
[62]Z. W. Lebens-Higgins, N. V. Faenza, M. D. Radin, H. Liu, S. Sallis, J. Rana, J. Vinckeviciute, P. J. Reeves, M. J. Zuba, F. Badway, N. Pereira, K. W. Chapman, T.-L. Lee, T. Wu, C. P. Grey, B. C. Melot, A. Van Der Ven, G. G. Amatucci, W. Yang, and L. F. J. Piper, Mater. Horiz. **6**, 2112 (2019).
[63]N. Li, S. Sallis, J. K. Papp, J. Wei, B. D. McCloskey, W. Yang, and W. Tong, ACS Energy Lett. **4**, 2836 (2019).
[64]E. Hu, Q. Li, X. Wang, F. Meng, J. Liu, J.-N. Zhang, K. Page, W. Xu, L. Gu, R. Xiao, H. Li, X. Huang, L. Chen, W. Yang, X. Yu, and X.-Q. Yang, Joule **5**, 720 (2021).
[65]W. Li, H. Y. Asl, Q. Xie, and A. Manthiram, J. Am. Chem. Soc. **141**, 5097 (2019).
[66]B. Song, W. Li, P. Yan, S.-M. Oh, C.-M. Wang, and A. Manthiram, J. Power Sources **325**, 620 (2016).
[67]B. Qiu, M. Zhang, S.-Y. Lee, H. Liu, T. A. Wynn, L. Wu, Y. Zhu, W. Wen, C. M. Brown, D. Zhou, Z. Liu, and Y. S. Meng, Cell Rep. Phys. Sci. **1**, 100028 (2020).
[68]T. Ohzuku, S. Takeda, and M. Iwanaga, J. Power Sources **81–82**, 90 (1999).
[69]S. H. Park, S.-W. Oh, S. H. Kang, I. Belharouak, K. Amine, and Y.-K. Sun, Electrochim. Acta **52**, 7226 (2007).
[70]M. Hu, X. Pang, and Z. Zhou, J. Power Sources **237**, 229 (2013).
[71]J. Song, D. W. Shin, Y. Lu, C. D. Amos, A. Manthiram, and J. B. Goodenough, Chem. Mater. **24**, 3101 (2012).
[72]J.-H. Kim, S.-T. Myung, C. S. Yoon, S. G. Kang, and Y.-K. Sun, Chem. Mater. **16**, 906 (2004).
[73]X. Ma, B. Kang, and G. Ceder, J. Electrochem. Soc. **157**, A925 (2010).
[74]J. Liu, A. Huq, Z. Moorhead-Rosenberg, A. Manthiram, and K. Page, Chem. Mater. **28**, 6817 (2016).
[75]M. Egashira, H. Takahashi, S. Okada, and J.-i. Yamaki, J. Power Sources **92**, 267 (2001).
[76]T.-F. Yi, J. Mei, and Y.-R. Zhu, J. Power Sources **316**, 85 (2016).
[77]M. Moshkovich, M. Cojocaru, H. E. Gottlieb, and D. Aurbach, J. Electroanal. Chem. **497**, 84 (2001).
[78]J.-H. Kim, N. P. W. Pieczonka, and L. Yang, ChemPhysChem **15**, 1940 (2014).
[79]X. Cao, X. He, J. Wang, H. Liu, S. Röser, B. R. Rad, M. Evertz, B. Streipert, J. Li, R. Wagner, M. Winter, and I. Cekic-Laskovic, ACS Appl. Mater. Interfaces **8**, 25971 (2016).
[80]N. P. W. Pieczonka, Z. Liu, P. Lu, K. L. Olson, J. Moote, B. R. Powell, and J.-H. Kim, J. Phys. Chem. C **117**, 15947 (2013).
[81]T. Liu, A. Dai, J. Lu, Y. Yuan, Y. Xiao, L. Yu, M. Li, J. Gim, L. Ma, J. Liu, C. Zhan, L. Li, J. Zheng, Y. Ren, T. Wu, R. Shahbazian-Yassar, J. Wen, F. Pan, and K. Amine, Nat. Commun. **10**, 4721 (2019).
[82]D. S. Lu, L. B. Yuan, J. L. Li, R. Q. Huang, J. H. Guo, and Y. P. Cai, J. Electroanal. Chem. **758**, 33 (2015).
[83]M. Lin, L. Ben, Y. Sun, H. Wang, Z. Yang, L. Gu, X. Yu, X.-Q. Yang, H. Zhao, R. Yu, M. Armand, and X. Huang, Chem. Mater. **27**, 292 (2015).
[84]K. W. Leitner, H. Wolf, A. Garsuch, F. Chesneau, and M. Schulz-Dobrick, J. Power Sources **244**, 548 (2013).
[85]O. (Youngman) Chusid, E. Ein Ely, D. Aurbach, M. Babai, and Y. Carmeli, J. Power Sources **43**, 47 (1993).
[86]G. Q. Liu, L. Wen, X. Wang, and B. Y. Ma, J. Alloys Compd. **509**, 9377 (2011).
[87]D. W. Shin, C. A. Bridges, A. Huq, M. P. Paranthaman, and A. Manthiram, Chem. Mater. **24**, 3720 (2012).
[88]G. T. K. Fey, C. Z. Lu, and T. Prem Kumar, J. Power Sources **115**, 332–345 (2003).
[89]J.-f. Wang, D. Chen, W. Wu, L. Wang, and G.-c. Liang, Trans. Nonferrous Met. Soc. China **27**, 2239 (2017).
[90]B. Xiao, H. Liu, J. Liu, Q. Sun, B. Wang, K. Kaliyappan, Y. Zhao, M. N. Banis, Y. Liu, R. Li, T.-K. Sham, G. A. Botton, M. Cai, and X. Sun, Adv. Mater. **29**, 1703764 (2017).
[91]G. B. Zhong, Y. Y. Wang, Y. Q. Yu, and C. H. Chen, J. Power Sources **205**, 385 (2012).
[92]Y. Luo, H. Li, T. Lu, Y. Zhang, S. S. Mao, Z. Liu, W. Wen, J. Xie, and L. Yan, Electrochim. Acta **238**, 237 (2017).
[93]Y. Shu, Y. Xie, W. Yan, S. Meng, D. Sun, Y. Jin, and K. He, J. Power Sources **433**, 226708 (2019).
[94]J.-H. Kim, N. P. W. Pieczonka, P. Lu, Z. Liu, R. Qiao, W. Yang, M. M. Tessema, Y.-K. Sun, and B. R. Powell, Adv. Mater. Interfaces **2**, 1500109 (2015).
[95]Q. Xia, X. Zhao, M. Xu, Z. Ding, J. Liu, L. Chen, D. G. Ivey, and W. Wei, J. Mater. Chem. A **3**, 3995 (2015).
[96]J. Liu, Y. Chen, J. Xu, W. Sun, C. Zheng, and Y. Li, RSC Adv. **9**, 3081 (2019).
[97]J. Chong, S. Xun, J. Zhang, X. Song, H. Xie, V. Battaglia, and R. Wang, Chem. - Eur. J. **20**, 7479 (2014).
[98]J. Chong, S. Xun, X. Song, G. Liu, and V. S. Battaglia, Nano Energy **2**, 283 (2013).
[99]Y. Deng, J. Mou, H. Wu, N. Jiang, Q. Zheng, K. H. Lam, C. Xu, and D. Lin, Electrochim. Acta **235**, 19 (2017).
[100]U. Nisar, S. A. J. A. Al-Hail, R. K. Petla, R. A. Shakoor, R. Essehli, R. Kahraman, S. Y. AlQaradawi, D. K. Kim, I. Belharouak, and M. R. Amin, ACS Appl. Energy Mater. **2**, 7263 (2019).
[101]Q. Chang, A. Wei, W. Li, X. Bai, L. Zhang, R. He, and Z. Liu, Ceram. Int. **45**, 5100 (2019).
[102]S. Deng, B. Wang, Y. Yuan, X. Li, Q. Sun, K. Doyle-Davis, M. N. Banis, J. Liang, Y. Zhao, J. Li, R. Li, T.-K. Sham, R. Shahbazian-Yassar, H. Wang, M. Cai, J. Lu, and X. Sun, Nano Energy **65**, 103988 (2019).
[103]H. Bouayad, Z. Wang, N. Dupré, R. Dedryvère, D. Foix, S. Franger, J.-F. Martin, L. Boutafa, S. Patoux, D. Gonbeau, and D. Guyomard, J. Phys. Chem. C **118**, 4634 (2014).

[104]J. C. Arrebola, A. Caballero, M. Cruz, L. Hernán, J. Morales, and E. R. Castellón, Adv. Funct. Mater. **16**, 1904 (2006).
[105]F. Wu, H. Zhou, Y. Bai, H. Wang, and C. Wu, ACS Appl. Mater. Interfaces **7**, 15098 (2015).
[106]Y. Abu-Lebdeh and I. Davidson, J. Power Sources **189**, 576 (2009).
[107]H. Xu, H. Zhang, J. Ma, G. Xu, T. Dong, J. Chen, and G. Cui, ACS Energy Lett. **4**, 2871 (2019).
[108]J. Wang, Y. Yamada, K. Sodeyama, C. H. Chiang, Y. Tateyama, and A. Yamada, Nat. Commun. **7**, 12032 (2016).
[109]Z. Zou, H. Xu, H. Zhang, Y. Tang, and G. Cui, ACS Appl. Mater. Interfaces **12**, 21368 (2020).
[110]R. J. Clément, Z. Lun, and G. Ceder, Energy Environ. Sci. **13**, 345 (2020).
[111]K. Kang and G. Ceder, Phys. Rev. B **74**, 094105 (2006).
[112]A. Van Der Ven, J. Bhattacharya, and A. A. Belak, Acc. Chem. Res. **46**, 1216 (2013).
[113]V. Pralong, V. Gopal, V. Caignaert, V. Duffort, and B. Raveau, Chem. Mater. **24**, 12–14 (2012).
[114]N. Yabuuchi, M. Takeuchi, M. Nakayama, H. Shiiba, M. Ogawa, K. Nakayama, T. Ohta, D. Endo, T. Ozaki, T. Inamasu, K. Sato, and S. Komaba, Proc. Natl. Acad. Sci. U. S. A. **112**, 7650 (2015).
[115]M. Diaz-Lopez, M. Freire, Y. Joly, C. V. Colin, H. E. Fischer, N. Blanc, N. Boudet, V. Pralong, and P. Bordet, Chem. Mater. **30**, 3060 (2018).
[116]M. Freire, N. V. Kosova, C. Jordy, D. Chateigner, O. I. Lebedev, A. Maignan, and V. Pralong, Nat. Mater. **15**, 173 (2016).
[117]Z. Lun, B. Ouyang, D.-H. Kwon, Y. Ha, E. E. Foley, T.-Y. Huang, Z. Cai, H. Kim, M. Balasubramanian, Y. Sun, J. Huang, Y. Tian, H. Kim, B. D. McCloskey, W. Yang, R. J. Clément, H. Ji, and G. Ceder, Nat. Mater. **20**, 214 (2021).
[118]R. Sharpe, R. A. House, M. J. Clarke, D. Förstermann, J.-J. Marie, G. Cibin, K.-J. Zhou, H. Y. Playford, P. G. Bruce, and M. S. Islam, J. Am. Chem. Soc. **142**, 21799 (2020).
[119]M. Freire, O. I. Lebedev, A. Maignan, C. Jordy, and V. Pralong, J. Mater. Chem. A **5**, 21898 (2017).
[120]M. Diaz-Lopez, P. A. Chater, Y. Joly, O. Proux, J.-L. Hazemann, P. Bordet, and V. Pralong, J. Mater. Chem. A **8**, 10998 (2020).
[121]M. A. Jones, P. J. Reeves, I. D. Seymour, M. J. Cliffe, S. E. Dutton, and C. P. Grey, Chem. Commun. **55**, 9027 (2019).
[122]Z. N. Taylor, A. J. Perez, J. A. Coca-Clemente, F. Braga, N. E. Drewett, M. J. Pitcher, W. J. Thomas, M. S. Dyer, C. Collins, M. Zanella, T. Johnson, S. Day, C. Tang, V. R. Dhanak, J. B. Claridge, L. J. Hardwick, and M. J. Rosseinsky, J. Am. Chem. Soc. **141**, 7333 (2019).
[123]Y. Gao, X. Wang, J. Ma, Z. Wang, and L. Chen, Chem. Mater. **27**, 3456 (2015).
[124]M. Diaz-Lopez, P. A. Chater, P. Bordet, M. Freire, C. Jordy, O. I. Lebedev, and V. Pralong, Adv. Energy Mater. **10**, 1902788 (2020).
[125]R. Chen, S. Ren, M. Yavuz, A. A. Guda, V. Shapovalov, R. Witter, M. Fichtner, and H. Hahn, Phys. Chem. Chem. Phys. **17**, 17288 (2015).
[126]B. Ouyang, N. Artrith, Z. Lun, Z. Jadidi, D. A. Kitchaev, H. Ji, A. Urban, and G. Ceder, Adv. Energy Mater. **10**, 1903240 (2020).
[127]D. Foix, M. Sathiya, E. McCalla, J.-M. Tarascon, and D. Gonbeau, J. Phys. Chem. C **120**, 862 (2016).
[128]P. E. Pearce, G. Assat, A. Iadecola, F. Fauth, R. Dedryvère, A. Abakumov, G. Rousse, and J.-M. Tarascon, J. Phys. Chem. C **124**, 2771 (2020).
[129]E. McCalla, A. M. Abakumov, M. Saubanère, D. Foix, E. J. Berg, G. Rousse, M.-L. Doublet, D. Gonbeau, P. Novák, G. Van Tendeloo, R. Dominko, and J.-M. Tarascon, Science **350**, 1516 (2015).
[130]C. J. Hansen, J. J. Zak, A. J. Martinolich, J. S. Ko, N. H. Bashian, F. Kaboudvand, A. Van Der Ven, B. C. Melot, J. Nelson Weker, and K. A. See, J. Am. Chem. Soc. **142**, 6737 (2020).
[131]M. Saubanère, E. McCalla, J.-M. Tarascon, and M.-L. Doublet, Energy Environ. Sci. **9**, 984 (2016).
[132]F. Wu and G. Yushin, Energy Environ. Sci. **10**, 435 (2017).
[133]S.-H. Yu, X. Feng, N. Zhang, J. Seok, and H. D. Abruña, Acc. Chem. Res. **51**, 273 (2018).
[134]X. Hua, R. Robert, L.-S. Du, K. M. Wiaderek, M. Leskes, K. W. Chapman, P. J. Chupas, and C. P. Grey, J. Phys. Chem. C **118**, 15169 (2014).
[135]X. Fan, E. Hu, X. Ji, Y. Zhu, F. Han, S. Hwang, J. Liu, S. Bak, Z. Ma, T. Gao, S. C. Liou, J. Bai, X. Q. Yang, Y. Mo, K. Xu, D. Su, and C. Wang, Nat. Commun. **9**, 2324 (2018).
[136]P. G. Bruce, S. A. Freunberger, L. J. Hardwick, and J.-M. Tarascon, Nat. Mater. **11**, 19 (2012).
[137]F. Wu, J. Maier, and Y. Yu, Chem. Soc. Rev. **49**, 1569 (2020).
[138]C. Chen, Y. Zuo, W. Ye, X. Li, Z. Deng, and S. P. Ong, Adv. Energy Mater. **10**, 1903242 (2020).
[139]M. T. Sougrati, A. Darwiche, X. Liu, A. Mahmoud, R. P. Hermann, S. Jouen, L. Monconduit, R. Dronskowski, and L. Stievano, Angew. Chem., Int. Ed. **55**, 5090 (2016).
[140]H. Zhang, B. M. May, F. Omenya, M. S. Whittingham, J. Cabana, and G. Zhou, Chem. Mater. **31**, 7790 (2019).
[141]S. Sharifi-Asl, J. Lu, K. Amine, and R. Shahbazian-Yassar, Adv. Energy Mater. **9**, 1900551 (2019).
[142]A. Hammami, N. Raymond, and M. Armand, Nature **424**, 635 (2003).
[143]S. Saha, G. Assat, M. T. Sougrati, D. Foix, H. Li, J. Vergnet, S. Turi, Y. Ha, W. Yang, J. Cabana, G. Rousse, A. M. Abakumov, and J.-M. Tarascon, Nat. Energy **4**, 977 (2019).
[144]J. Cabana, L. Monconduit, D. Larcher, and M. R. Palacín, Adv. Mater. **22**, E170 (2010).
[145]F. Badway, F. Cosandey, N. Pereira, and G. G. Amatucci, J. Electrochem. Soc. **150**, A1318 (2003).
[146]A. R. Armstrong and P. G. Bruce, Nature **381**, 499 (1996).
[147]E. A. Olivetti, G. Ceder, G. G. Gaustad, and X. Fu, Joule **1**, 229 (2017).
[148]B. Simon, S. Ziemann, and M. Weil, Resour. Conserv. Recycl. **104**, 300 (2015).
[149]J. Lee, J. K. Papp, R. J. Clément, S. Sallis, D. H. Kwon, T. Shi, W. Yang, B. D. McCloskey, and G. Ceder, Nat. Commun. **8**, 981 (2017).
[150]W. Lee, S. Muhammad, C. Sergey, H. Lee, J. Yoon, Y. M. Kang, and W. S. Yoon, Angew. Chem., Int. Ed. **59**, 2578 (2020).
[151]K. T. Lai, I. Antonyshyn, Y. Prots, and M. Valldor, J. Am. Chem. Soc. **139**, 9645 (2017).
[152]D. Mikhailova, L. Giebeler, S. Maletti, S. Oswald, A. Sarapulova, S. Indris, Z. Hu, J. Bednarcik, and M. Valldor, ACS Appl. Energy Mater. **1**, 6593 (2018).
[153]Z. Lu and F. Ciucci, J. Mater. Chem. A **6**, 5185 (2018).
[154]T. Matsumura, R. Kanno, Y. Inaba, Y. Kawamoto, and M. Takano, J. Electrochem. Soc. **149**, A1509 (2002).
[155]S.-H. Wu and H.-Y. Liu, J. Power Sources **174**, 789 (2007).
[156]M. A. Hayward, M. A. Green, M. J. Rosseinsky, and J. Sloan, J. Am. Chem. Soc. **121**, 8843 (1999).
[157]A. Manthiram, Nat. Commun. **11**, 1550 (2020).
[158]A. D. Becke, J. Chem. Phys. **140**, 18A301 (2014).
[159]A. R. Oganov, C. J. Pickard, Q. Zhu, and R. J. Needs, Nat. Rev. Mater. **4**, 331 (2019).
[160]H. Guo, H. Ping, J. Hu, X. Song, J. Zheng, and F. Pan, J. Mater. Chem. A **5**, 14294 (2017).
[161]X. Zhao, S. Wu, X. Lv, M. C. Nguyen, C.-Z. Wang, Z. Lin, Z.-Z. Zhu, and K.-M. Ho, Sci. Rep. **5**, 15555 (2015).
[162]G. Hautier, C. Fischer, V. Ehrlacher, A. Jain, and G. Ceder, Inorg. Chem. **50**, 656 (2011).
[163]D. J. Wales and J. P. K. Doye, J. Phys. Chem. A **101**, 5111 (1997).
[164]S. Goedecker, J. Chem. Phys. **120**, 9911 (2004).
[165]A. R. Oganov, C. W. Glass, and S. Ono, Earth Planet. Sci. Lett. **241**, 95 (2006).
[166]Y. Wang, J. Lv, L. Zhu, and Y. Ma, Comput. Phys. Commun. **183**, 2063 (2012).
[167]C. J. Pickard and R. J. Needs, Phys. Rev. Lett. **97**, 045504 (2006).
[168]C. J. Pickard and R. J. Needs, J. Phys.: Condens. Matter **23**, 053201 (2011).
[169]R. J. Nicholls, N. Ni, S. Lozano-Perez, A. London, D. W. McComb, P. D. Nellist, C. R. M. Grovenor, C. J. Pickard, and J. R. Yates, Adv. Eng. Mater. **17**, 211 (2015).
[170]Z. Lu, B. Zhu, B. W. B. Shires, D. O. Scanlon, and C. J. Pickard, J. Chem. Phys. **154**, 174111 (2021).

[171]B. Zhu and D. Scanlon, ChemRxiv (2021).
[172]S. L. Dudarev G. A. Botton, S. Y. Savrasov, C. J. Humphreys, and A. P. Sutton, Phys. Rev. B **57**, 1505 (1998).
[173]A. V. Krukau, O. A. Vydrov, A. F. Izmaylov, and G. E. Scuseria, J. Chem. Phys. **125**, 224106 (2006).
[174]D. W. Davies, K. T. Butler, A. J. Jackson, A. Morris, J. M. Frost, J. M. Skelton, and A. Walsh, Chem **1**, 617 (2016).
[175]E. B. Isaacs, S. Patel, and C. Wolverton, Phys. Rev. Mater. **4**, 065405 (2020).
[176]J. Sun, A. Ruzsinszky, and J. Perdew, Phys. Rev. Lett. **115**, 036402 (2015).
[177]J. Behler and M. Parrinello, Phys. Rev. Lett. **98**, 146401 (2007).
[178]A. P. Bartók, M. C. Payne, R. Kondor, and G. Csányi, Phys. Rev. Lett. **104**, 136403 (2010).
[179]V. L. Deringer, D. M. Proserpio, G. Csányi, and C. J. Pickard, Faraday Discuss. **211**, 45 (2018).
[180]B. Cheng, R.-R. Griffiths, S. Wengert, C. Kunkel, T. Stenczel, B. Zhu, V. L. Deringer, N. Bernstein, J. T. Margraf, K. Reuter, and G. Csanyi, Acc. Chem. Res. **53**, 1981 (2020).
[181]A. Jain, S. P. Ong, G. Hautier, W. Chen, W. D. Richards, S. Dacek, S. Cholia, D. Gunter, D. Skinner, G. Ceder, and K. A. Persson, APL Mater. **1**, 011002 (2013).
[182]S. Kirklin, J. E. Saal, B. Meredig, A. Thompson, J. W. Doak, M. Aykol, S. Rühl, and C. Wolverton, npj Comput. Mater. **1**, 15010 (2015).
[183]C. Chen, W. Ye, Y. Zuo, C. Zheng, and S. P. Ong, Chem. Mater. **31**, 3564 (2019).
[184]D. W. Davies, B. J. Morgan, D. O. Scanlon, and A. Walsh, IOP SciNotes **1**, 024805 (2020).
[185]J. Zheng, Y. Ye, and F. Pan, Natl. Sci. Rev. **7**, 242 (2020).
[186]P. Hou, H. Zhang, Z. Zi, L. Zhang, and X. Xu, J. Mater. Chem. A **5**, 4254 (2017).
[187]F. Zhou, X. Zhao, A. Van Bommel, A. W. Rowe, and J. R. Dahn, Chem. Mater. **22**, 1015 (2010).
[188]M.-H. Lee, Y.-J. Kang, S.-T. Myung, and Y.-K. Sun, Electrochim. Acta **50**, 939 (2004).
[189]Y.-K. Sun, S.-T. Myung, M.-H. Kim, J. Prakash, and K. Amine, J. Am. Chem. Soc. **127**, 13411 (2005).
[190]L. Liang, X. Sun, C. Wu, L. Hou, J. Sun, X. Zhang, and C. Yuan, ACS Appl. Mater. Interfaces **10**, 5498 (2018).
[191]X. Dong, J. Yao, W. Zhu, X. Huang, X. Kuai, J. Tang, X. Li, S. Dai, L. Shen, R. Yang, L. Gao, and J. Zhao, J. Mater. Chem. A **7**, 20262 (2019).
[192]P. Hou, J. Guo, D. Song, J. Zhang, E. Zhou, and L. Zhang, Chem. Lett. **41**, 1712 (2012).
[193]Y.-K. Sun, S.-T. Myung, B.-C. Park, J. Prakash, I. Belharouak, and K. Amine, Nat. Mater. **8**, 320 (2009).
[194]Y.-K. Sun, Z. Chen, H.-J. Noh, D.-J. Lee, H.-G. Jung, Y. Ren, S. Wang, C. S. Yoon, S.-T. Myung, and K. Amine, Nat. Mater. **11**, 942 (2012).
[195]B.-B. Lim, S.-J. Yoon, K.-J. Park, C. S. Yoon, S.-J. Kim, J. J. Lee, and Y.-K. Sun, Adv. Funct. Mater. **25**, 4673 (2015).
[196]D. Song, P. Hou, X. Wang, X. Shi, and L. Zhang, ACS Appl. Mater. Interfaces **7**, 12864 (2015).
[197]C. Xu, K. Märker, J. Lee, A. Mahadevegowda, P. J. Reeves, S. J. Day, M. F. Groh, S. P. Emge, C. Ducati, B. Layla Mehdi, C. C. Tang, and C. P. Grey, Nat. Mater. **20**, 84 (2021).
[198]R. J. Mou and K. P. C. Yao, J. Electrochem. Soc. **168**, 020503 (2021).
[199]M. Park, X. Zhang, M. Chung, G. B. Less, and A. M. Sastry, J. Power Sources **195**, 7904 (2010).
[200]Y.-H. Chen, C.-W. Wang, X. Zhang, and A. M. Sastry, J. Power Sources **195**, 2851 (2010).
[201]B. L. Trembacki, A. N. Mistry, D. R. Noble, M. E. Ferraro, P. P. Mukherjee, and S. A. Roberts, J. Electrochem. Soc. **165**, E725 (2018).
[202]G. Inoue and M. Kawase, J. Power Sources **342**, 476 (2017).
[203]Q. Cao, H. P. Zhang, G. J. Wang, Q. Xia, Y. P. Wu, and H. Q. Wu, Electrochem. Commun. **9**, 1228 (2007).
[204]J. Kim, B. Kim, J.-G. Lee, J. Cho, and B. Park, J. Power Sources **139**, 289 (2005).
[205]H.-S. Kim, M. Kong, K. Kim, I.-J. Kim, and H.-B. Gu, J. Power Sources **171**, 917 (2007).
[206]S. Lee, Y. Cho, H.-K. Song, K. T. Lee, and J. Cho, Angew. Chem., Int. Ed. **124**, 8878 (2012).
[207]J.-H. Kim, S. J. Kim, T. Yuk, J. Kim, C. S. Yoon, and Y.-K. Sun, ACS Energy Lett. **3**, 3002 (2018).
[208]Y. K. Lee, Energies **12**, 658 (2019).
[209]F. Lin, D. Nordlund, I. M. Markus, T.-C. Weng, H. L. Xin, and M. M. Doeff, Energy Environ. Sci. **7**, 3077 (2014).
[210]M. Kerlau, M. Marcinek, V. Srinivasan, and R. M. Kostecki, Electrochim. Acta **53**, 1386 (2007).
[211]G.-L. Xu, Q. Liu, K. K. S. Lau, Y. Liu, X. Liu, H. Gao, X. Zhou, M. Zhuang, Y. Ren, J. Li, M. Shao, M. Ouyang, F. Pan, Z. Chen, K. Amine, and G. Chen, Nat. Energy **4**, 484 (2019).
[212]W. Liu, Q. Wang, C. Cao, X. Han, J. Zhang, X. Xie, and B. Xia, J. Alloys Compd. **621**, 162 (2015).
[213]S. Chae, M. Ko, S. Park, N. Kim, J. Ma, and J. Cho, Energy Environ. Sci. **9**, 1251 (2016).
[214]J. T. Lee, C. Jo, and M. De Volder, Proc. Natl. Acad. Sci. U. S. A. **117**, 21155 (2020).
[215]J.-H. Kim, N. P. W. Pieczonka, Z. Li, Y. Wu, S. Harris, and B. R. Powell, Electrochim. Acta **90**, 556 (2013).
[216]N. J. J. De Klerk, E. Van Der Maas, and M. Wagemaker, ACS Appl. Energy Mater. **1**, 3230 (2018).
[217]X. Yu and A. Manthiram, Energy Environ. Sci. **11**, 527 (2018).
[218]J. Xie, A. D. Sendek, E. D. Cubuk, X. Zhang, Z. Lu, Y. Gong, T. Wu, F. Shi, W. Liu, E. J. Reed, and Y. Cui, ACS Nano **11**, 7019 (2017).
[219]G. Chen, B. Peng, R. Han, N. Chen, Z. Wang, and Q. Wang, Ceram. Int. **46**, 20985 (2020).
[220]L. Ma, S. Young, L. D. Ellis, Q. Huang, X. Ma, M. Chatzidakis, H. Li, L. Thompson, A. Eldesoky, C. R. M. McFarlane, G. A. Botton, I. G. Hill, and J. R. Dahn, ACS Appl. Energy Mater. **1**, 7052 (2018).
[221]W. Bao, G. Qian, L. Zhao, Y. Yu, L. Su, X. Cai, H. Zhao, Y. Zuo, Y. Zhang, H. Li, Z. Peng, L. Li, and J. Xie, Nano Lett. **20**, 8832 (2020).
[222]J.-Z. Kong, C. Ren, G.-A. Tai, X. Zhang, A.-D. Li, D. Wu, H. Li, and F. Zhou, J. Power Sources **266**, 433 (2014).
[223]W. Liu, M. Wang, X. L. Gao, W. Zhang, J. Chen, H. Zhou, and X. Zhang, J. Alloys Compd. **543**, 181 (2012).
[224]B. Han, B. Key, S. H. Lapidus, J. C. Garcia, H. Iddir, J. T. Vaughey, and F. Dogan, ACS Appl. Mater. Interfaces **9**, 41291 (2017).
[225]B. Song, W. Li, S.-M. Oh, and A. Manthiram, ACS Appl. Mater. Interfaces **9**, 9718 (2017).
[226]W. Cho, S.-M. Kim, J. H. Song, T. Yim, S.-G. Woo, K.-W. Lee, J.-S. Kim, and Y.-J. Kim, J. Power Sources **282**, 45 (2015).
[227]F. Xin, H. Zhou, X. Chen, M. Zuba, N. Chernova, G. Zhou, and M. S. Whittingham, ACS Appl. Mater. Interfaces **11**, 34889 (2019).
[228]K. Nie, Y. Hong, J. Qiu, Q. Li, X. Yu, H. Li, and L. Chen, Front. Chem. **6**, 616 (2018).
[229]T. Nakamura, K. Amezawa, J. Kulisch, W. G. Zeier, and J. Janek, ACS Appl. Mater. Interfaces **11**, 19968 (2019).
[230]T. Famprikis, P. Canepa, J. A. Dawson, M. S. Islam, and C. Masquelier, Nat. Mater. **18**, 1278 (2019).
[231]P.-J. Lian, B.-S. Zhao, L.-Q. Zhang, N. Xu, M.-T. Wu, and X.-P. Gao, J. Mater. Chem. A **7**, 20540 (2019).
[232]A. Banerjee, X. Wang, C. Fang, E. A. Wu, and Y. S. Meng, Chem. Rev. **120**, 6878 (2020).
[233]K. Beltrop, S. Klein, R. Nölle, A. Wilken, J. J. Lee, T. K.-J. Köster, J. Reiter, L. Tao, C. Liang, M. Winter, X. Qi, and T. Placke, Chem. Mater. **30**, 2726 (2018).
[234]B. Qiu, M. Zhang, L. Wu, J. Wang, Y. Xia, D. Qian, H. Liu, S. Hy, Y. Chen, K. An, Y. Zhu, Z. Liu, and Y. S. Meng, Nat. Commun. **7**, 12108 (2016).
[235]X. Lu, A. Bertei, D. P. Finegan, C. Tan, S. R. Daemi, J. S. Weaving, K. B. O'Regan, T. M. M. Heenan, G. Hinds, E. Kendrick, D. J. L. Brett, and P. R. Shearing, Nat. Commun. **11**, 2079 (2020).

[236]X. Xu, H. Huo, J. Jian, L. Wang, H. Zhu, S. Xu, X. He, G. Yin, C. Du, and X. Sun, Adv. Energy Mater. **9**, 1803963 (2019).
[237]N. D. Phillip, C. Daniel, and G. M. Veith, J. Electrochem. Soc. **167**, 040521 (2020).
[238]Z. Deng, X. Lin, Z. Huang, J. Meng, Y. Zhong, G. Ma, Y. Zhou, Y. Shen, H. Ding, and Y. Huang, Adv. Energy Mater. **11**, 2000806 (2021).
[239]T. L. Burnett and P. J. Withers, Nat. Mater. **18**, 1041 (2019).
[240]D. P. Finegan, M. Scheel, J. B. Robinson, B. Tjaden, I. Hunt, T. J. Mason, J. Millichamp, M. Di Michiel, G. J. Offer, G. Hinds, D. J. L. Brett, and P. R. Shearing, Nat. Commun. **6**, 6924 (2015).
[241]T. M. M. Heenan, C. Tan, J. Hack, D. J. L. Brett, and P. R. Shearing, Mater. Today **31**, 69 (2019).
[242]S. R. Daemi, C. Tan, T. Volkenandt, S. J. Cooper, A. Palacios-Padros, J. Cookson, D. J. L. Brett, and P. R. Shearing, ACS Appl. Energy Mater. **1**, 3702 (2018).
[243]S. L. Morelly, J. Gelb, F. Iacoviello, P. R. Shearing, S. J. Harris, N. J. Alvarez, and M. H. Tang, ACS Appl. Energy Mater. **1**, 4479 (2018).
[244]A. Quinn, H. Moutinho, F. Usseglio-Viretta, A. Verma, K. Smith, M. Keyser, and D. P. Finegan, Cell Rep. Phys. Sci. **1**, 100137 (2020).
[245]D. Zeibig, T. Bernthaler, G. Schneider, and S. Freitag, Microsc. Microanal. **24**, 1512 (2018).
[246]W. Li, A. Dolocan, P. Oh, H. Celio, S. Park, J. Cho, and A. Manthiram, Nat. Commun. **8**, 14589 (2017).
[247]E. M. Erickson, W. Li, A. Dolocan, and A. Manthiram, ACS Appl. Mater. Interfaces **12**, 16451 (2020).
[248]L. Wheatcroft, N. Klingner, R. Heller, G. Hlawacek, D. Özkaya, J. Cookson, and B. J. Inkson, ACS Appl. Energy Mater. **3**, 8822 (2020).
[249]M. Gu, L. R. Parent, B. L. Mehdi, R. R. Unocic, M. T. McDowell, R. L. Sacci, W. Xu, J. G. Connell, P. Xu, P. Abellan, X. Chen, Y. Zhang, D. E. Perea, J. E. Evans, L. J. Lauhon, J.-G. Zhang, J. Liu, N. D. Browning, Y. Cui, I. Arslan, and C.-M. Wang, Nano Lett. **13**, 6106 (2013).
[250]C. Y. Chen, T. Sano, T. Tsuda, K. Ui, Y. Oshima, M. Yamagata, M. Ishikawa, M. Haruta, T. Doi, M. Inaba, and S. Kuwabata, Sci. Rep. **6**, 36153 (2016).
[251]E. Fahrenkrug, D. H. Alsem, N. Salmon, and S. Maldonado, J. Electrochem. Soc. **164**, H358 (2017).
[252]J. Hou, R. Girod, N. Nianias, T.-H. Shen, J. Fan, and V. Tileli, J. Electrochem. Soc. **167**, 110515 (2020).
[253]P. Abellan, B. L. Mehdi, L. R. Parent, M. Gu, C. Park, W. Xu, Y. Zhang, I. Arslan, J.-G. Zhang, C.-M. Wang, J. E. Evans, and N. D. Browning, Nano Lett. **14**, 1293 (2014).
[254]Z. Wang, D. Santhanagopalan, W. Zhang, F. Wang, H. L. Xin, K. He, J. Li, N. Dudney, and Y. S. Meng, Nano Lett. **16**, 3760 (2016).
[255]D. Chen, S. Indris, M. Schulz, B. Gamer, and R. Mönig, J. Power Sources **196**, 6382 (2011).
[256]M. I. Nandasiri, L. E. Camacho-Forero, A. M. Schwarz, V. Shutthanandan, S. Thevuthasan, P. B. Balbuena, K. T. Mueller, and V. Murugesan, Chem. Mater. **29**, 4728 (2017).
[257]M. E. Holtz, Y. Yu, D. Gunceler, J. Gao, R. Sundararaman, K. A. Schwarz, T. A. Arias, H. D. Abruña, and D. A. Muller, Nano Lett. **14**, 1453 (2014).
[258]G. Rong, X. Zhang, W. Zhao, Y. Qiu, M. Liu, F. Ye, Y. Xu, J. Chen, Y. Hou, W. Li, W. Duan, and Y. Zhang, Adv. Mater. **29**, 1606187 (2017).
[259]R. R. Unocic, R. L. Sacci, G. M. Brown, G. M. Veith, N. J. Dudney, K. L. More, F. S. Walden, D. S. Gardiner, J. Damiano, and D. P. Nackashi, Microsc. Microanal. **20**, 452 (2014).
[260]G. Xu, X. Zhang, M. Liu, H. Li, M. Zhao, Q. Li, J. Zhang, and Y. Zhang, Small **16**, 1906499 (2020).
[261]Y. Xie, H. Wang, G. Xu, J. Wang, H. Sheng, Z. Chen, Y. Ren, C.-J. Sun, J. Wen, J. Wang, D. J. Miller, J. Lu, K. Amine, and Z.-F. Ma, Adv. Energy Mater. **6**, 1601306 (2016).
[262]J. Wang, Y. C. K. Chen-Wiegart, and J. Wang, Nat. Commun. **5**, 4570 (2014).
[263]D. J. Miller, C. Proff, J. G. Wen, D. P. Abraham, and J. Bareño, Adv. Energy Mater. **3**, 1098 (2013).
[264]O. J. Borkiewicz, B. Shyam, K. M. Wiaderek, C. Kurtz, P. J. Chupas, and K. W. Chapman, J. Appl. Crystallogr. **45**, 1261 (2012).
[265]J. J. Biendicho, M. Roberts, C. Offer, D. Noréus, E. Widenkvist, R. I. Smith, G. Svensson, K. Edström, S. T. Norberg, S. G. Eriksson, and S. Hull, J. Power Sources **248**, 900 (2014).
[266]W. R. Brant, D. Li, Q. Gu, and S. Schmid, J. Power Sources **302**, 126 (2016).
[267]O. J. Borkiewicz, K. M. Wiaderek, P. J. Chupas, and K. W. Chapman, J. Phys. Chem. Lett. **6**, 2081 (2015).
[268]H. Liu, P. K. Allan, O. J. Borkiewicz, C. Kurtz, C. P. Grey, K. W. Chapman, and P. J. Chupas, J. Appl. Crystallogr. **49**, 1665 (2016).
[269]M. Diaz-Lopez, G. L. Cutts, P. K. Allan, D. S. Keeble, A. Ross, V. Pralong, G. Spiekermann, and P. A. Chater, J. Synchrotron Radiat. **27**, 1190 (2020).
[270]F. Rosciano, M. Holzapfel, H. Kaiser, W. Scheifele, P. Ruch, M. Hahn, R. Kötz, and P. Novák, J. Synchrotron Radiat. **14**, 487 (2007).
[271]R. Petibon, J. Li, N. Sharma, W. K. Pang, V. K. Peterson, and J. R. Dahn, Electrochim. Acta **174**, 417 (2015).
[272]V. A. Godbole, M. Heß, C. Villevieille, H. Kaiser, J.-F. Colin, and P. Novák, RSC Adv. **3**, 757 (2013).
[273]H. Liu, F. C. Strobridge, O. J. Borkiewicz, K. M. Wiaderek, K. W. Chapman, P. J. Chupas, and C. P. Grey, Science **344**, 1252817 (2014).
[274]Z. Lun, B. Ouyang, Z. Cai, R. J. Clément, D.-H. Kwon, J. Huang, J. K. Papp, M. Balasubramanian, Y. Tian, B. D. McCloskey, H. Ji, H. Kim, D. A. Kitchaev, and G. Ceder, Chem **6**, 153 (2020).
[275]K. M. Wiaderek, O. J. Borkiewicz, E. Castillo-Martínez, R. Robert, N. Pereira, G. G. Amatucci, C. P. Grey, P. J. Chupas, and K. W. Chapman, J. Am. Chem. Soc. **135**, 4070 (2013).
[276]A. Simonov, T. De Baerdemaeker, H. L. B. Boström, M. L. Ríos Gómez, H. J. Gray, D. Chernyshov, A. Bosak, H.-B. Bürgi, and A. L. Goodwin, Nature **578**, 256 (2020).
[277]H. Ji, A. Urban, D. A. Kitchaev, D. H. Kwon, N. Artrith, C. Ophus, W. Huang, Z. Cai, T. Shi, J. C. Kim, H. Kim, and G. Ceder, Nat. Commun. **10**, 592 (2019).
[278]S. Permien, T. Neumann, S. Indris, G. Neubüser, L. Kienle, A. Fiedler, A.-L. Hansen, D. Gianolio, T. Bredow, and W. Bensch, Phys. Chem. Chem. Phys. **20**, 19129 (2018).
[279]G. Tonin, G. Vaughan, R. Bouchet, F. Alloin, M. Di Michiel, L. Boutafa, J. F. Colin, and C. Barchasz, Sci. Rep. **7**, 2755 (2017).
[280]D. P. Finegan, A. Vamvakeros, C. Tan, T. M. M. Heenan, S. R. Daemi, N. Seitzman, M. Di Michiel, S. Jacques, A. M. Beale, D. J. L. Brett, P. R. Shearing, and K. Smith, Nat. Commun. **11**, 631 (2020).
[281]S. R. Daemi, C. Tan, A. Vamvakeros, T. M. M. Heenan, D. P. Finegan, M. Di Michiel, A. M. Beale, J. Cookson, E. Petrucco, J. S. Weaving, S. Jacques, R. Jervis, D. J. L. Brett, and P. R. Shearing, Phys. Chem. Chem. Phys. **22**, 17814 (2020).
[282]K. M. Ø. Jensen, X. Yang, J. V. Laveda, W. G. Zeier, K. A. See, M. D. Michiel, B. C. Melot, S. A. Corr, and S. J. L. Billinge, J. Electrochem. Soc. **162**, A1310 (2015).
[283]S. D. M. Jacques, M. Di Michiel, S. A. J. Kimber, X. Yang, R. J. Cernik, A. M. Beale, and S. J. L. Billinge, Nat. Commun. **4**, 2536 (2013).
[284]K. W. Chapman, S. H. Lapidus, and P. J. Chupas, J. Appl. Crystallogr. **48**, 1619 (2015).
[285]H. S. Geddes, H. Blade, J. F. McCabe, L. P. Hughes, and A. L. Goodwin, Chem. Commun. **55**, 013346 (2019).
[286]V. L. Deringer, C. Merlet, Y. Hu, T. H. Lee, J. A. Kattirtzi, O. Pecher, G. Csányi, S. R. Elliott, and C. P. Grey, Chem. Commun. **54**, 5988 (2018).
[287]T. Q. Nguyen and C. Breitkopf, J. Electrochem. Soc. **165**, E826 (2018).
[288]S.-M. Park and J.-S. Yoo, Anal. Chem. **75**, 455A (2003).
[289]A. Nickol, T. Schied, C. Heubner, M. Schneider, A. Michaelis, M. Bobeth, and G. Cuniberti, J. Electrochem. Soc. **167**, 090546 (2020).
[290]L. S. Cahill, R. P. Chapman, J. F. Britten, and G. R. Goward, J. Phys. Chem. B **110**, 7171 (2006).
[291]C. V. Chandran, C. E. A. Kirschhock, S. Radhakrishnan, F. Taulelle, J. A. Martens, and E. Breynaert, Chem. Soc. Rev. **48**, 134 (2019).
[292]I. McClelland, B. Johnston, P. J. Baker, M. Amores, E. J. Cussen, and S. A. Corr, Annu. Rev. Mater. Res. **50**, 371–393 (2020).
[293]A. Van Der Ven and G. Ceder, "Lithium diffusion mechanisms in layered intercalation compounds," J. Power Sources **97–98**, 529 (2001).

[294]T. E. Ashton, P. J. Baker, D. Bauer, A. R. Groves, C. Sotelo-Vazquez, T. Kamiyama, T. Matsukawa, K. M. Kojima, and J. A. Darr, J. Mater. Chem. A **8**, 11545 (2020).
[295]O. Pecher, J. Carretero-González, K. J. Griffith, and C. P. Grey, Chem. Mater. **29**, 213 (2017).
[296]I. McClelland, S. G. Booth, H. El-Shinawi, B. I. J. Johnston, J. Clough, W. Guo, E. J. Cussen, P. J. Baker, and S. A. Corr, ACS Appl. Energy Mater. **4**, 1527 (2021).
[297]A. J. Rossini, A. Zagdoun, M. Lelli, A. Lesage, C. Copéret, and L. Emsley, Acc. Chem. Res. **46**, 1942 (2013).
[298]A. S. Lilly Thankamony, J. J. Wittmann, M. Kaushik, and B. Corzilius, Prog. Nucl. Magn. Reson. Spectrosc. **102–103**, 120 (2017).
[299]A. G. M. Rankin, J. Trébosc, F. Pourpoint, J.-P. Amoureux, and O. Lafon, Solid State Nucl. Magn. Reson. **101**, 116 (2019).
[300]C. Song, K.-N. Hu, C.-G. Joo, T. M. Swager, and R. G. Griffin, J. Am. Chem. Soc. **128**, 11385 (2006).
[301]M. A. Hope, D. M. Halat, P. C. M. M. Magusin, S. Paul, L. Peng, and C. P. Grey, Chem. Commun. **53**, 2142 (2017).
[302]M. Leskes, G. Kim, T. Liu, A. L. Michan, F. Aussenac, P. Dorffer, S. Paul, and C. P. Grey, J. Phys. Chem. Lett. **8**, 1078 (2017).
[303]Y. Jin, N.-J. H. Kneusels, L. E. Marbella, E. Castillo-Martínez, P. C. M. M. Magusin, R. S. Weatherup, E. Jónsson, T. Liu, S. Paul, and C. P. Grey, J. Am. Chem. Soc. **140**, 9854 (2018).
[304]T. Wolf, S. Kumar, H. Singh, T. Chakrabarty, F. Aussenac, A. I. Frenkel, D. T. Major, and M. Leskes, J. Am. Chem. Soc. **141**, 451 (2019).
[305]D. Jardón-Álvarez, G. Reuveni, A. Harchol, and M. Leskes, J. Phys. Chem. Lett. **11**, 5439 (2020).
[306]M. A. Hope, B. L. D. Rinkel, A. B. Gunnarsdóttir, K. Märker, S. Menkin, S. Paul, I. V. Sergeyev, and C. P. Grey, Nat. Commun. **11**, 2224 (2020).
[307]K. W. Chapman, P. J. Chupas, and C. J. Kepert, J. Am. Chem. Soc. **127**, 11232 (2005).
[308]W. Li, R. Harrington, Y. Tang, J. D. Kubicki, M. Aryanpour, R. J. Reeder, J. B. Parise, and B. L. Phillips, Environ. Sci. Technol. **45**, 9687 (2011).
[309]R. Harrington, D. B. Hausner, N. Bhandari, D. R. Strongin, K. W. Chapman, P. J. Chupas, D. S. Middlemiss, C. P. Grey, and J. B. Parise, Inorg. Chem. **49**, 325 (2010).
[310]P. J. Chupas, K. W. Chapman, G. Jennings, P. L. Lee, and C. P. Grey, J. Am. Chem. Soc. **129**, 13822 (2007).
[311]K. T. Mukaddem, P. A. Chater, L. R. Devereux, O. K. Al Bahri, A. Jain, and J. M. Cole, J. Phys. Chem. C **124**, 11935 (2020).
[312]M. Zobel, R. B. Neder, and S. A. J. Kimber, Science **347**, 292 (2015).
[313]H. S. Geddes, H. D. Hutchinson, A. R. Ha, N. P. Funnell, and A. L. Goodwin, ChemRxiv:14318741 (2021).
[314]S. Shiotani, K. Ohara, H. Tsukasaki, S. Mori, and R. Kanno, Sci. Rep. **7**, 6972 (2017).
[315]O. J. Borkiewicz, K. W. Chapman, and P. J. Chupas, Phys. Chem. Chem. Phys. **15**, 8466 (2013).
[316]E. Morenzoni, H. Glückler, T. Prokscha, H. P. Weber, E. M. Forgan, T. J. Jackson, H. Luetkens, C. Niedermayer, M. Pleines, M. Birke, A. Hofer, J. Litterst, T. Riseman, and G. Schatz, Physica B **289–290**, 653 (2000).
[317]G. Zhou, X. Sun, Q.-H. Li, X. Wang, J.-N. Zhang, W. Yang, X. Yu, R. Xiao, and H. Li, J. Phys. Chem. Lett. **11**, 3051 (2020).
[318]J. Behler, J. Chem. Phys. **145**, 170901 (2016).
[319]W. Jia, H. Wang, M. Chen, D. Lu, L. Lin, R. Car, W. E, and L. Zhang, in International Conference for High Performance Computing, Networking, Storage and Analysis, SC, November 2020.
[320]D. Lu, H. Wang, M. Chen, L. Lin, R. Car, W. E, W. Jia, and L. Zhang, Comput. Phys. Commun. **259**, 107624 (2021).
[321]S. Chen, L. Qiu, and H.-M. Cheng, Chem. Rev. **120**, 2811 (2020).
[322]H. H. Ryu, N. Y. Park, D. R. Yoon, U. H. Kim, C. S. Yoon, and Y. K. Sun, Adv. Energy Mater. **10**, 2000495 (2020).
[323]Y. Zhao, P. Stein, Y. Bai, M. Al-Siraj, Y. Yang, and B.-X. Xu, J. Power Sources **413**, 259 (2019).
[324]A. Singer, M. Zhang, S. Hy, D. Cela, C. Fang, T. A. Wynn, B. Qiu, Y. Xia, Z. Liu, A. Ulvestad, N. Hua, J. Wingert, H. Liu, M. Sprung, A. V. Zozulya, E. Maxey, R. Harder, Y. S. Meng, and O. G. Shpyrko, Nat. Energy **3**, 641 (2018).
[325]W. Huddleston, F. Dynys, and A. Sehirlioglu, J. Am. Ceram. Soc. **103**, 1527 (2020).
[326]R. Xu, H. Sun, L. Scalco De Vasconcelos, and K. Zhao, J. Electrochem. Soc. **164**, A3333 (2017).
[327]D. Dang, Y. Wang, and Y.-T. Cheng, J. Electrochem. Soc. **166**, A2749 (2019).
[328]W. C. Oliver and G. M. Pharr, J. Mater. Res. **7**, 1564 (1992).
[329]G. R. Anstis, P. Chantikul, B. R. Lawn, and D. B. Marshall, J. Am. Ceram. Soc. **64**, 533 (1981).
[330]J. Wolfenstine, J. L. Allen, T. R. Jow, T. Thompson, J. Sakamoto, H. Jo, and H. Choe, Ceram. Int. **40**, 13673 (2014).
[331]M. Qu, W. H. Woodford, J. M. Maloney, W. C. Carter, Y.-M. Chiang, and K. J. Van Vliet, Adv. Energy Mater. **2**, 940 (2012).
[332]P. Yan, J. Zheng, M. Gu, J. Xiao, J. G. Zhang, and C. M. Wang, Nat. Commun. **8**, 14101 (2017).
[333]J. J. Vlassak and W. D. Nix, J. Mech. Phys. Solids **42**, 1223 (1994).
[334]K. Märker, P. J. Reeves, C. Xu, K. J. Griffith, and C. P. Grey, Chem. Mater. **31**, 2545 (2019).
[335]H. Tavassol, E. M. C. Jones, N. R. Sottos, and A. A. Gewirth, Nat. Mater. **15**, 1182 (2016).

AFFILIATIONS

[1]Department of Chemical and Biological Engineering, University of Sheffield, Sheffield S1 3JD, United Kingdom
[2]The Faraday Institution, Quad One, Harwell Campus, Didcot OX11 0RA, United Kingdom
[3]ISIS Neutron and Muon Source, STFC Rutherford Appleton Laboratory, Didcot OX11 0QX, United Kingdom
[4]Department of Materials Science and Engineering, The University of Sheffield, Sheffield S1 3JD, United Kingdom
[5]Department of Chemistry, University of Cambridge, Cambridge CB2 1EW, United Kingdom
[6]Department of Chemistry, University of Oxford, Inorganic Chemistry Laboratory, Oxford OX1 3QR, United Kingdom
[7]Cavendish Laboratory, University of Cambridge, Cambridge CB3 0HE, United Kingdom
[8]Institute for Manufacturing, Department of Engineering, University of Cambridge, Cambridge CB3 0FS, United Kingdom
[9]Department of Engineering, University of Cambridge, Cambridge CB2 1PZ, United Kingdom
[10]Department of Chemistry, Lancaster University, Lancaster LA1 4YB, United Kingdom
[11]Department of Materials Science and Metallurgy, University of Cambridge, Cambridge CB3 0FS, United Kingdom
[12]WMG, University of Warwick, Coventry CV4 7AL, United Kingdom
[13]Exawatt, Sheffield S10 2LR, United Kingdom
[14]Department of Chemistry, University College London, London WC1H 0AJ, United Kingdom
[15]Diamond Light Source Ltd., Diamond House, Harwell Science and Innovation Campus, Didcot OX11 0DE, United Kingdom

[a)]**Authors to whom correspondence should be addressed:** s.g.booth@sheffield.ac.uk; a.nedoma@sheffield.ac.uk; and s.cussen@sheffield.ac.uk